2007

Characterization of S-denitrosation and disulfide reductase activity of protein disulfide isomerase

Arun Raturi
University of Windsor

Characterization of *S*-Denitrosation and Disulfide Reductase Activity of Protein Disulfide Isomerase: Role in Vascular Function

by

Arun Raturi

A Dissertation
Submitted to the Faculty of Graduate Studies and Research
through Chemistry and Biochemistry
in Partial Fulfillment of the Requirements for
the Degree of Doctor of Philosophy at the
University of Windsor

Windsor, Ontario, Canada
2007

Your file Votre référence
ISBN: 978-0-494-35093-5
Our file Notre référence
ISBN: 978-0-494-35093-5

ABSTRACT

PDI (protein disulphide-isomerase) is widely distributed across eukaryotic tissues, making up approximately 1% of the total protein content of cells. One of the most studied functions of PDI is its ability to catalyze isomerization and rearrangement of disulphide bonds in the endoplasmic reticulum. Recently, its *S*-denitrosation activity has also been demonstrated. The present study was initiated to characterize PDI mediated denitrosation as well as disulfide reduction by using novel assays and methods.

We present here simple UV-visible spectrophotometric and fluorometric assays to monitor denitrosation of *S*-nitrosoglutathione (GSNO) by PDI. This was achieved by monitoring the loss of the S-NO absorbance at 343 nm as well as with the aid of the fluorogenic nitric oxide (NOx) probe 2,3-diaminonaphthalene. Our results further suggested that final product of this catalytic denitrosation is NO$^{\bullet}$. Overall, we have provided evidence that PDI can be *S*-nitrosated to form PDI-SNO which, in turn, can be denitrosated by PDI suggesting the potential role of this enzyme in the transport of nitric oxide across the membrane.

We have utilized oxidized glutathione to develop a series of fluorescent probes and to establish sensitive fluorometric assays for the continuous determination of disulphide reductase activity of PDI. The most effective probe was dieosin glutathione disulfide

(Di-E-GSSG) that gave ~70-fold increase in the fluorescence signal upon reduction of the disulfide bond. This probe was used to monitor disulfide reductase activity of PDI with a sensitivity range that has not been reported in literature. The assay was used to study the dithiol equilibrium state of PDI under variable [GSH] / [GSSG] ratios.

We have shown that platelet derived microparticles contain protein disulfide isomerase and this surface associated PDI is involved in promoting platelet aggregation. We also detected increased levels of PDI-containing microparticles in patients with type II diabetes (T2D). These findings strongly suggest that platelet hypersensitivity observed in T2D can partially be attributed to microparticle-surface-PDI activity.

Dedicated to my wife, Ritu, my daughter, Avani and my Parents

ACKNOWLEDGEMENTS

First and foremost I would like to thank Dr. Bulent Mutus for his enthusiastic supervision, constant guidance and the trust he has bestowed on me over the years. My gratitude is extended to my committee members Dr. Lana Lee, Dr. Panayiotis O Vacratsis, Dr. Dennis Higgs and external examiner Dr. Hiram F Gilbert for their contributions. My thanks to Dr. John Hudson, Dr. Siyaram Pandey, Dr. James Gauld and Dr. Sirinart Ananvoranich for all the scientific discussions I had with them over the years.

This work would not have been possible without the helping hands of Inga Sliskovic, Shane Miersch and Paul Root. Their contribution to my thesis has been indispensable. Many thanks to former and current members of Mutus group: Shirin Akhter, Arzu Akarca, Jiung Wang, Nabiha Hamaed, Khaled Elmosrati, Ruchi Chaube, Harmanpreet Kaur, Gaurav Saluja, Suzie Durocher and Danijela Domazet.

I would like to extend my gratitude to my colleagues Jafar Naderi, Mallika Somayjulu-Nitu, Priya Sharda, Anna Kozarova, Ahmed, John Mucaki and David for their support and concern.

I am forever indebted to my parents for their endless love and trust on me that will always remain the prime source of inspiration for me.

Finally, I would like to thank my wife Ritu for her constant support, understanding, endless patience and encouragement when it was most required. This work would not have been remotely possible without her love.

TABLE OF CONTENTS

LIST OF FIGURES

LIST OF SCHEMES

LIST OF TABLES

LIST OF ABBRIVIATIONS

ACD:	Acid Citrate Dextrose
ADP:	Adenosine diphosphate
ATP:	Adenosine triphosphate
BH_4:	Tetrahydrobiopterin
BSA:	Bovine serum albumin
BSA-NO:	*S*-nitroso bovine serum albumin
CaM:	Calmodulin
cGMP:	Cyclic guanosine monophosphate
CGSNO:	*S*-nitrosocysteinyl glycine
csPDI:	cell surface protein disulfide isomerase
DAN:	2,3 diamino napthalene
Diabz:	di (o-amino benzoyl) glutathione disulfide
Di-E-GSSG:	Dieosin glutathione disulfide
Di-E-Insulin:	Dieosin insulin
DM:	Diabetes Mellitus
DMF:	N,N-Dimethyl formamide
DNA:	Deoxyribonucleic acid
DTNB:	5,5'-dithio bis (2-nitrobenzoic acid)
DTT:	Dithiothreitol
EDTA:	Ethylene diamine tetraacetic acid
ER:	Endoplasmic reticulum

E.coli	Escherichia *coli*
EITC:	eosin isothiocyanate
eNOS:	Endothelial nitric oxide Synthase
FAD:	Flavin adenine dinucleotide
FITC:	Fluorescein isothiocyanate
FMN:	Flavin mononucleotide
FRET:	Fluorescence resonance energy transfer
FSQ:	Fluorescence self quenching
GC:	Guanylate cyclase
GP:	Glycoprotein
γGT :	γ glutamyl transpeptidases
GSH:	Reduced glutathione
GSNO:	*S*-nitroso glutathione
GSSG:	Oxidized glutathione
iNOS:	Inducible nitric oxide synthase
IAA:	Iodo acetic acid
IPA:	Isopropyl alcohol or isopropanol
IPTG:	Isopropyl β-D-1-thiogalactopyranoside
IP_3:	Inositol 1,4,5 biphosphate
MP:	Microparticle
msPDI:	microparticle surface protein disulfide isomerase
NADPH:	Nicotinamide adenine dinucleotide phosphate (reduced form)
NAT:	Napthatriazole

NEM:	N-ethylmaleimide
nNOS:	neuronal nitric oxide synthase
$NO^{\cdot}$:	Nitric oxide
NO_2 :	Nitrogen dioxide
NOS:	Nitric oxide synthase
OD:	Optical Density
PAO:	Phenylarsine oxide
PBS:	Phosphate buffer saline
PDI:	Protein disulfide isomerase
PMP:	Platelet derived microparticle
PRP:	Platelet rich plasma protein disulfide isomerase
psPDI:	Platelet surface protein disulfide isomerase
PS:	Phosphatidylserine
RFU:	Relative fluorescence unit
ROS:	Reactive oxygen species
$RS^{\cdot}$:	thiyl radical
RSH:	Thiols
RSNO:	*S*-nitrosothiols
SOD:	Super oxide dismutase
sGC:	soluble guanylate cyclase
T2D:	Type 2 Diabetes
TF:	Tissue factor
UV:	Ultraviolet

CHAPTER 1

General Introduction

Protein Disulfide Isomerase:

Structure, Function and Localization

1.1 Protein disulfide isomerase

Protein disulfide isomerase (PDI) (E.C. 5.3.4.1) is a ~55 kDa protein that was first isolated and characterized by Anfinsen and coworkers (Goldberger *et al.*, 1963). It is primarily located in the endoplasmic reticulum (ER) where it assists in the proper folding of proteins through disulfide isomerization. However, this enzyme has been extensively studied in past decades for its multifunctional roles and non- ER locations (Turano *et al.*, 2002).

1.1.1 Overall Structural Organization

PDI is a multidomain protein and, as shown in Figure 1.1, its structure is organized in five domains (***a, b, b', a', c***) (Darby *et al.*, 1996). The ***a*** and ***a'*** domains are catalytically active due to the presence of one active site in each domain and show high degree of homology to each other as well as to thioredoxin. In contrast, ***b*** and ***b'*** are inactive domains and show homology only to each other but not to thioredoxin. The active site present in ***a*** or ***a'*** domain has two cysteine residues separated by two amino acids, glycine and histidine, through which PDI mediates its activity.

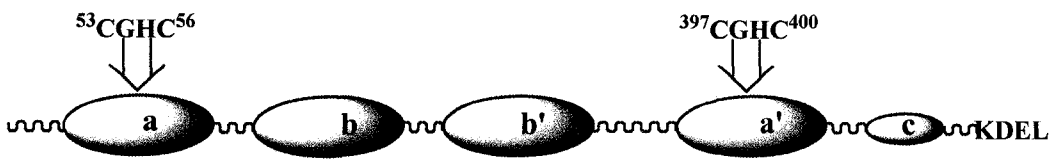

Figure 1.1 Simple domain architecture of human PDI (Darby *et al.*, 1996).

1.1.2 Crystal Structure of Yeast PDI

Most of the information related to structural organization of human PDI in the literature has come from the NMR studies on individual ***a*** and ***b*** domains conducted by Kemmink *et al.* (1996, 1997). However, very recently, Schindelin and coworkers (Tian *et al.*, 2006) have obtained the crystal structure of full length yeast PDI and have extensively described its three dimensional structure which has tremendously improved our knowledge towards better understanding of PDI structure. Although the described crystal structure is of yeast PDI, it is expected that mammalian PDI will share structural homology with the former owing to similarities in primary structure and domain boundaries.

The crystal structure showed that PDI active sites, as predicted earlier, adopt a thioredoxin fold that is composed of five β sheets and 4 α helices in the sequence of βαβαβαββα (Figure 1.2). The active site consensus sequence (CGHC) in ***a*** or ***a'*** domain is present towards the N-terminus of second α helix. The ***b*** and ***b'*** domains also resemble the thioredoxin fold with noted differences. While the ***b*** domain lacks the third α helix and has a shorter second helix, ***b'*** domain lacks the first β strand and has an extra short α helix before the fourth helix. The overall arrangement of four domains is asymmetrical in such a way that ***a*** domain is in contact with both ***b*** and ***b'*** domains, whereas ***a'*** domain only interacts with ***b'*** domain. In addition, ***a*** and ***a'*** domains are more flexible in spatial movement as compared to rigid ***b*** and ***b'*** domains.

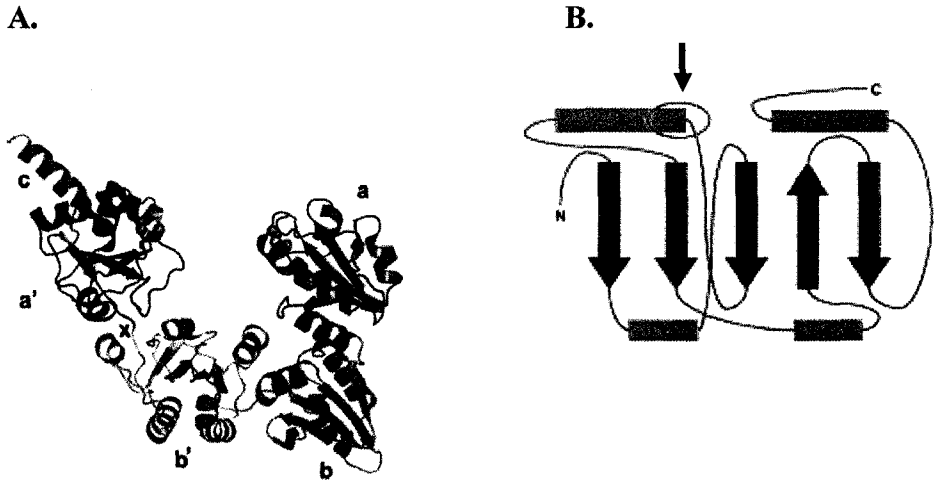

Figure 1.2 Structure of yeast PDI (Tian *et al.*, 2006)

A. Ribbon diagram of PDI: ***a*** domain in violet, ***b*** domain in cyan, ***b'*** domain in golden, ***a'*** domains in red, and the ***c*** domain in green. '**x**' represents the loop connecting ***a'*** and ***b'*** domains. **B.** Secondary structure diagram of the canonical thioredoxin fold with α helices in green and β strands in red. The location of the active site is indicated by a red oval and arrow. Reprint with permission from Elsevier (Tian *et. al*, 2006)

1.1.3 Active site arrangement

One of the most important findings derived from the crystal structure of PDI is the determination of the adjacent positioning of the two active sites with respect to each other. The structure shows that PDI adopts a 'U' shape in such a way that ***b*** and ***b'*** domains form its base and ***a*** and ***a'*** domains are facing each other in the inside of 'U' structure. The proper folding of proteins by PDI is potentially facilitated by this shape in two ways: 1) Internal surface of 'U' is rich in hydrophobic residues that participate in the interaction of PDI with misfolded proteins and 2) The two active sites are separated by a distance of 28 Å that can accommodate a protein of ~100 residues.

1.1.4 Hydrophobic features of *b* and *b'* domains

The NMR study of human PDI (Kemmink *et al.*, 1996) as well as the crystal structure of yeast PDI has shown that both ***b*** and ***b'*** domains have hydrophobic patches surrounding the active sites (Figure 1.3). These patches, in association with hydrophobic residues of the ***a*** and ***a'*** domains, form a continuous hydrophobic surface that provides an ideal substrate binding platform for misfolded proteins. Although the ***b*** domain has a hydrophobic patch that contributes to the overall hydrophobic platform and makes it larger, the primary substrate binding site is present in ***b'*** domain. Pimeskoski *et al.* (2004) have shown that in human PDI, residue I272 of ***b'*** domain is crucial for the substrate binding. Overall, it has been suggested that while ***b'*** domain is important for the effective protein folding, ***b*** domain potentially increases the rate of refolding (Tian *et al.*, 2006).

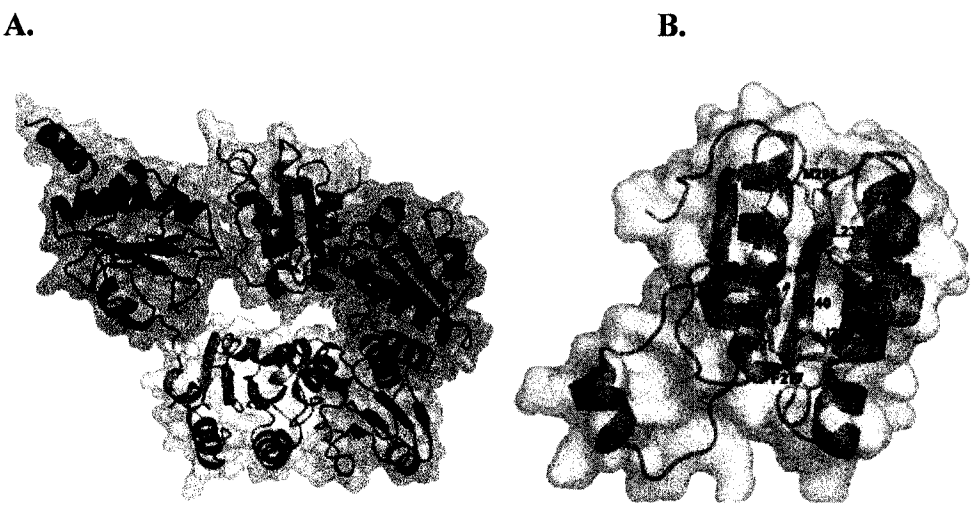

Figure 1.3 Hydrophobic Surface Features of PDI (Tian *et al.*, 2006)

A. Packing interactions in PDI. The ***b*** domain (cyan) is located between the ***a*** and ***a'*** domains. **B.** Peptide binding pockets in the ***b'*** domain. Residues in the center are present at the bottom of the hydrophobic pocket. Reprint with permission from Elsevier (Tian *et. al*, 2006)

1.1.5 PDI family proteins

To date, there are seventeen members of human PDI family that have been identified and are shown to be present in endoplasmic reticulum (Table 1.1) (Ellgaard and Ruddock, 2005a). Although members of the same family, these homologues may differ from each other in many features such as number of active sites, length, N-glycosylation or domain architecture. For example ERdj5 contains 4 active site domains, ERp72, ERp46 and PDIr contain 3 active site domains whereas ERp27, ERp28, ERdj5, ERp18 and TMX4 contain only one active site domain. PDI, ERp57, PDIp, ERp65 and P5 contain 2 active site domains and show high degree of sequence similarity as well as similar domain organization suggesting their similar physiological function(s).

Table 1.1 Members of PDI family. Adapted from Ellgaard and Ruddock (2005a)

Name	SwissProt accession	Length	ER retention	*a*-Like domains
ERdj5	Q8IXB1	793	KDEL	4
ERp72	PI3667	645	KEEL	3
PDIr	QI4554	519	KEEL	3
ERp46	Q8NBS9	432	KDEL	3
PDI	P07237	508	KDEL	2
ERp57	P30101	505	QEDL	2
PDIp	Q13087	525	KEEL	2
ERp65	Q8N807	584	KEEL	2
P5	Q15084	440	KDEL	2
ERp18	Q95881	172	EDEL	1
ERp44	Q9BS26	406	RDEL	1
TMX	Q9H3N1	280	Unknown	1
TMX2	Q9Y320	296	KKDK	1
TMX3	Q96JJ7	454	KKKD	1
TMX4	Q9H1E5	349	Unknown	1
ERp27	Q96DN0	273	KVEL	0
ERp28	P30040	261	KEEL	0

1.1.6 Physiological role in the endoplasmic reticulum

Depending upon its redox state, PDI can catalyze three types of reactions: oxidation, reduction or isomerization. As shown in Figure 1.4A, in completely oxidized state, PDI would preferably perform oxidation of protein thiols by transferring oxidizing equivalents from its active site. On the other hand, in completely reduced state, it can either perform reduction or isomerization of disulfide bonds (Wilkinson and Gilbert, 2004) (Figure 1.4B). Note that there is no net change in redox state of PDI in the isomerization reaction.

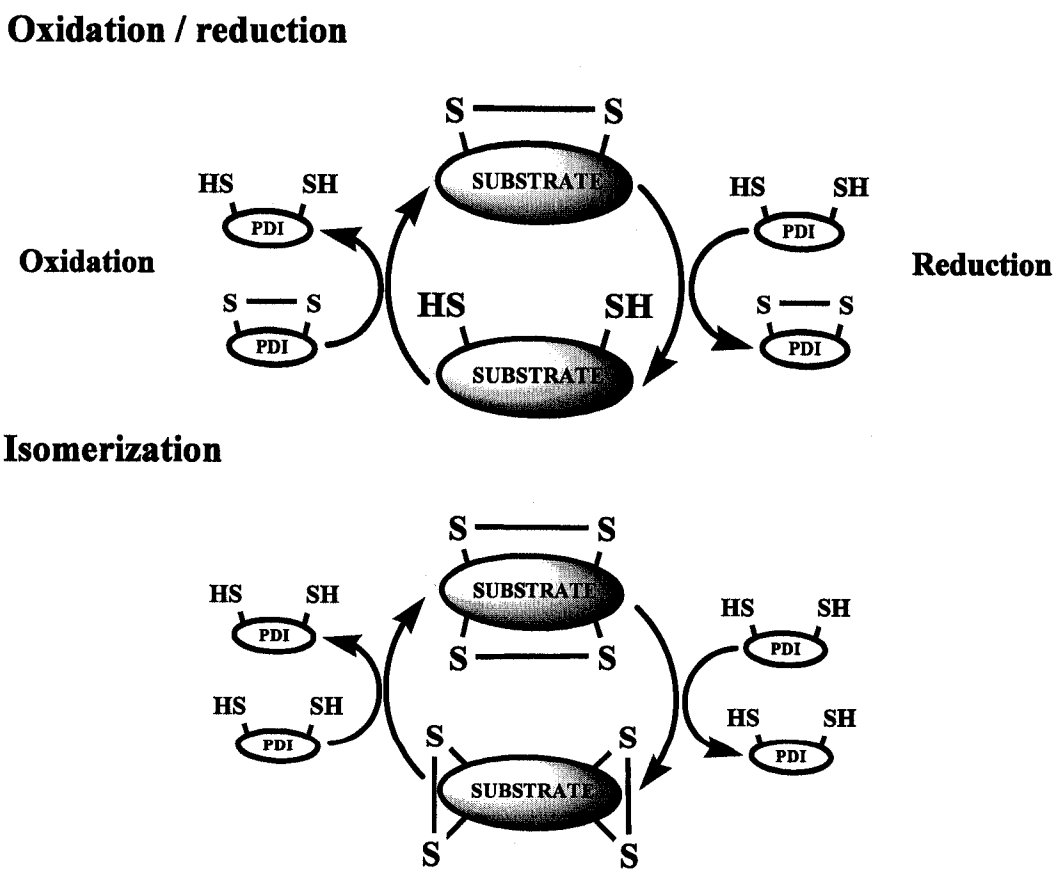

Figure 1.4 Reduction, oxidation (A) and isomerization (B) of disulfide by PDI.

PDI is primarily located in the ER where its concentration is very high (Terada *et al.*, 1995) (~7 μg per mg of total ER protein) because of higher level of expression as well as its high stability (Ohba *et al.*, 1981). Here, its primary function is isomerization of disulfide bonds required for the proper folding of proteins and polypeptides.

The rearrangement of misfolded proteins requires breaking of improperly paired disulfide bonds and then reforming them in correct disulfide format. The first step in this process is the nucleophilic attack by the N-terminal active site cysteine which is exposed to the solvent and has an unusually low pKa. This leads to the formation of a trans-disulfide intermediate between PDI and substrate. At this stage, according to Gilbert and coworkers (Schwaller *et al.*, 2003), there are two possibilities (Figure 1.5):

i) The second cysteine in the substrate, with spatial proximity to reaction site, displaces PDI thereby starting an intramolecular disulfide rearrangement within the substrate until the C-terminal active site cysteine reduces the substrate-PDI disulfide. This mode of rearrangement of disulfide bonds requires only reduced form of PDI.

ii) PDI escapes after reducing the substrate which initiates intermolecular disulfide rearrangement. This leads to cycles of reduction and oxidation of substrate until it attains stability to resist any further isomerization. Unlike intramolecular rearrangement, this mechanism requires both reduced and oxidized PDI.

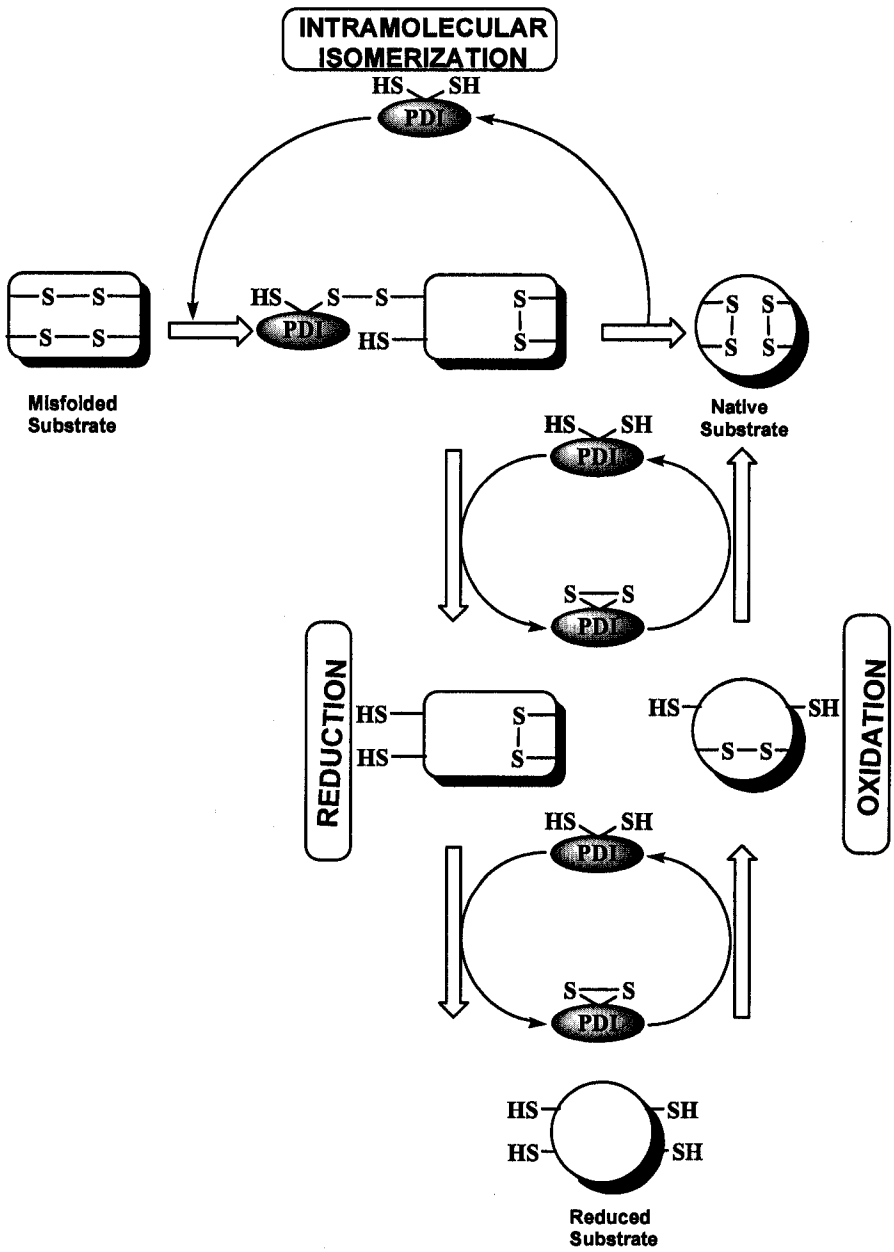

Figure 1.5 Intra- and Inter-molecular rearrangements of disulfides by PDI (Schwaller *et al.*, 2003).

1.1.7 Non-ER location of PDI: Cell surface protein disulfide isomerase (csPDI)

As previously described, PDI is primarily located in endoplasmic reticulum and is known for its ability to catalyze rearrangement of disulphide bonds in its lumen. However, it is now well established that PDI is also secreted from a variety of cell types like hepatocytes (Terada *et al.*, 1995), endothelial cells (Hotchkiss *et al.*, 1998), pancreatic cells (Yoshimori *et al.*, 1990), leukocytes (Bennett *et al.*, 2000) and platelets (Chen *et al.*, 1995) and binds to the cell surface through electrostatic interactions (Terada *et al.*, 1995). The mechanism by which PDI escapes from the ER is not well understood as it contains an ER-retention sequence and, ideally, should not leave the ER lumen. One mechanism proposed for its escape is through its association with other proteins that are destined for secretion (Johnson *et al.*, 2001). This mechanism is supported by the fact that ***b'*** domain of PDI contains large hydrophobic patches that may serve as suitable binding site for peptides and proteins.

The physiological role of csPDI in different cell lines is currently under investigation in various studies where it has been reported to play important role in cell adhesion and in many diseases.

1.1.7.1 csPDI in cell adhesion

The role of PDI in cell adhesion is attributed to reduction or reshuffling of exofacial disulfides by its catalytic activity. For example, Bennett *et al.* (2000) have shown evidence that PDI regulates leukocyte adhesion by maintaining the conformation of L-selectin. L-selectin is a cell membrane adhesion protein that is expressed on the majority

of leukocytes, including peripheral blood T and B lymphocytes, neutrophils, eosinophils, basophils, monocytes and NK cells. Shedding of L-selectin is regulated by its redox state. When in reduced state, its conformation is resistant to proteolytic cleavage (Figure 1.6) whereas in oxidized state the extracellular moiety of L-selectin is cleaved resulting in loss of adhesive property of the leukocytes. It was proposed that reduced csPDI prevents the shedding of L-selectin by maintaining it in reduced state. This observation was supported by the fact that treatment of non-activated leukocytes with anti-PDI antibody also promoted L-selectin shedding (Bennett *et al.*, 2000).

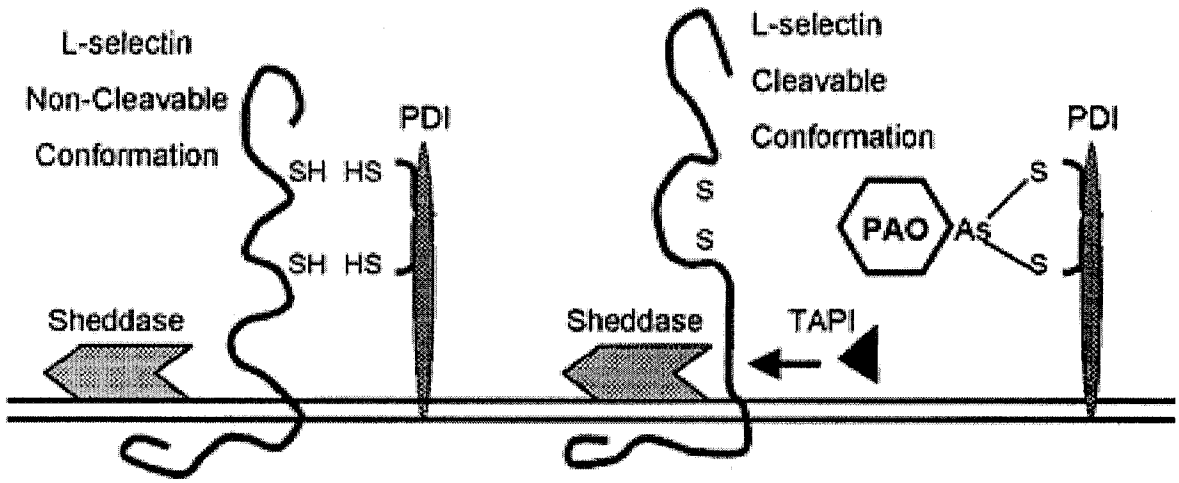

Figure 1.6 Regulation of L-selectin shedding by reduced csPDI (Bennett *et al.*, 2000)

Sheddase mediated proteolytic cleavage of L-selection is only possible after blocking reductive activity of PDI.

1.1.7.2 csPDI in platelet activation

The role of surface thiols in platelet response was first studied by Aledort *et al.* (1968) when they showed that platelet aggregation can be inhibited by pre-treating them with membrane impermeable thiol blocker. This observation was further supported by Macintyre and Gordon (1974) who showed that addition of DTT potentiates platelet aggregation only in the presence of fibrinogen. It is now well established that exofacial thiols are required for reshuffling of disulfide bonds in integrins causing its activation that eventually mediates platelet aggregation. The role of PDI in integrin activation was demonstrated by the observations that platelet aggregation was inhibited in the presence of its inhibitors (Essex and Li 1999; Essex *et al.*, 2001; Lahav *et al.*, 2000). Later, Lahav *et al.*. (2002) studied the binding of fibrinogen to its integrin receptor, GPIIbIIIa, and demonstrated that the stable binding between the two requires disulfide reshuffling that is mediated by PDI.

1.1.7.3 csPDI in NO transport

Nitric oxide ($NO^{\cdot}$) is a heterodiatomic free radical with multiple physiological actions such as vaso-relaxation, neurotransmission, regulation of platelet function, and non-specific immune responses (Ignarro, 1991; Kandel and O'Dell, 1992; Radomski *et al.*, 1987). $NO^{\cdot}$ mediated induction of vasorelaxation or inhibition of platelet function is, in part, through activation of soluble guanylyl cyclase. Nitrosation of cellular thiols results in the formation of *S*-nitrosothiols that prolongs its half-life and may act as an alternative source of cellular $NO^{\cdot}$ (Stamler *et al.*, 1992a, 1992b).

The transport of NO· across the membrane is presumed to be mainly by diffusion (Goretski and Hollocher, 1988) that is facilitated by its charge neutrality, small size and relative low reactivity. As thiols can liberate NO· from *S*-nitrosothiols, it is possible that NO· transport across the membrane may be regulated by transnitrosation reactions involving membrane thiols. Zai *et al.*, (1999) presented a transnitrosation mechanism catalyzed by cell-surface PDI that may regulate cellular entry of NO·. Later, a mechanism was proposed by which the NO· released from *S*-nitrosothiols by csPDI can nitrosate intracellular thiols at the membrane-cytosol interface (Ramachandran *et al.*, 2001) (Figure 1.7). The role of csPDI in denitrosation, and *S*-nitrosation is described in detail in Chapter 2.

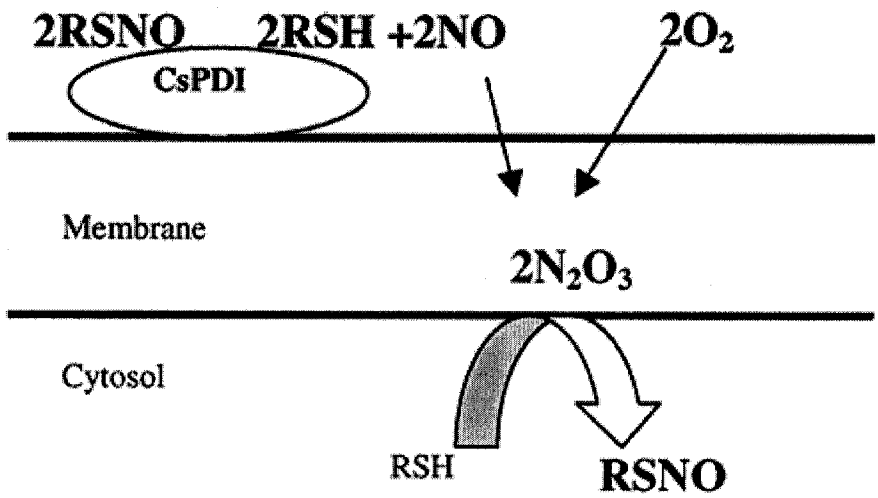

Figure 1.7 Postulated mechanism for intracellular NO transport catalyzed by csPDI (Ramachandran *et al.*, 2001).

1.1.7.4 csPDI in diseases

Several independent studies have demonstrated the involvement of csPDI in pathogen-host cell interactions. For example, it was shown that uptake of diphtheria toxin by host is possible only after the reduction of its disulfide bond by csPDI (Mandel *et al.*, 1993). Abell and Brown (1993) further showed that entry of Sindbis virus requires PDI reductase activity. Interestingly, it has been reported that csPDI is crucial for human immuno deficiency (HIV) envelope fusion as well as virus entry (Ryser *et al.*, 1994; Fenouillet *et al.*, 2001, Markovic *et al.* 2004). It was suggested that entry of virus requires PDI mediated disulfide reduction of viral envelope glycoprotein gp120. Recently, it was shown that presence of native PDI on the surface of epithelial cells is required for the infection by Chlamydia *trachomatis* which is a leading bacterial agent causing sexually transmitted disease (Stephens and Carolyn, 2006). The attachment of Neospora *caninum*, a protozoan that causes abortion in cattles, to its host cell was also shown to be regulated by csPDI (Naguleswaran *et al.*, 2005).

1.1.8 Chaperone activity of PDI

A protein is defined as a chaperone if it assists the correct, non-covalent assembly of a protein but is not a component of this protein when performing its normal biological function(s). PDI falls in this category because, apart from its isomerase activity, it inhibits the aggregation of misfolded or partially folded proteins in the ER lumen by binding to protein domains that are prone to self assembly. The chaperone activity of PDI is independent of its isomerase activity and does not require the -CGHC- active sites as

demonstrated by its ability to promote *in vitro* reactivation and inhibition of aggregation during refolding of denatured proteins with no disulfide. It is suggested that the peptide binding site of PDI required for chaperone activity is located between ***a'*** and ***c*** domain because PDI without ***c*** domain does not show any chaperone activity (Dai and Wang, 1997). Chaperone activity of PDI has been shown to assist *in-vitro* folding of proteins like rhodonase (Song and Wang, 1995), lysozyme (Puig and Gilbert, 1994), alcohol dehydrogenase (Prim *et al.*, 1996), glyceraldehyde-3-phosphate dehydrogenase (Cai *et al.*, 1994) and citrate synthase (Primm *et al.*, 1996), by inhibiting their aggregation.

1.1.9 PDI as a subunit of other enzymes

PDI functions as a subunit in two enzyme complexes, the collagen prolyl 4-hydroxylases (Kivirikko and Myllyharju, 1998) and microsomal triglyceride transfer protein (Wetterau *et al.*, 1990). Prolyl 4-hydroxylase is essential for the synthesis of collagen and catalyzes the hydroxylation of prolines in procollagen during its synthesis (Kivirikko and Myllyharju, 1998). It is a tetramer consisting of two catalytic α subunits and two β subunits identical to PDI (Pihlajaniemi *et al.*, 1987). PDI is also a component of microsomal triacylglycerol transfer protein (an $\alpha\beta$ heterodimer of PDI and a 88 kDa β subunit), that is essential for the assembly of apoB lipoproteins and catalyzes the transfer of neutral lipid onto nascent lipoprotein particles (Wetterau *et al.*., 1990). When complexed with either prolyl-4-hydroxylase or the microsomal triacylglycerol transfer protein, PDI does not show isomerase activity and its role is to keep highly insoluble α subunits of both enzymes catalytically active and in solution (Vuori *et al.*, 1992; Wetterau *et al.* 1990). This function is likely to be related to the peptide binding and

chaperone functions of PDI, and therefore does not have involvement of active site dithiols (Lamberg *et al.*, 1996). Also, PDI might help in keeping the prolyl-4-hydroxylase in the ER lumen, since the α subunits lack the ER retention sequence.

Chapter 2

Characterization of *S*-Denitrosation Activity of PDI

2.1 Introduction

2.1.1 Nitric oxide

The identification of Nitric oxide (NO·) as endothelium-derived relaxing factor (EDRF) was one of the most fascinating discoveries of 1980s (Furchgott and Vanhoutt, 1989; Ignarro *et al.* 1987; Moncada *et al.*, 1987; Palmer *et al.*, 1987) which had a great impact on our understanding of signal transduction and many cellular processes in mammals. It is now well established that, owing to its unique chemical properties, NO· is a potent biological mediator and regulate many cellular processes in the body.

2.1.1.1 Chemical properties

NO· is a simple, diatomic molecule that exists in the colorless gaseous form at room temperature. The Lewis dot structure of NO· clearly demonstrates that it is a free radical with one unpaired electron (Figure 2.1A). In order to complete its octet, it is expected that NO· would diamerize to form N_2O_4. However, this is not the case and can be explained by its molecular orbital diagram. The molecular orbital diagram of NO· shows one unpaired electron in π^* antibonding orbital which gives it a bond order of 2.5 (Figure 2.1B). Upon dimerization, NO would form N_2O_4 with no net gain in the bonding (overall bond order of 5). Therefore dimerization is not entropically favored and NO· exists as a monomer at room temperature. Moreover, The N-N bond distance in N_2O_4 is unusually long (2.263 Å) (McKellar *et al.*, 1995) which makes this bond very weak (bond energy 2-4 kcal/mol) (East *et al.*, 1998).

A.

B.

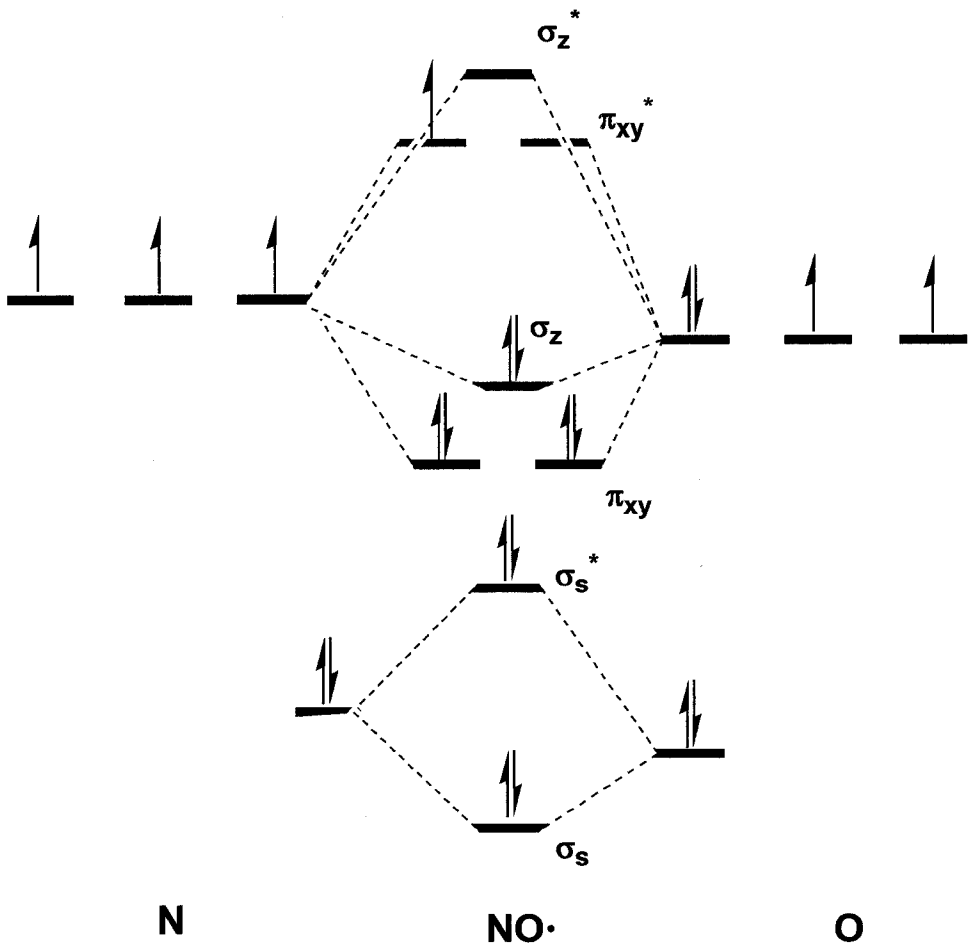

Figure 2.1 Lewis diagram (A) and molecular orbital diagram (B) of NO·

2.1.1.2 Biosynthesis of NO·

NO· is synthesized by a group of enzymes called nitric oxide synthase (NOS) which are found in three forms: Neuronal NOS (nNOS or NOS 1), Inducible NOS (iNOS or NOS 2) and Endothelial NOS (eNOS or NOS 3). Irrespective of its form, the catalytic formation of NO· by NOS is by 5 electron oxidation of terminal guanidium nitrogen of L-arginine (Figure 2.2) in the presence of O_2 and the cofactors nicotinamide adenine dinucleotide phosphate (NADPH), flavin adenine dinucleotide (FAD), flavin mononucleotide (FMN), heme and tetrahydrobiopterin (BH_4). The overall reaction consumes 1.5 moles of NADPH and 2 moles of oxygen to form 1 mole of NO·.

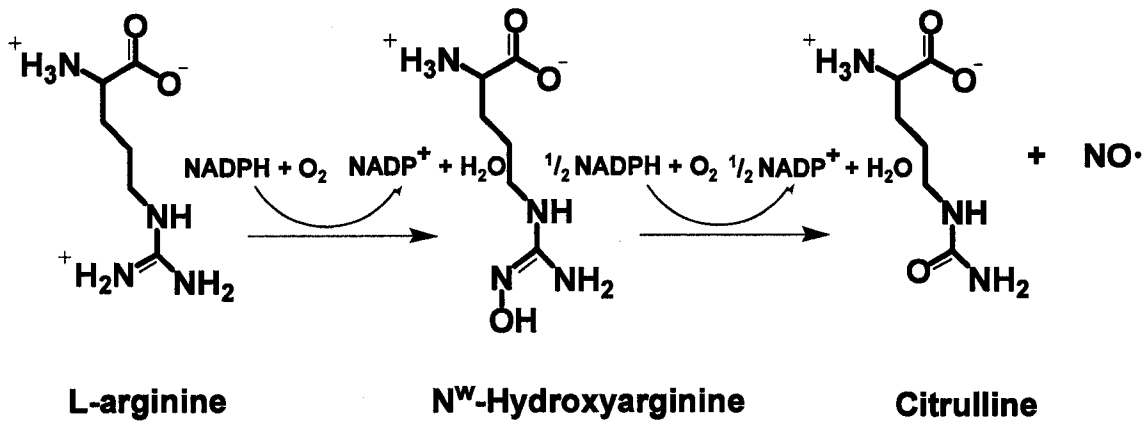

Figure 2.2 Synthesis of NO· from L-arginine (Ignarro, 2000)

A schematic alignment of cofactor binding sites of the three NOS isozymes is as follows:

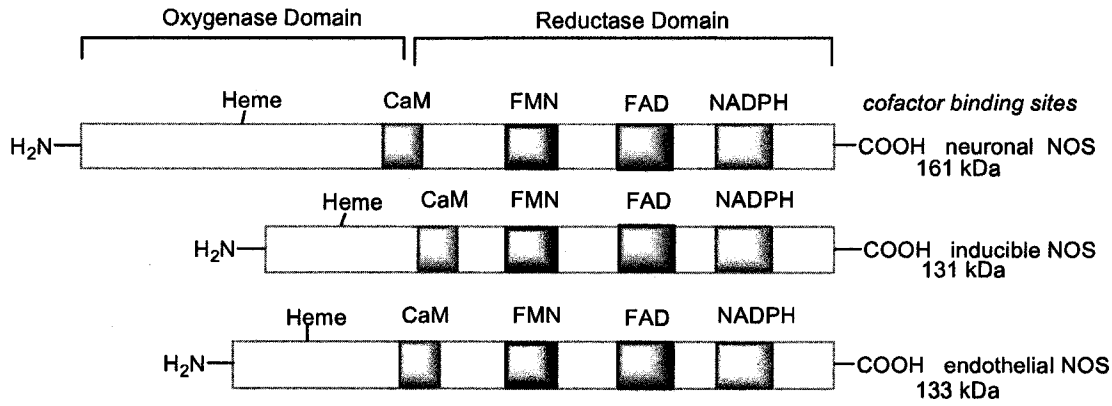

Figure 2.3 Comparison of three NOS forms (Ignarro, 2000)

All three forms of NOS exist as homodimer where each monomer consists of two major domains: i) N-terminal oxygenase domain that has binding site for BH_4 and L-arginine and ii) C-terminal reductase domain that binds to FMN, FAD and NADPH. The calmodulin (CaM) binding sequence is present in the interdomain linker between the oxygenase and reductase domains. The physiological concentrations of Ca^{2+} in cells regulate the binding of CaM to NOS 1 and NOS 3 that initiates the electron transfer from the flavins to the heme moieties leading to the formation of $NO^{\cdot}$. On the contrary, CaM is always tightly bound to the NOS 2 and therefore is a Ca^{2+}-insensitive isoform.

2.1.1.3 Other Nitrogen oxide species

In the aqueous solution, $NO^{\cdot}$ reacts with O_2 to form NO^{-}_2 (nitrite) (Eq-1):

$$4NO^{\cdot} + O_2 + H_2O \longrightarrow 4NO_2^{-} + H^{+} \qquad \text{Eq. 1}$$

This reaction is of second order with respect to $NO^{\cdot}$ and therefore the half life of $NO^{\cdot}$ depends upon its initial concentration (Ford *et al.*, 1993). If we assume that $NO^{\cdot}$ reacts only with O_2, its half life would be 100 to 500 seconds. However, it has been shown that $NO^{\cdot}$ can react with numerous other biological molecules and therefore have a half life of few seconds in biological systems (Stamler *et al.*, 1992b).

Other possible $NO^{\cdot}$ derivatives are listed in Figure 2.4. $NO^{\cdot}$ can undergo one electron reduction to form NO^{-} with a bond order of 2 or one electron oxidation to form NO^{+} with a bond order of 3. Reaction of $NO^{\cdot}$ with oxygen generates nitrogen dioxide (NO_2), which is a stronger oxidizing agent with the reduction potential of 1.04 V for NO_2/NO_2^{-} couple (Stanbury, 1989). These derivatives are implicated in some important biological reactions (Stamler *et al.*, 1992b).

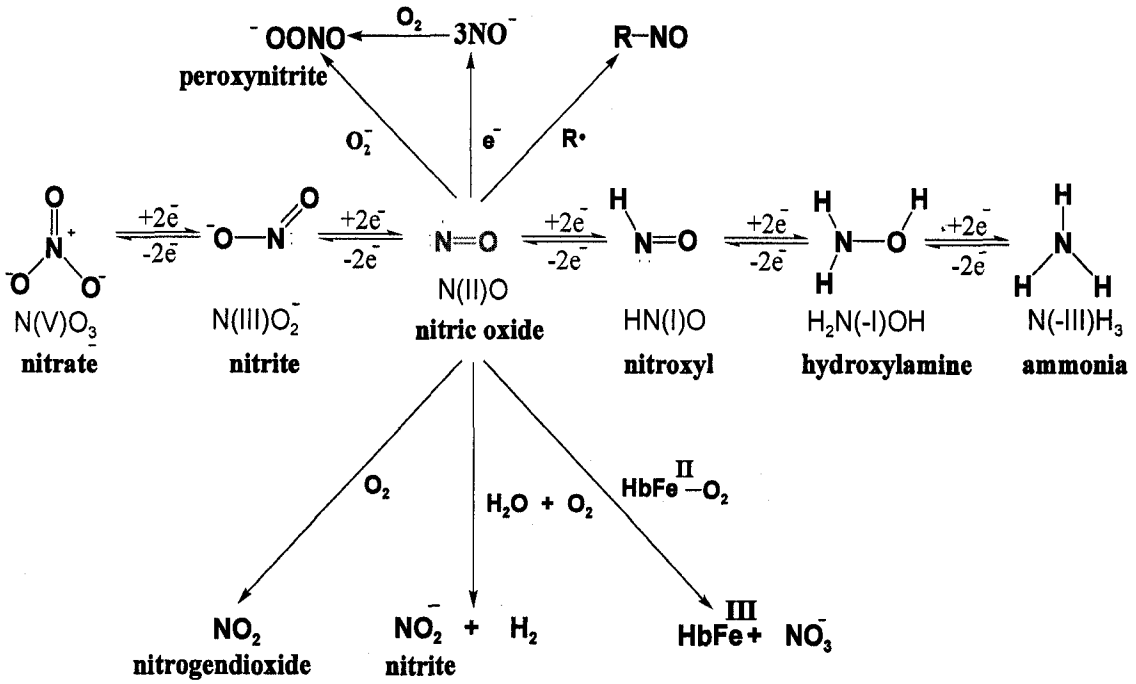

Figure 2.4 Redox derivatives of NO· (Ignarro, 2000).

2.1.1.4 Physiological function of NO· : Activation of soluble guanylate cyclase (sGC)

sGC is an enzyme that catalyzes the conversion of guanosine triphosphate (GTP) to cyclic guanosine monophosphate (cGMP) in the presence of magnesium ion (Mg^{2+}) (Figure 2.5A). This reaction has a K_M value of ~100 μM and Vmax of 0.1 μmol/min/mg of protein. Interestingly, in the presence of NO·, the Km and Vmax for the same reaction is 30 μM and 10-20 μmol/min/mg respectively indicating a 3-fold increase in the affinity for substrate and 100-200-fold increase in the specific activity of the enzyme (Ignarro, 1991). These data clearly demonstrate that NO· activates sGC.

The mechanism of activation of sGC by NO· involves its binding to heme group of the enzyme. This has been proposed because addition of NO· to heme-deficient sGC did not cause any activation of enzyme (Ignarro *et al.*, 1984). When heme is bound to sGC, the axial ligand bonding imparts steric hindrance to the binding of substrate (GTP) that results in low catalytic activity (Figure 2.5B). Upon binding of NO· to the iron of heme group, there is a conformational change that leads to the cleavage of axial bond between iron and the enzyme (Figure 2.5B). This conformational change exposes the catalytic site of enzyme resulting in higher V_{max} and lower K_M.

cGMP is one of the most important secondary messengers and is widely known for the relaxation of smooth muscles by activating cGMP dependent protein kinases (Lincoln and Cornwell, 1993). This effect can be enhanced by activation of sGC by NO· or NO· donors (Butler *et al.* 1995). In platelets, NO· mediated activation of sGC results in the inhibition of platelet aggregation (Radomski *et al.*, 1987). Activation of sGC by nNOS generated NO· in the neurons has been shown to modulate neurotransmission (Kandel and O'Dell, 1992). In addition to the NO· responses through sGC activation, it has been suggested that NO· produced in macrophages is involved in non specific immune response by phagocytic and non-phagocytic removal of invading pathogens (Beckman *et al.*, 1990; Moncada *et al.*, 1991).

A.

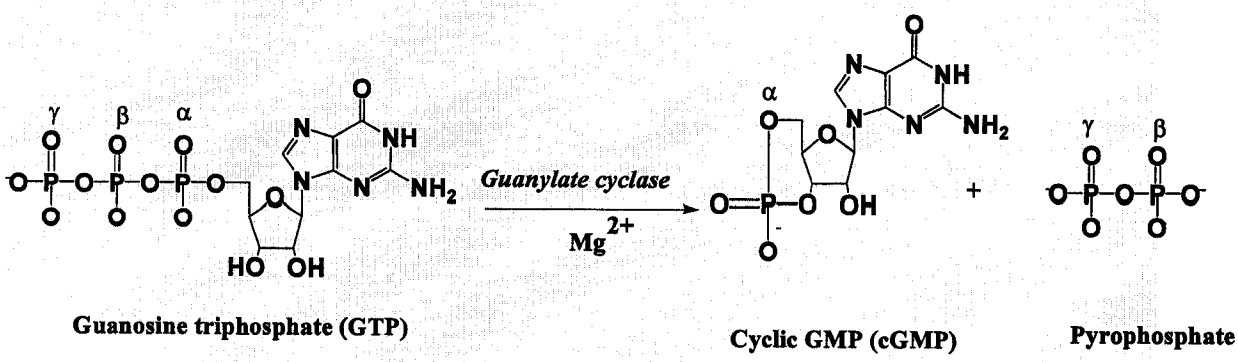

B.

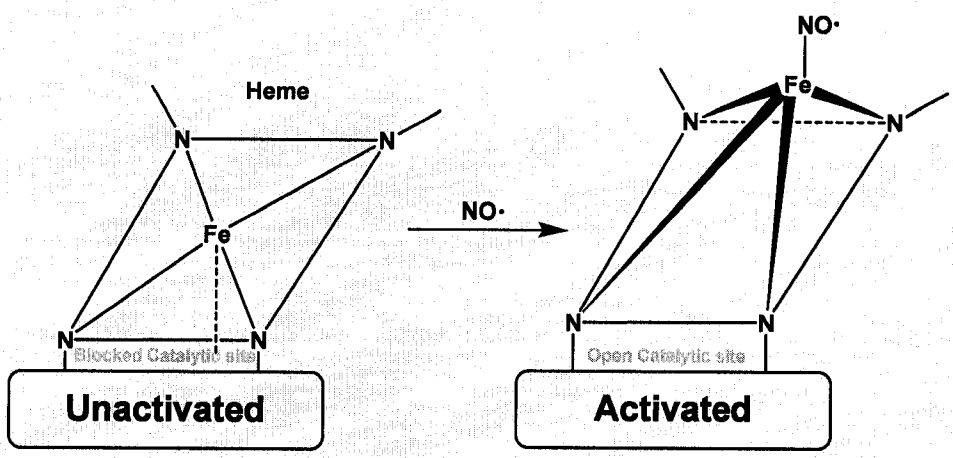

Figure 2.5 Synthesis of cGMP (A) and mechanism of activation of sGC (B). (Ignarro, 2000)

2.1.2 *S*-Nitrosothiols

Thiols (RSH) are the most abundant electrophiles present *in vivo* that readily reacts with NO· to form *S*-Nitrosothiols (RSNOs). It has been demonstrated that RSNOs, like NO·, exhibit vasorelaxant and antiplatelet activities through the release of NO· (Myers *et al.*, 1990; Stamler *et al.*, 1992a, 1992b). RSNOs are more stable than NO· and therefore it is suggested to be 'store house' of NO· in the body.

2.1.2.1 Formation of RSNOs

RSNOs are synthesized *in vitro* by the reaction of RSH with nitrous acid (HNO_2) at lower pH (less than 3) (Eq-2):

$$HNO_2 + RSH \longrightarrow RSNO + H_2O \qquad \text{Eq. 2}$$

However, use of extremely low pH in this reaction limits this method for the synthesis of only low molecular weight RSNOs (CysNO or GSNO) and not for protein *S*-nitrosothiols because:

i) At low pH, proteins are susceptible for denaturation

ii) Acidified nitrite can modify non-thiols such as aromatic ring, alcohol or amines.

The most common method for the synthesis of protein-*S*-nitrosothiols is the transnitrosation reaction between small molecular weight RSNOs and protein thiols (Eq-3):

$$RSNO + R'SH_{protein} \longrightarrow R'SNO_{protein} + RSH \qquad \text{Eq. 3}$$

Although the exact mechanism by which RSNOs are formed *in vivo* is still unclear, it has been suggested that the primary nitrosating agent under physiological condition is dinitrogen trioxide (N_2O_3). The overall reaction can be represented as follows (Scheme 1.1):

$$2NO + O_2 \Longrightarrow 2NO_2$$
$$NO_2 + NO^{\cdot} \Longrightarrow N_2O_3 = {}^{+}ON\text{----}NO_2^{-}$$
$${}^{+}ON\text{----}NO_2^{-} + RSH \Longrightarrow RSNO + HNO_2$$

Scheme 1.1 Nitrosation of RSH under physiological conditions

The solubility of $NO^{\cdot}$ in water is 2 mM at 1 atmospheric pressure which increases 6- to 8-fold in nonpolar solvents or in lipid membrane (Shaw and Vosper, 1977). Therefore, formation of N_2O_3 would be favored in hydrophobic environment owing to the higher concentrations of $NO^{\cdot}$ and O_2.

RSNOs are characterized by absorbance band in UV-VIS region at 343 nm and 540 nm with the extinction coefficient of 980 $M^{-1}cm^{-1}$ and 18 $M^{-1}cm^{-1}$ respectively (Williams 1996). Therefore the formation or consumption of RSNOs can be monitored spectrophotometrically by monitoring change in absorbance at 343 nm.

2.1.2.2 Decomposition of RSNOs

i) By Metal ions: The stability of RSNOs in the solution greatly depends upon the presence of contaminating metal ions such as copper, mercury and iron (Vanin *et al.*, 1997; Williams, 1996). Copper mediated degradation of RSNOs is a two step process (Askew *et al.*, 1995). In the first step cupric ion (Cu^{2+}) reacts with thiolate to generate cuprous ion (Cu^{+}). In the second step, Cu^{+} reacts with RSNO to generate NO, Cu^{2+} and RSSR (Vanin *et al.*, 1997) (Scheme 2.1):

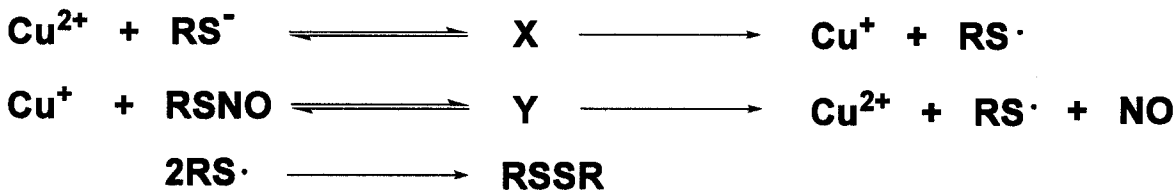

Scheme 2.1 Denitrosation of RSNO by copper (Askew *et al.*, 1995; Vanin *et al.*, 1997)

ii) By transnitrosation: In this process the NO· group is transferred directly from donor S-nitrosothiols to acceptor thiol without net release of NO·. However, the release of NO· can be facilitated by this process if the transfer is from more stable RSNO such as GSNO and generate less stable RSNO such as CysNO.

iii) By photochemical decomposition: It has been reported that UV radiation of RSNO causes hemolytic fission of S-NO bond to generate alkyl thiyl free radical (RS·) and NO· (Sexton *et al.*, 1994). The RS· then reacts with another molecule of RSNO to generate

disulfide (RSSR) and NO·. Similar products are shown to be formed upon thermal decomposition of RSNOs (Scheme 2.2).

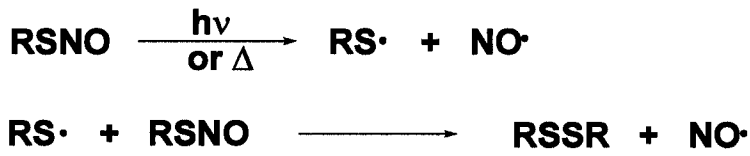

Scheme 2.2 Photolysis and thermal decomposition of RSNO.

iv) By enzymatic decomposition: It has been demonstrated in many *in vitro* studies that RSNO degradation can be mediated by many enzyme systems such as γ glutamyl transpeptidases (γGT) (Lipton *et al.*, 2001), xanthine / xanthine oxidase (Trujillo *et al.*, 1998), thioredoxin/thioredoxin reductase (Nikitovic and Holmgren, 1996), Cu/Zn superoxide dismutase (SOD) (Johnson *et al.*, 2001; Jourd'heuil *et al.*, 1999) and glutathione dependent formaldehyde dehydrogenase (GDFDH) (Jensen *et al.*, 1998; Liu *et al.*, 2001). Liu *et al.*, (2001) have shown that GDFDH deficient *E.coli*, yeast and mice have increased levels of cytosolic S-NO proteins as compared to wild types, suggesting its role in RSNO degradation. Similarly, consumption of GSNO by SOD has been reported in various studies where it is suggested to play neuroprotective role in central nervous system (Johnson *et al.*, 2001; Jourd'heuil *et al.*, 1999). γGT catalyzes the breakdown of GSNO to form glutamate and S-nitrosocysteinyl glycine (CGSNO). CGSNO is less stable than GSNO and therefore release of NO· is facilitated by γGT activity. Moreover, CGSNO diffuse across the cell membrane more readily than GSNO.

Although PDI is primarily known for isomerization of disulfide bonds, an additional novel activity of PDI is its ability to denitrosate RSNO. On the cell surface, the RSNO denitrosation activity of PDI has been shown to play a role in the transfer of *S*-nitrosothiol-bound NO into cytosol (Bell *et al.*, 2006; Ramachandran *et al.*, 2001; Zai *et al.*, 1999).

The present study was initiated because the RSNO denitrosation activity of PDI has not been well characterized. Here this was accomplished by directly monitoring the PDI-dependent loss in the S–NO bond at 343 nm and by using a fluorogenic NO_x trapping probe. We have also shown that PDI stores the NO$^{\cdot}$ released from RSNOs, probably in the form of N_2O_3 and can transfer it to intra- and intermolecular thiols. These significant findings could implicate PDI in both efflux and influx of RSNO-bound NO$^{\cdot}$.

2.2 Materials and Equipment

2.2.1 Materials

Acetone; Sigma-Aldrich Canada Ltd., Oakville, Ontario

4-(9-Acridinecarbonyl)-amino)-2,2,6,6-tetramethylpiperidine-1-oxyl (Ac-Tempo); Sigma-Aldrich Canada Ltd., Oakville, Ontario

Ammonium persulfate; Sigma-Aldrich Canada Ltd., Oakville, Ontario

Ammonium sulfate; Sigma-Aldrich Canada Ltd., Oakville, Ontario

Biorad Protein Assay (Bradford Reagent); Bio-Rad Laboratories USA, Hercules, California

Dimethyl formamide (DMF); Sigma-Aldrich Canada Ltd., Oakville, Ontario

2,3-diaminonaphthalene (DAN); Sigma-Aldrich Canada Ltd., Oakville, Ontario

4,4-difluoro-5,7-dimethyl-4-bora-3a,4a-diaza-*s*-indacene-3-propionic acid (BODIPY FL), Invitrogen Canada Inc., Burlington, Ontario

Copper sulfate; Sigma-Aldrich Canada Ltd., Oakville, Ontario

Eosin isothiocyanate; Sigma-Aldrich Canada Ltd., Oakville, Ontario

Ethylene diamine tetraacetic acid; Sigma-Aldrich Canada Ltd., Oakville, Ontario

Fluoroscein isothiocyanate; Sigma-Aldrich Canada Ltd., Oakville, Ontario

Homocysteine; Sigma-Aldrich Canada Ltd., Oakville, Ontario

Monoclonal anti-PDI antibody RL90; Abcam USA, Cambridge, MA

Oxidized glutathione; Sigma-Aldrich Canada Ltd., Oakville, Ontario

Phenylarsine oxide; Sigma-Aldrich Canada Ltd., Oakville, Ontario

Potassium phosphate; Sigma-Aldrich Canada Ltd., Oakville, Ontario

Reduced glutathione; Sigma-Aldrich Canada Ltd., Oakville, Ontario

Rhodamine 1,2,3; Invitrogen Canada Inc., Burlington, Ontario

Sephadex G-25; Sigma-Aldrich Canada Ltd., Oakville, Ontario

Sodium Chloride; Sigma-Aldrich Canada Ltd., Oakville, Ontario

Sodium phosphate monobasic; Sigma-Aldrich Canada Ltd., Oakville, Ontario

2.2.2 Equipment

Agilent 8453 UV-VIS Spectrophotometer;
Agilent Technologies Canada Inc, Mississauga, Ontario

BioRad Fraction Collector Model 2110;
Bio-Rad Laboratories (Canada) Ltd., Mississauga, Ontario

Hemocytometer;
Reichert Co, Buffalo, NY

Jouan CR3i Centrifuge;
Jouan Inc., Winchester, Virginia

Labconco FreeZone 4.5 Liter Benchtop Freeze Dry Systems;
Laconoco Corporation, Kansas City, Missouri

Mettler AJ100 Balance;
Mettler Toledo Canada, Mississauga, Ontrio

Microtiter 96-well Solid Plate;
Thermo Electron Corp. Canada, Burlington, Ontario

Northen Eclipse 6.0 Imaging Software;
Empix Imaging Inc., Mississauga, Ontario

NUAIRE Biological Safety Cabinet Class II Type A/B3;
Thermo Electron Corp. Canada, Burlington, Ontario

Orion Model 420A pH Meter;
Thermo Electron Corp. Canada, Burlington, Ontario

Stir Plate 360 Series;
VWR International, Mississauga, Ontario

Varian Eclipse Fluorescence Spectrophotometer;
Varian Canada, Mississauga, Ontario

Zeiss Axiovert 200inverted Fluorescence Microscope;
Empix Imaging Inc., Mississauga, Ontario

2.3 Methods

2.3.1 Purification of Protein Disulfide Isomerase

E. *coli* strain BL21 (DE3) and expression vector pET-28a were used for expression of recombinant human PDI. Cloning and expression of PDI gene was performed by Dana Seslija as described earlier (Seslija, 2005). The plasmid encodes a fusion protein containing the entire human PDI sequence with an N-terminal His_6 tag (Pihlajaniemi *et al.*., 1987). Purification of recombinant PDI from the soluble fraction of cell lysate was done using Ni-CAM™ HC Resin (Sigma), a high capacity nickel affinity matrix. PDI bound to the resin was eluted using 250 mM imidazole in 50 mM Tris-HCl, pH 8.0, and was collected in 2.0-mL fractions. The fractions containing PDI were pooled and dialyzed against 0.1 M potassium phosphate buffer, pH 7. Protein quantification was performed using the Bradford assay (Bradford, 1976). The purity of protein was ascertained by gel electrophoresis and Western blot.

2.3.2 PDI Assay Buffer

PDI assay buffer contained 0.1 M potassium phosphate buffer, pH 7.0, and 2 mM EDTA. This buffer was used throughout the study unless otherwise specified.

2.3.3 Synthesis of *S*-Nitrosoglutathione

Prior to synthesis of *S*-nitrosoglutathione, [free thiol] in the GSH was determined with DTNB (Jiang *et al.*., 1999). A stoichiometric amount of acidified $NaNO_2$ was reacted with GSH for 30 min at 4 °C. Upon completion of reaction, the pH of the solution was

then adjusted to 7.4. Lastly, GSNO was recrystallized by the slow addition of ice-cold acetone and was resuspended in the appropriate buffer.

2.3.4 Direct Monitoring of PDI Denitrosation Activity with UV-visible Spectroscopy

The denitrosation activity of PDI was determined by monitoring the changes in absorption of GSNO (343 nm) as a function of time with different reducing agents. The reaction was performed in PDI assay buffer containing 100 μM GSNO and 3 μM PDI with varying concentrations of GSH (25 μM to 10 mM) to determine the ideal GSH concentration for optimizing GSNO denitrosation. The activity was also monitored with a fixed concentration of GSH (1.2 mM) and varying concentrations of GSNO (10–500 μM) to estimate its K_M. All measurements were performed using a Bio-tek Instruments $EL_{X\ 808ru}$ Ultra microplate reader and Agilent 8453 UV-visible spectrophotometer at 25 °C.

2.3.5 Monitoring PDI denitrosation activity by fluorescent spectroscopy

2,3 diamino naphthalene (DAN) (10 mM) was prepared in dimethyl formamide and used as a stock solution for all the studies. DAN (100 μM) was incubated with varying [GSNO] (0.5 μM to 8 μM) for 15 min in the presence of $HgCl_2$ (100 μM) in PBS buffer (0.1 mM, pH 7.4). The final pH was increased to 11 by adding 10 μL of NaOH (10 mM) and the reading was taken flurometrically between 390 nm and 500 nm with excitation at 375 nm.

For measuring catalytic denitrosation, GSNO (20 μM) was incubated without or with PDI (1 μM) in PBS buffer (0.1 mM, pH 7.4) supplemented with GSH (100 μM) for 15 min

followed by the addition of 10 μL NaOH (10 mM, final pH 11). Net naphthatrizole (NAT) formation was monitored fluorometrically with excitation at 375 nm and emission between 390 and 500 nm. All the fluorescence studies were performed at 25 °C using a Varian Eclipse fluorometer. Study of PDI denitrosation kinetics was done using 1 μM PDI dissolved in PBS buffer (0.1 mM, pH 7.4) containing 100 μM DAN in the presence of 500 μM GSH and varying concentrations of GSNO (10–200 μM) in a fluorescence cuvette (total volume 2.5 mL).

2.3.6 Preparation of Oxyhemoglobin and Methemoglobin

Oxyhemoglobin was prepared by reduction of human hemoglobin with dithionite in 100 mM potassium phosphate, pH 7.4, followed by chromatographic separation on Sephadex G-25 column (10 mm x 100 mm) using the same buffer. Methemoglobin was prepared by oxidizing human hemoglobin with 5% excess of potassium ferricyanide in 100 mM potassium phosphate, pH 7.0, followed by chromatographic separation of unreacted species using Sephadex G-25 column equilibrated with the same buffer. Oxyhemoglobin and methemoglobin were prepared fresh prior to each experiment.

2.3.7 Hemoglobin Assay

The final product of GSNO cleavage by PDI was examined using the hemoglobin assay (Arnelle and Stamler, 1995). Oxyhemoglobin assay is used to detect NO·, which serves as an oxidizing agent thereby converting oxyhemoglobin to methemoglobin (Bazylinski and Hollocher, 1985; Stone and Marletta, 1994).The reaction is accompanied by a decrease in

absorbance at 542 and 580 nm and an increase at 630 nm, indicative of methemoglobin formation. The reaction mixture contained 30 μM oxyhemoglobin, 1.2 mM GSH, 100 μM GSNO (blank), and 2 μM PDI (sample), in 100 mM potassium phosphate buffer, pH 7.4, containing 1 mM EDTA. NO^- generation was monitored by methemoglobin reduction to oxyhemoglobin and subsequent increase in 542 and 580 nm accompanied by a decrease in 630 nm. Assay solution contained 30 μM methemoglobin, 1.2 mM GSH, 100 μM GSNO (blank), and 2 μM PDI (sample), in 100 mM potassium phosphate buffer, pH 7.0, including 1 mM EDTA. All spectra were recorded from 500 to 700 nm at specified time intervals. The extinction coefficient for oxyhemoglobin at pH 7.0 is 13,900 $M^{-1}cm^{-1}$ and 14,400 $M^{-1}cm^{-1}$ at 542 and 580 nm, respectively, whereas the GSNO extinction coefficient at 545 nm is 15 $M^{-1}cm^{-1}$ (Hart, 1985) and is therefore considered insignificant. All measurements were performed using Agilent 8453 UV-visible spectrophotometer in a 1-cm path length quartz cuvette.

2.3.8 Detection of PDI Radicals with Ac-Tempo

According to previous reports, Ac-Tempo, a paramagnetic nonfluorescent conjugate of nitroxide and acridine, interacts with glutathionyl radicals resulting in increased fluorescence of the acridine moiety of Ac-Tempo (Borisenko el al., 2004). Ac-Tempo concentration was determined by measuring absorbance at 359 nm (ε = 10.4 mM^{-1} cm^{-1}) (Borisenko el al., 2004) using an Agilent 8453 UV-visible spectrophotometer. Fluorescence measurements were recorded on a Varian Cary Eclipse fluorescence spectrometer, with the excitation and emission wavelengths of 360 and 440 nm, respectively. PDI radical formation was detected by mixing stoichiometric amounts of

PDI and GSNO (2 μM) with Ac-Tempo (10 μM) followed by a time-based measurement of radical generation. The possibility of Ac-Tempo reacting with GS· coming from GSNO was eliminated by separate experiments that used DTT and GSH as reducing agents (data not shown). Also, additional evidence that PDI is responsible for GSNO denitrosation that results in PDI radical formation was conducted with the use of BSA (2 μM) instead of PDI. The standard plot of free radical formation was constructed by photolysis (355 nm) using an Applied Photophysics Laser Flash photolysis spectrometer; varying concentrations of GSNO (1–20 μM) were photolyzed for 40 s in the presence of Ac-Tempo, and the fluorescence was observed at 440 nm (ex. 360 nm). The standard plot was generated and used for thiyl/dithiyl radical quantification whenever required.

2.3.9 Generation of a Standard Curve with DAN

Varying concentrations of GSNO (200 nM to 25 μM) were incubated with DAN (200 μM) and $HgCl_2$ (100 μM) for 10 min in PBS (0.1 mM, pH 7.4) at room temperature. The fluorescence readings were taken at 415 nm (ex. 375 nm). The quantification of released NO_x, when required, was estimated using this standard curve.

2.3.10 Preparation of red-PDI and S-Nitrosated PDI (PDI-SNO)

PDI was treated with 10-fold molar excess of DTT for 30 min at room temperature and dialyzed overnight in 20 mM phosphate buffer, pH 6.3, at 4 °C. The concentration of free thiols was measured with DTNB (Jiang *et al.*., 1999). PDI-NO was prepared by incubating reduced PDI with 5-fold molar excess of DEA-NO for 30 min at room

temperature. The NO· concentration was determined by NO· meter using $HgCl_2$ (Borisenko *et al.*., 2004) as described below.

2.3.11 Nitric Oxide Determinations Using NO Meter

The NO-meter experiments in this chapter were performed by my colleague, Inga Sliskovic.Soluble nitric oxide was measured using the ISO-NO Mark II equipped with WPI MKII NO electrode. A standard curve for NO· was generated by adding GSNO (10–100 μM) to 0.1 M phosphate buffer, pH 7.0, containing 100 μM $HgCl_2$.

PDI-NO (1.0 μM) was placed in the vial containing 0.1 mM phosphate buffer, pH 7.4, and the electrode was blanked using this mixture. At 20 s, 100 μM $HgCl_2$ was added, and the NO generation was monitored until NO was no longer detected. In the parallel experiment, 2.0 μM red-PDI was added to PDI-NO to verify whether PDI alone could act upon PDI-NO. In a control experiment, BSA (2.0 μM), used instead of red-PDI, did not result in NO generation.

To demonstrate the involvement of the active-site thiols, NEM-blocked PDI was incubated with DEA-NO for 30 min at room temperature, generating NO-saturated PDI. 3.0 μM of this NO-saturated PDI was placed in the vial containing 0.1 mM phosphate buffer, pH 7.4, and the current was measured for 2 min. At 40 s, 100 μM $HgCl_2$ was added to remove any S–NO present in the sample. Finally, at 130 s, 500 μM GSH was added to potentially scavenge N_2O_3 postulated to be present in hydrophobic domains of PDI. Also, this experiment was preformed in the reverse order by first adding GSH (500 μM) followed by the addition of $HgCl_2$ (100 μM). The control was obtained in a similar

way, using NEM-blocked PDI without exposure to DEA-NO. Actual NO concentration was determined from the standard curve. The control was obtained in a similar manner, using the buffer without PDI.

2.3.12 Quantification of Thiols in PDI

10 μM PDI was incubated with 10 mM DTT for 1 h and then separated through a G-25 sephadex column. 1.2 μM PDI was then incubated with DTNB for 30 min at different time intervals, and absorbance was monitored at 412 nm in 100 mM Tris-HCL buffer, pH 8 (ϵ = 13600 M^{-1} cm^{-1} at 412 nm) (Ellman, 1959).

2.3.13 Monitoring PDI-SNO Formation by UV-visible Spectroscopy

Freshly isolated native PDI (10 μM) was treated with DEA-NO for 30 min and then separated through a G-25 column. The absorption spectrum of PDI-SNO was then monitored between 300 and 450 nm. The NO was removed by adding Hg to the above solution, and the quantification of *S*-nitrosation was done at 340 nm by taking the molar extinction coefficient of 980 M^{-1} cm^{-1} (Williams, 1996).

2.4 Results

2.4.1 The effect of GSH on PDI denitrosation activity

It is well established that free thiols like dithiothreitol or GSH are required to maintain the thiol-disulfide exchange activity of PDI (Grey, 1997; Lyles and Gilbert, 1991; Primm and Gilbert, 2001; Ramachandran *et al.*., 2001; Sideraki and Gilbert, 2000; Zheng and Gilbert, 2001). The same should be true for the PDI mediated RSNO denitrosation activity because denitrosation would also require the regeneration of free thiols. In an attempt to determine the ideal RSNO / RSH ratio for maximal PDI denitrosation activity, the denitrosation of a constant amount of GSNO (100 μM) was monitored as a function of [GSH] in the presence and absence of PDI (Figure 2.6). The largest ratio of enzymatic rate to blank rate of ~6 was obtained with 1.2 mM GSH. This concentration of GSH was subsequently used in the K_M estimations. At higher concentrations of reducing agent, it is expected that the transnitrosation reaction will take over thr net denitrosation reaction and therefore there would be decrease in the activity at higher [GSH] (Figure 2.6). Interestingly, no enzymatic denitrosation was observed when DTT or homocysteine were the reducing agent (Figure 2.7 and Figure 2.8).

2.4.2 Kinetic Characterization of PDI-catalyzed RSNO Denitrosation

The initial rates of denitrosation were monitored spectrophotometrically at 340 nm for the loss of S–NO absorbance with 3 μM human recombinant PDI and 1.2 mM GSH as a function of [GSNO] (10–500 μM). Initial rates versus [GSNO] data were well

accommodated with the Michealis-Menten equation and the apparent K_M estimated for GSNO was 65 ± 5 μM (Figure 2.9).

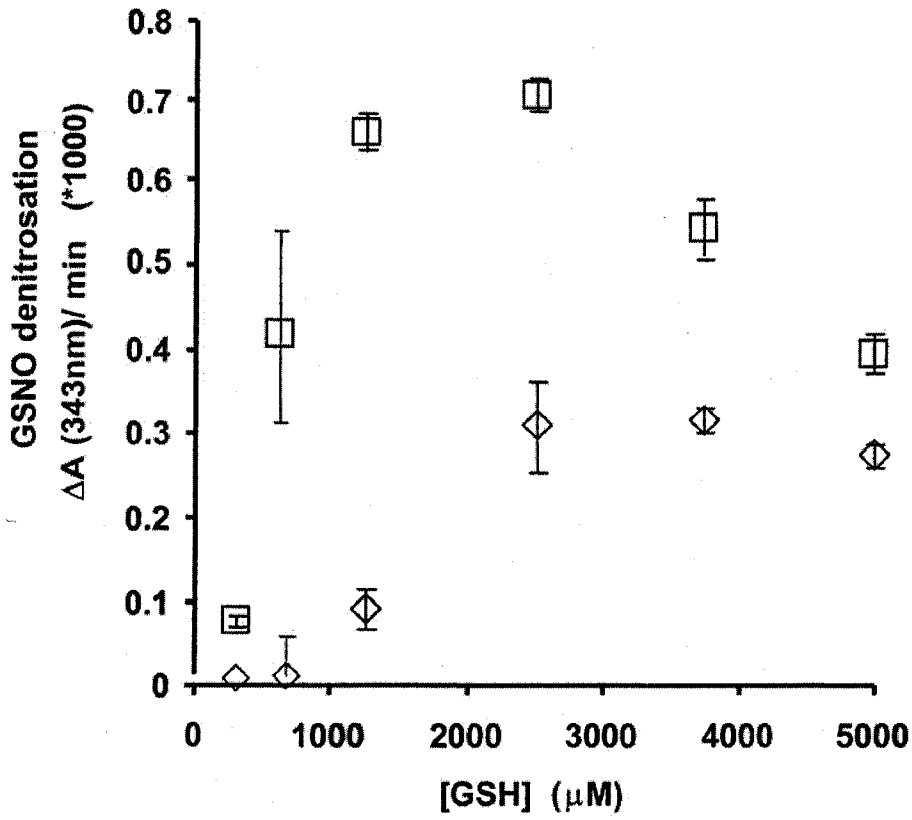

Figure 2.6 Denitrosation of GSNO by PDI in the presence of GSH.

The rate of denitrosation of GSNO (100 μM) as a function of [GSH] in the presence (squares) and absence (diamonds) of PDI (3 μM) was monitored by the loss of the S–NO absorbance at 343 nm. The experiment was performed in PDI assay buffer. The error bars represent S.D. (n = 5).

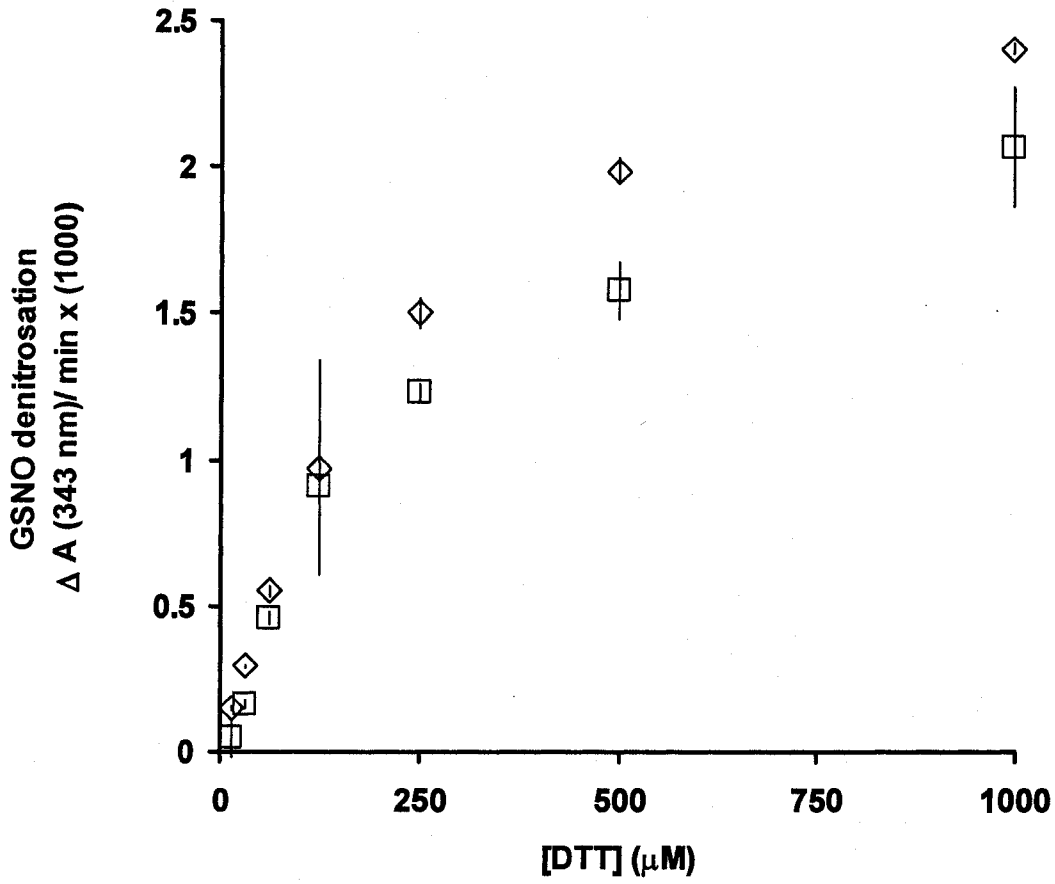

Figure 2.7 Denitrosation of GSNO by PDI in the presence of DTT

The rate of denitrosation of GSNO (100 μM) as a function of [DTT] in the presence (squares) and absence (diamonds) of PDI (3 μM) was monitored by the loss of the S–NO absorbance at 343 nm. The experiment was performed in PDI assay buffer.

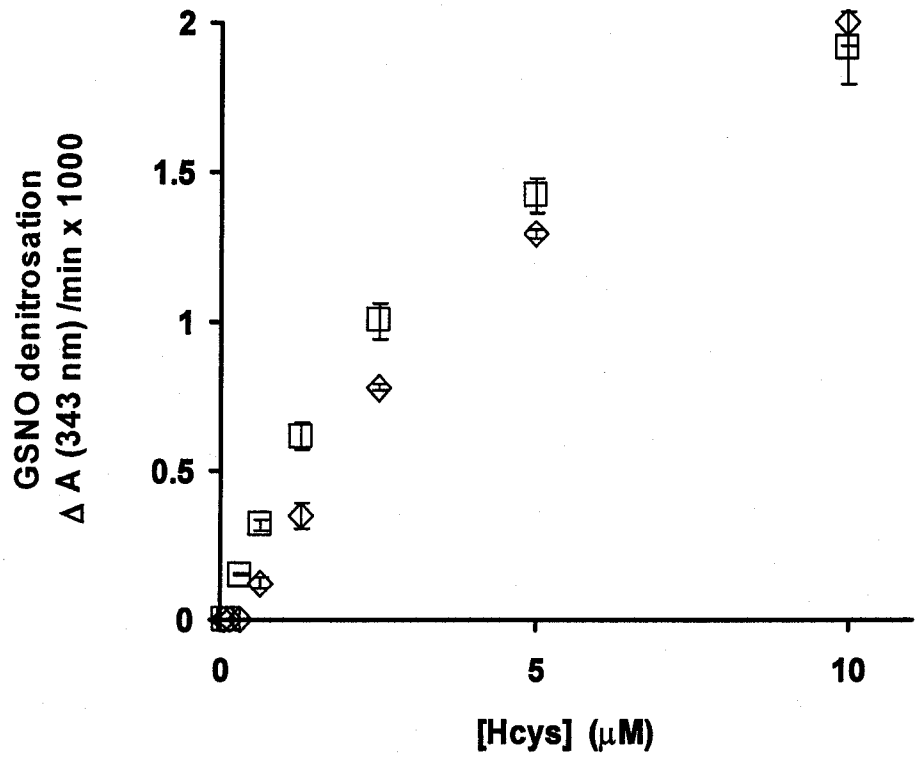

Figure 2.8 Denitrosation of GSNO by PDI in the presence of Hcys

The rate of denitrosation of GSNO (100 μM) as a function of [Hcys] in the presence (squares) and absence (diamonds) of PDI (3 μM) was monitored by the loss of the S–NO absorbance at 343 nm.

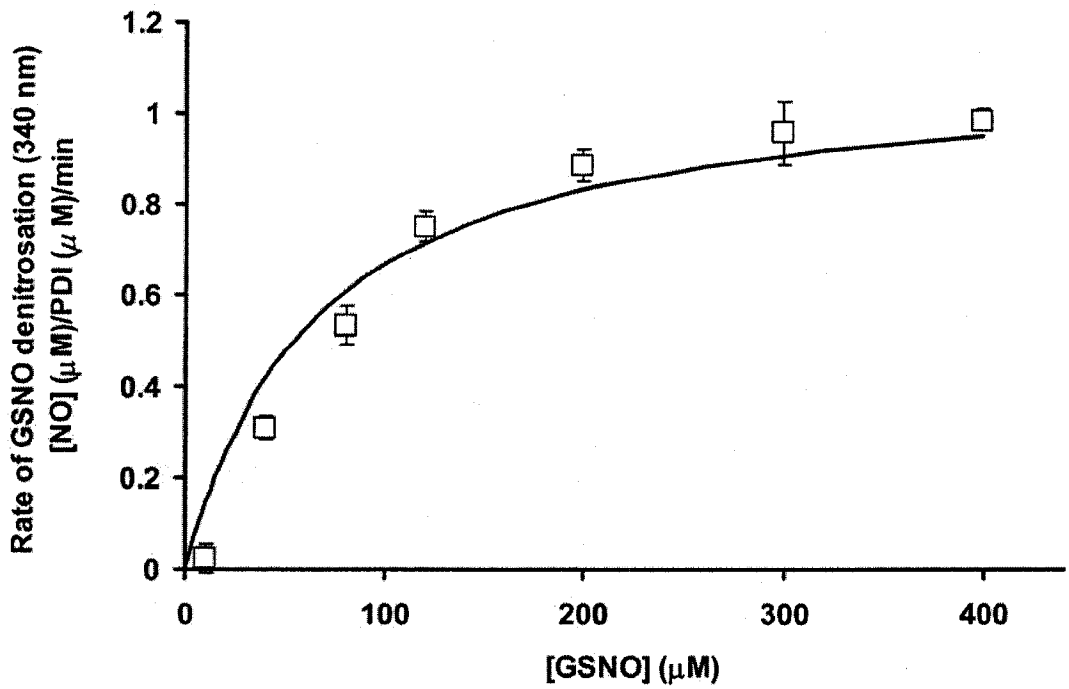

Figure 2.9 PDI denitrosation kinetics and estimation of K_M

Samples containing PDI (3 μM) were mixed with 1.2 mM GSH, and denitrosation was monitored at 343 nm as a function of time. The rates were corrected by subtracting the blank rates (without PDI) and plotted against increasing GSNO concentrations.

2.4.3 Use of DAN to develop fluorescent assay for PDI denitrosation

This is the first time that DAN was used to study PDI denitrosation activity. DAN is relatively non fluorescent compound. However, when incubated with NOx (NO_2^-, NO_3^-, and N_2O_3 (Girard and Potier, 1993; Jourd'heuil *et al.*., 2000), its amino group gets N-nitrosated and forms napthotriazole (NAT) (Figure 2.10) which is a highly fluorescent compound with characteristic peaks at 390, 406, 427, and 450 nm when excited at 375 nm (Figure 2.11). Therefore, the release of nitric oxide from RSNOs by metals such as copper or mercury (Figure 2.10) can be detected and quantified by monitoring the increase in the fluorescence at these wavelengths. As evident from Figure 2.11, the fluorescence increase is proportional to [GSNO] even at lower micromolar range. The fluorescence measurement in these samples were done after increasing the pH to 11 as NAT fluorescence is more sensitive and stable at higher pH (Wink *et al.*, 1999).

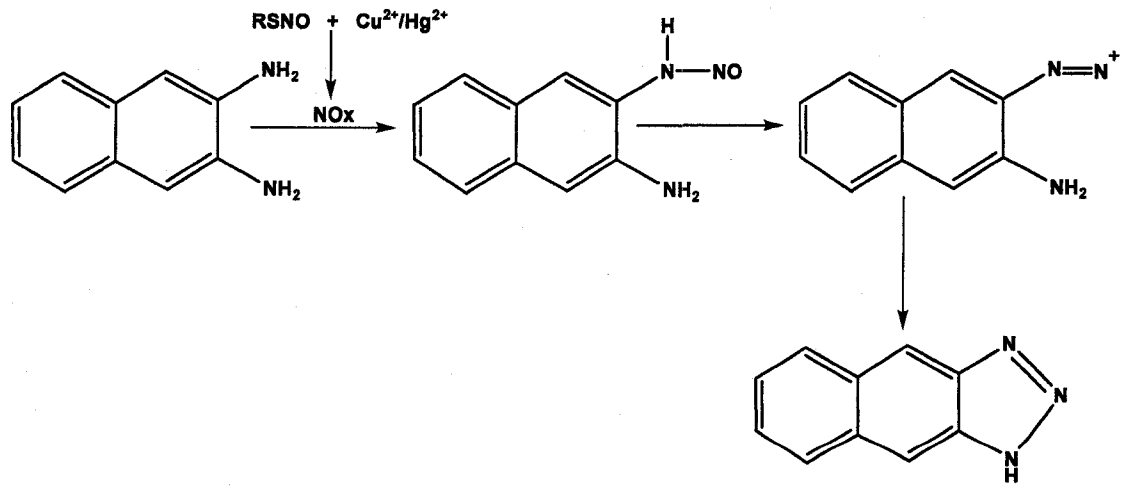

Figure 2.10 Reaction of DAN with NO derivatives.

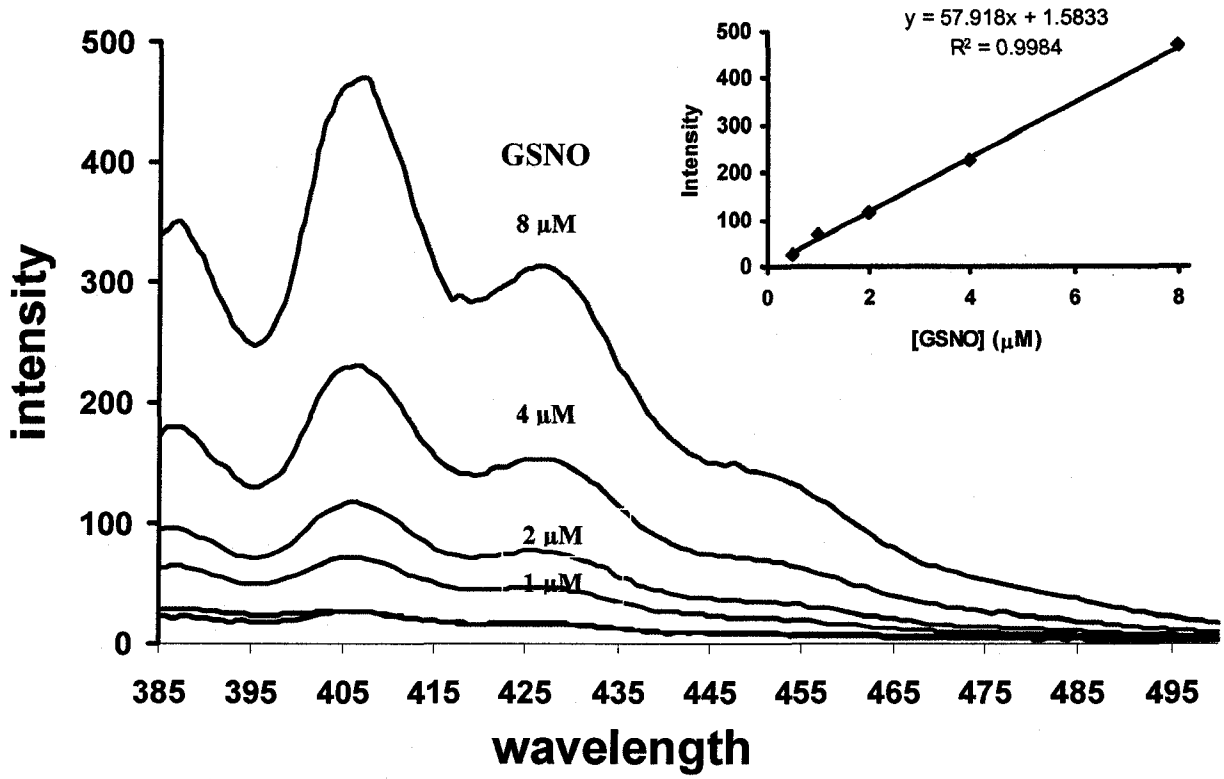

Figure 2.11 Reaction of DAN with GSNO

DAN (100 μM) was incubated with varying [GSNO] (0.5 μM to 8 μM) for 15 min in the presence of $HgCl_2$ (100 μM) in PBS buffer (0.1 mM, pH 7.4). The final pH was increased to 11 by adding NaOH (10 mM) and the fluorescence was measured between between 390 nm and 500 nm (ex. 375 nm).

The denitrosation of GSNO by using DAN was studied in the presence of GSH which acted as a reducing agent for reactivating the oxidized PDI active-site thiols after one denitrosation cycle. As can be seen in Figure 2.12, the increase in fluorescence was ~8-fold higher in the presence of PDI as compared to GSH alone indicating catalytic reduction of S-NO bond by PDI.

DAN was then tested for its ability to continuously report on the PDI denitrosation activity at physiological pH (7.4) (Figure 2.13). In these experiments DAN was mixed with GSNO and GSH and the fluorescence was monitored at 406 nm (ex. 375 nm) with respect to time. Under these conditions fluorescence did not increase. Upon addition of PDI there was a rapid increase in the rate of fluorescence, indicating that DAN could be employed for monitoring the kinetics of PDI-catalyzed RSNO denitrosation. The initial rates of NAT formation were monitored as a function of [GSNO] with a view of estimating the affinity of PDI for GSNO. The initial rate vs [GSNO] data were well accommodated by the Michaelis–Menten equation with a K_M of 65 ± 5 μM for GSNO (Figure 2.14).

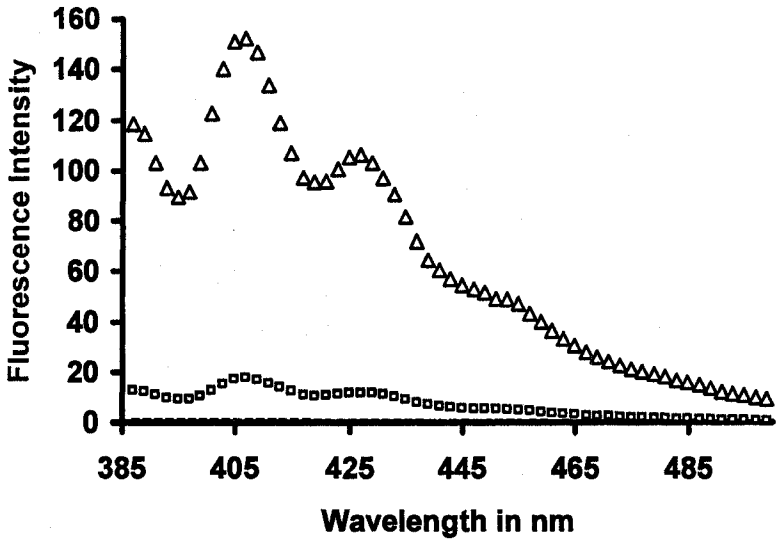

Figure 2.12 Denitrosation with and without PDI

DAN incubated with GSNO and PDI (triangles) for 30 min showed eightfold higher fluorescence than GSNO alone (squares) in PBS buffer. The final pH was increased to 11 by adding NaOH (10 mM) and the fluorescence was measured between between 390 nm and 500 nm (ex. 375 nm).

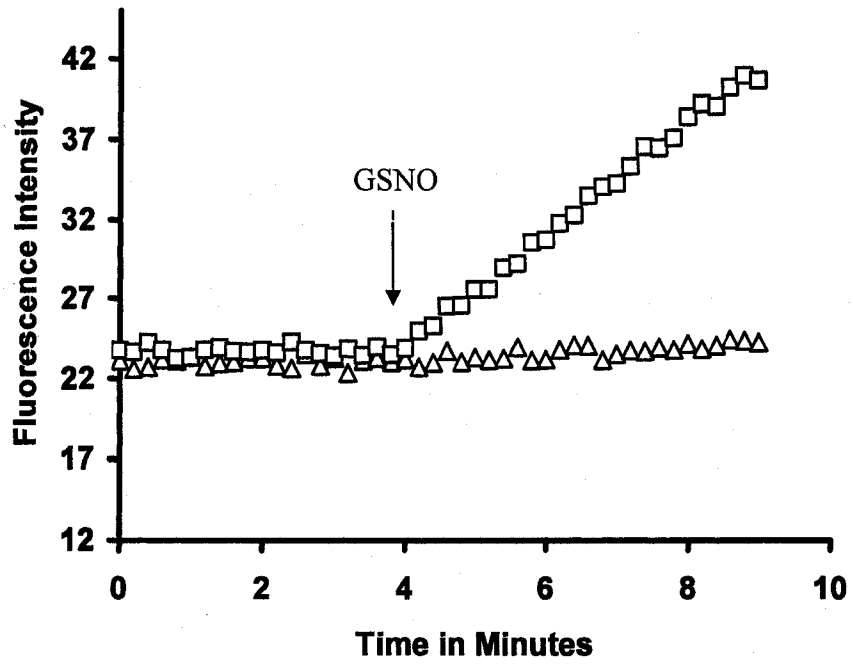

Figure 2.13 Effect of PDI addition on the rate of NAT formation

The initial mixture contained DAN (100 μM) and GSH (500 μM) in PBS (pH 7.4) (triangles). Sample cuvette (squares) contained additional PDI (1 μM). GSNO was added with mixing to sample cuvette and blank cuvette after 4 min and the rate was monitored for another 10 min.

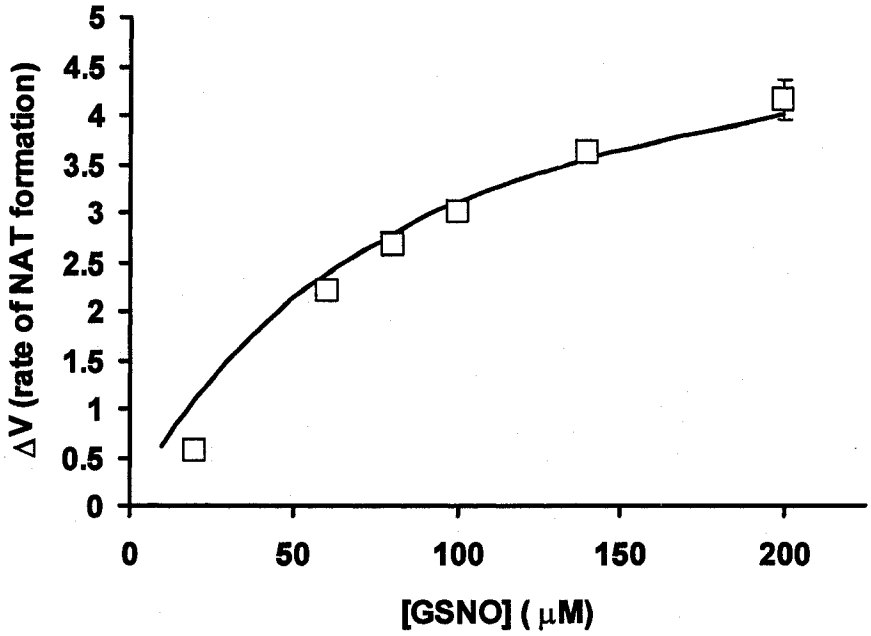

Figure 2.14 Fluorometric study of PDI kinetics

GSH (500 μM) was mixed with variable [GSNO] in 3 mL cuvette containing PDI (1 μM) in PBS (pH 7.4) and denitrosation rate was monitored with emission at 406 nm and excitation at 375 nm. Experimental values (squares) were plotted against best-fit line (dark line). The blank rates were subtracted from the net rate to get normalized PDI denitrosation rate.

The end product of PDI-dependent GSNO denitrosation could be either NO^- or NO·. To this end, hemoglobin assay was performed (Arnelle and Stamler, 1995) for identifying the actual product of PDI denitrosation activity. Oxyhemoglobin assay has been used in past to detect NO·, which serves as an oxidizing agent and converts oxyhemoglobin to methemoglobin (Bazylinski and Hollocher, 1985; Stone and Marletta, 1994). The reaction is accompanied by a decrease in absorbance at 542 and 580 nm and an increase at 630 nm, indicative of methemoglobin formation. Upon incubation of oxyhemoglobin with GSNO, GSH, and PDI, a time-dependent decrease at 542 and 580 nm and an increase at 630 nm indicated methemoglobin formation, suggesting that the major product of reaction was NO· (Figure 2.15). To eliminate the possibility that NO^- was produced, which can under certain circumstances be converted to NO·, we did a methemoglobin assay with PDI and GSNO (data not shown). If NO^- were produced, it would reduce methemoglobin that could be monitored by an increase in absorbance at 540 nm and 580 nm accompanied by a decrease at 630 nm. Because methemoglobin spectrum in the presence of PDI and GSNO was stable for over 20 min, we concluded the amount of NO^- possibly being produced was below the detection limit.

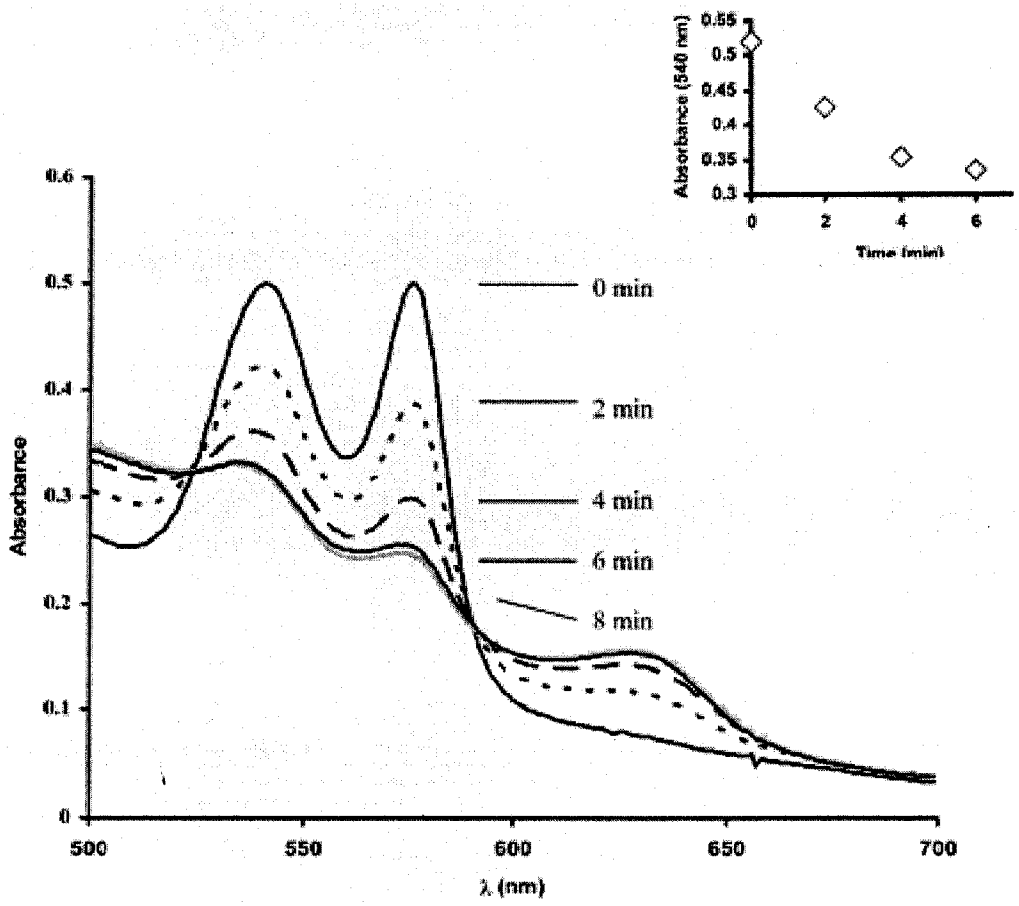

Figure 2.15 Monitoring NO release by hemoglobin assay

Oxyhemoglobin assay contained 30 μM oxyhemoglobin, 1.2 mM GSH, 100 μM GSNO, and 2 μM PDI in 100 mM potassium phosphate, 1.0 mM EDTA, pH 7.4. A decrease at 542 and 580 nm and a resulting increase at 630 nm were an indication of NO· production. The reaction was over in ~6 min. *Inset*, plot of decrease in absorbance at 540 nm as a function of time.

2.4.4 PDI Radical Formation as a Result of GSNO Denitrosation

To obtain additional evidence for the catalytic mechanism of PDI denitrosation activity, a fluorogenic thiyl radical probe, Ac-Tempo, was used. Previous studies have shown that Ac-Tempo, upon interacting with thiyl radicals, produces a fluorescent signal (Borisenko el al, 2004). Here we set out to determine whether PDI would form a thiyl radical as a result of GSNO denitrosation. First, GSNO was added to Ac-Tempo alone. The lack of fluorescent product formation suggested that there is no spontaneous interaction between probe and GSNO. However, when equimolar (2 μM) PDI plus GSNO were added to Ac-Tempo (10 μM), a continuous, time-dependent increase in fluorescence was observed. The rate of thiyl radical formation (Figure 2.16, squares) closely paralleled NO production upon mixing of equimolar (2 μM) PDI and GSNO (Figure 2.16, diamonds). A comparison of the NO and thiyl/dithiyl stoichiometry indicated that 0.8 ± 0.12 mol NO was produced per 3.0 ± 0.43 mol thiyl/dithiyl radical formed.

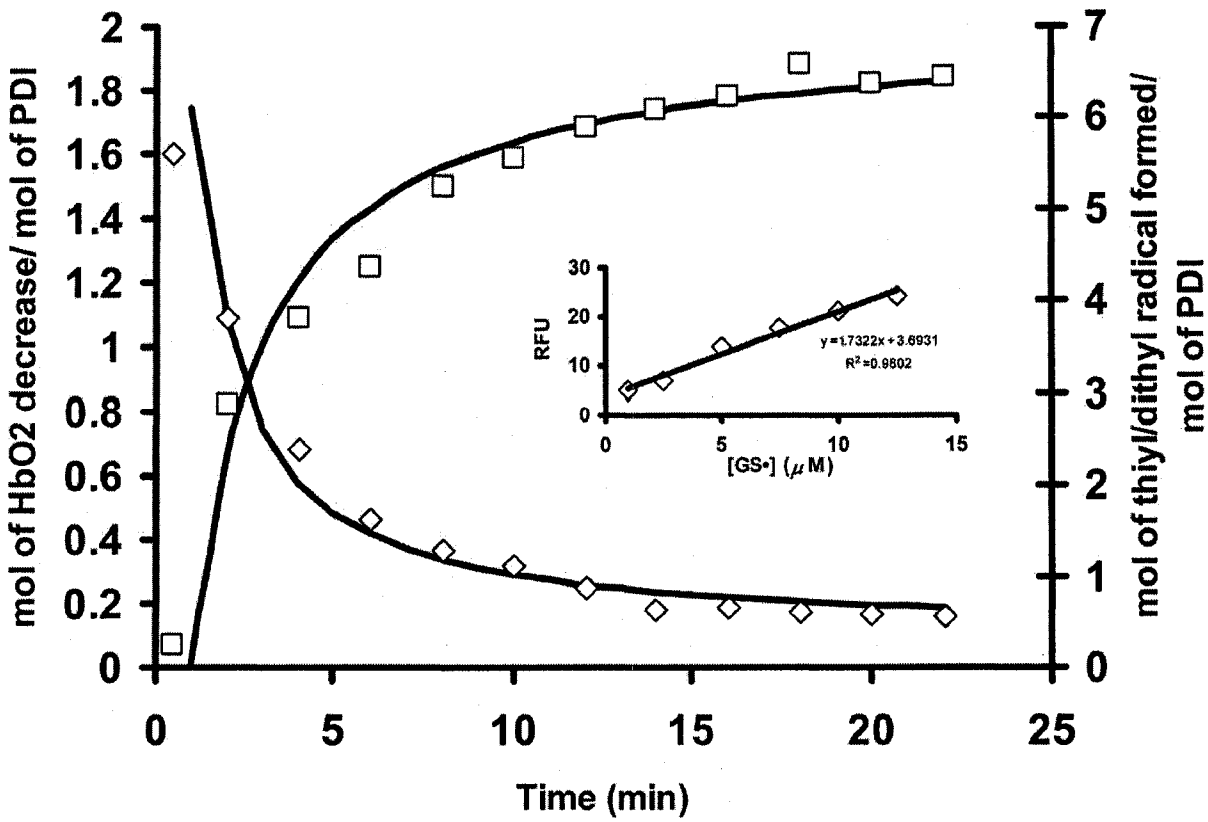

Figure 2.16 Detection of thiyl/dithiyl radical formation by Ac-Tempo and NO production by oxyhemoglobin

Ac-Tempo (10 μM) was mixed with 2 μM PDI (homodimer) and 2 μM GSNO, and the fluorescent signal was measured over time (squares). In parallel experiments, ~40 mM oxyhemoglobin (HbO_2) was mixed with 2 μM PDI and 2 μM GSNO, and the decrease at 542 nm (indicative of NO-induced methemoglobin formation) was monitored over time (diamonds). *Inset*, standard plot of Ac-Tempo fluorescence (in relative fluorescence units (RFU) as a function of [GS·] generated by flash photolysis (355 nm) of varying concentration of GSNO.

2.4.5 PDI Can Release NO from PDI-SNO

Many studies have indicated that NO$^{\bullet}$ and O_2 concentrate in hydrophobic loci of biological milieus and react to produce the highly reactive nitrosating agent N_2O_3 (Goss *et al.*., 1999; Liu *et al.*., 1998; Nedospasov *et al.*., 2000; Rafikova *et al.*., 2000). Nudler and co-workers (2002) have shown that the accumulated N_2O_3 in the hydrophobic pockets of BSA could nitrosate thiols. In the case of PDI, the most likely candidate for *S*-nitrosation would be the active site thiols of PDI itself. If this is the case, the PDI-SNO could be denitrosated by metals such as copper or mercury. For these experiments, a NO electrode was used as a direct method for measuring soluble [NO] (Pfeiffer *et al.*., 1998; Zhang *et al.*., 2000)

The NO electrode was placed in the buffer containing NO-saturated PDI (1.0 μM) (Figure 2.17A and 2.17B) and the current was monitored for 20 s to ensure that there was not a spontaneous generation of NO occurring. At 20 s, $HgCl_2$ (100 μM) was added. This resulted in an instantaneous increase in current that corresponded to [NO] of 4 ± 0.5 μM/1.0 μM PDI (Figure 2.17A). A similar experiment was performed, using red-PDI (2 μM) instead of $HgCl_2$. This also resulted in an increase in current corresponding to 4 ± 0.5 μM NO (Figure 2.17B) suggesting that PDI-SNO can also be denitrosated by another molecule of catalytically active PDI. Therefore, the possible NO$^{\bullet}$ released from PDI-SNO was determined to be ~ 4.5 μM NO/1.0 μM PDI, under our experimental conditions.

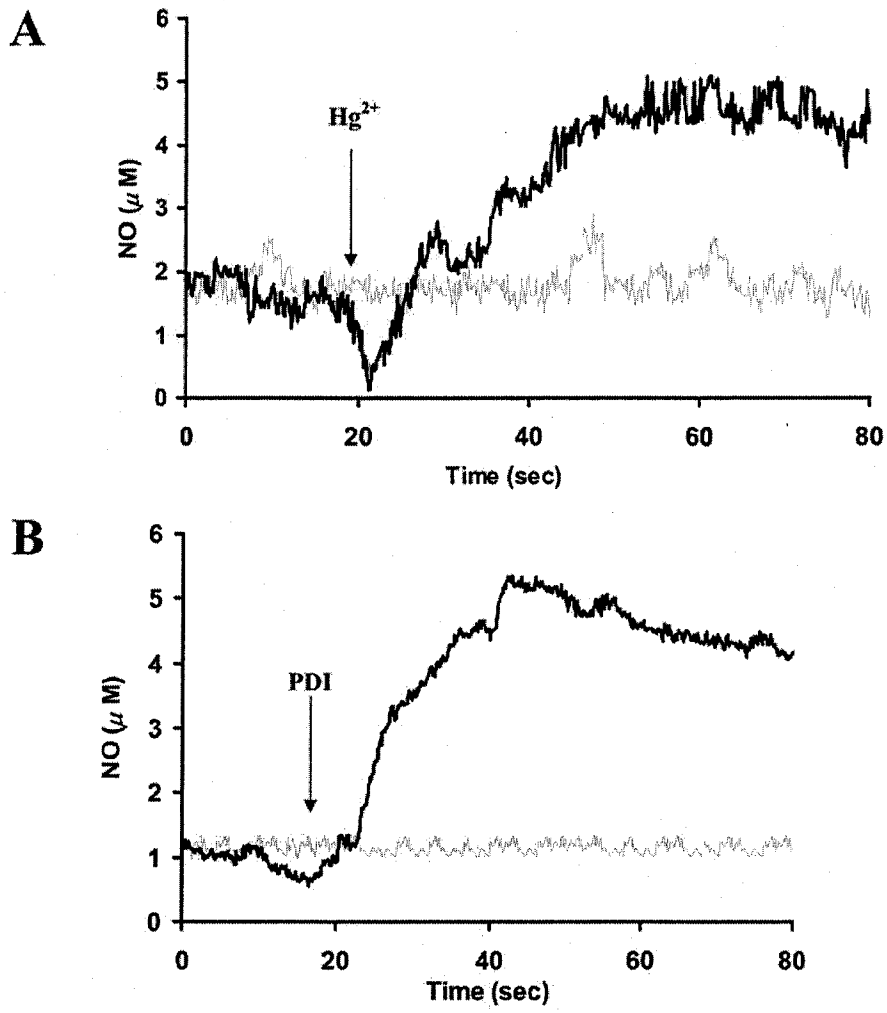

Figure 2.17 Monitoring denitrosation rate using NO meter

A. PDI-SNO (1 μM) was placed in the vial and the NO meter was blanked using this solution. After a stable signal was obtained, at 20 s, 100 μM $HgCl_2$ was added, and the NO generation was monitored until saturation was obtained. The blank that was used contained only buffer instead of PDI-SNO. **B**. PDI-SNO denitrosation by PDI was same as the above except that PDI was added instead of $HgCl_2$.

To investigate the possibility that PDI is able to store NO in the form of N_2O_3 in its hydrophobic pockets (Rafikova *et al.*., 2000), we incubated NEM-blocked PDI with DEA-NO. This method ensured that there is no PDI-SNO formation. Upon addition of 100 μM $HgCl_2$ to NEM-blocked NO-saturated PDI, no change in current was observed. However, when 100 μM GSH was added to the sample, a slower increase of current was observed (Figure 2.18), and the concentration of NO generated was found to be ~10 ± 1 μM NO/1.0 μM PDI. The interpretation of these results is that in NEM blocked PDI, intramolecular S–N=O cannot be formed. Therefore NO generated in the presence of $HgCl_2$ (Figure 2.18) is coming from GSNO that is formed from the reaction between N_2O_3 in NEM-PDI hydrophobic domains with added GSH. Addition of GSH in NEM-blocked PDI not exposed to DEA-NO (data not shown) did not produce any NO, supporting our hypothesis. The same experiment was preformed in reverse order. Upon adding GSH to NEM-blocked PDI previously exposed to DEA-NO, no NO generation was observed (Figure 2.18, thick line). However, upon adding $HgCl_2$, NO release was observed.

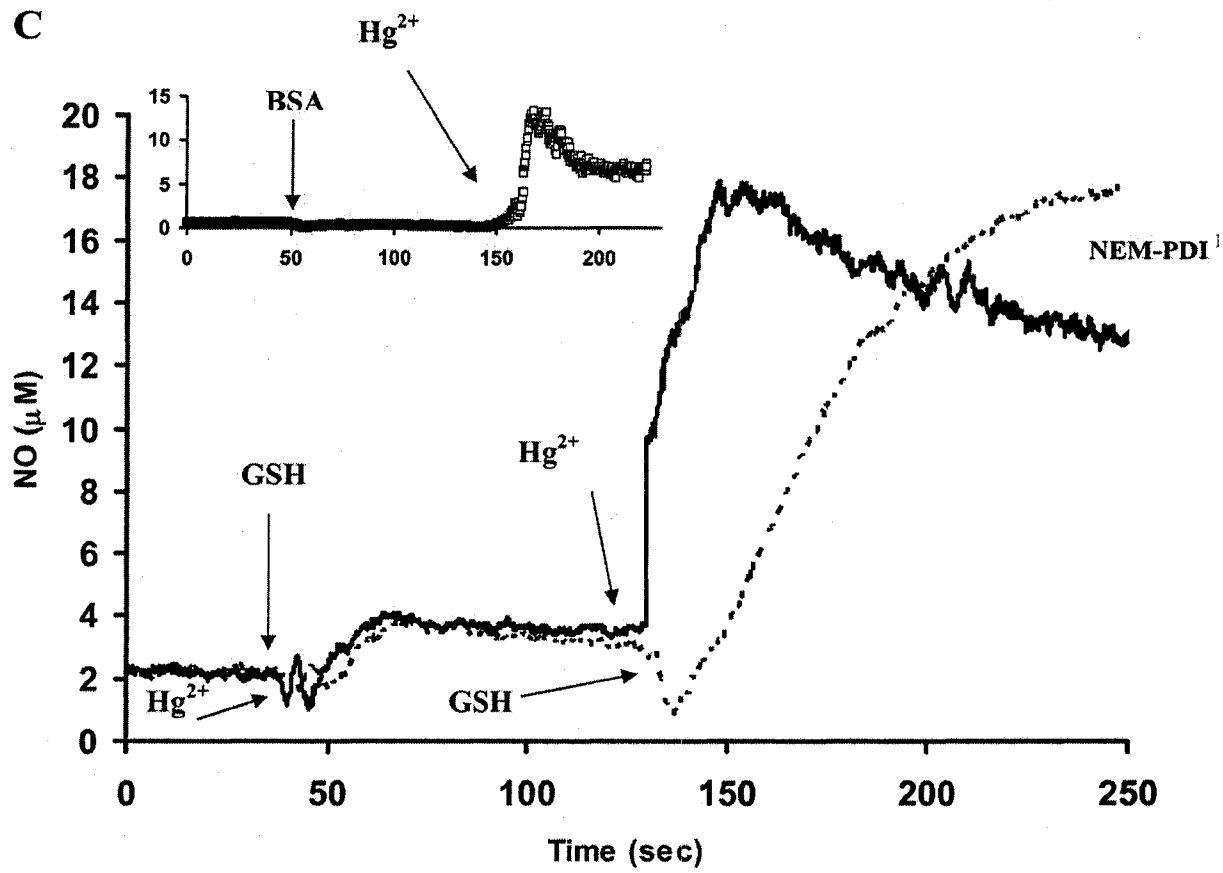

Figure 2.18 PDI ability to store NO

NEM-blocked PDI (3 μM) was saturated with NO, as described under "Experimental Procedures." At 50 s, addition of 100 μM $HgCl_2$ (dashed line) or 500 μM GSH (thick line) did not result in change in current. Addition of 500 μM GSH (thick line) or 100 μM $HgCl_2$ (dashed line) at 120 s resulted in a steady increase in current until saturation was reached. *Inset*, control obtained by addition of BSA instead of PDI to PDI-SNO, followed by the addition of $HgCl_2$.

2.4.6 Monitoring oxidation of red-PDI and PDI-SNO formation

The stability of PDI thiols was tested by first fully reducing it and then monitoring the thiol decay at room temperature by DTNB assay (Figure 2.19A). It was observed that almost ~50% of the thiols were reoxidized in 2.5–3 h. Freshly purified PDI was also found to have 50–60% reduced thiols. When freshly purified PDI was nitrosated by DEA-NO and then separated by G-25 column, it showed a peak at ~340 nm (Figure 2.19B, dark line). The peak disappeared after the addition of 100 μM Hg (Figure 2.19B, dashed line). The corrected spectrum showed 50% PDI nitrosation (Figure 2.19B, *inset*). To compare the activity of native PDI and PDI-SNO, the insulin turbidity method was employed. The assay was performed in the absence of any reducing agent. Whereas native PDI was found to be active (no turnover), no activity was observed with PDI-SNO (Figure 2.20). PDI-SNO, once formed, was fairly stable for more than 2.5 h and could be denitrosated by DTT.

A

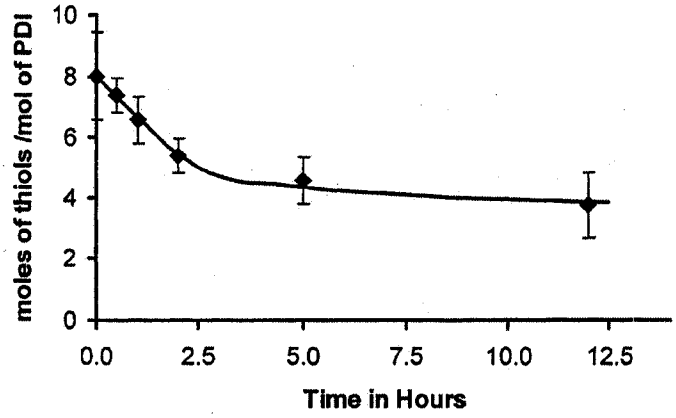

B

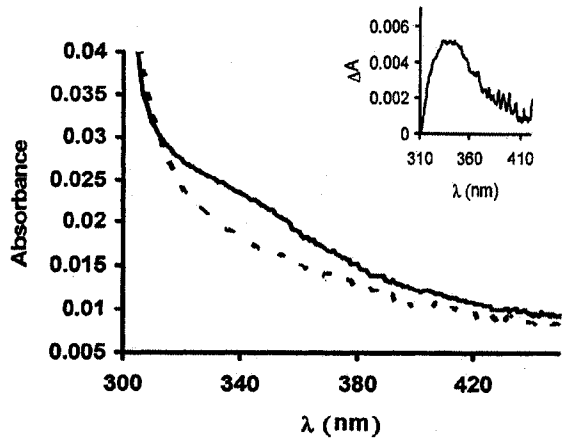

Figure 2.19 Monitoring oxidation of red-PDI and PDI-SNO formation

A. 10 μM PDI was incubated with 10 mM DTT for 1 h and then separated through a G-25 column. 1.2 μM PDI was then incubated with DTNB at different time intervals, and absorbance (A) was monitored at 412 nm in 100 mM Tris-HCL buffer, pH 8. **B.** 10 μM freshly isolated native PDI was treated with DEA-NO for 30 min and then separated through a G-25 column. The absorption spectrum of PDI-SNO was then monitored between 300 and 450 nm before (dark line) and after (dotted line) the addition of 100 μM $HgCl_2$.

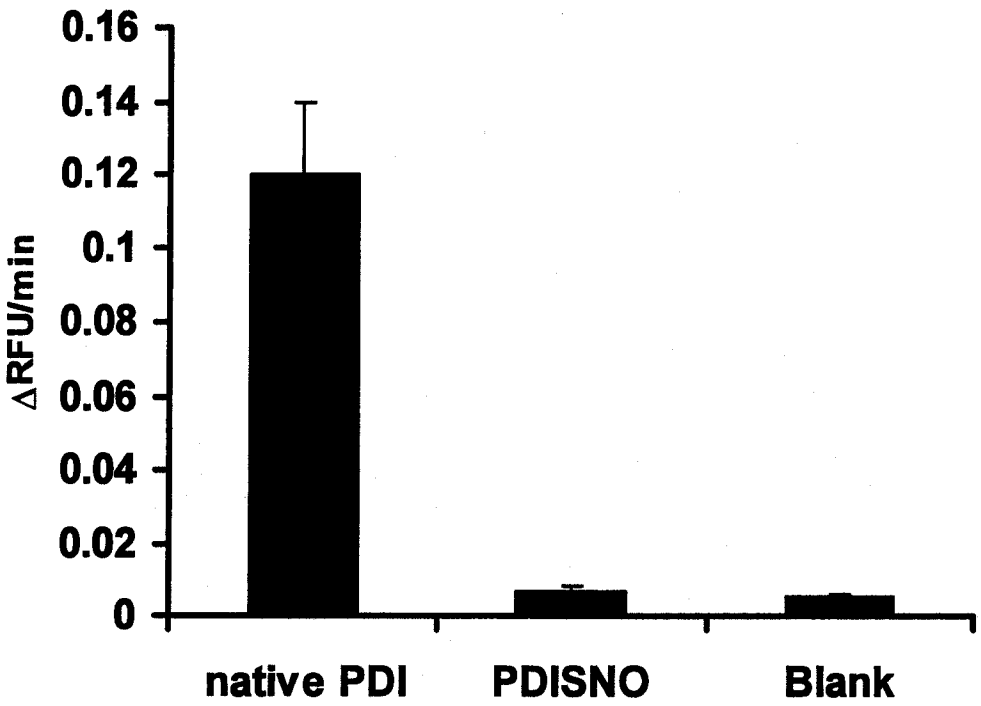

Figure 2.20 Insulin turbidity assay of native-PDI and PDISNO

Insulin (100 μM) was incubated with native-PDI (10 μM) or PDISNO (10 μM) and increase in absorbance was monitored at 630 nm as a function of time.

2.5 Discussion

The *S*-denitrosation activity of PDI, although demonstrated in several studies (Ramachandran *et al.*., 2001; Zai *et al.*., 1999), has not been well characterized. Here we set out to kinetically analyze the GSNO denitrosation activity of human recombinant PDI. It has been well established that PDI requires thiol reductants to perform its thiol-disulfide exchange activity (Essex *et al.*., 1999). Therefore, it is not surprising that the GSNO denitrosation activity probed here was also dependent on thiol-reducing agents. GSH turned out to be the best reducing agent when the loss in the absorbance of S–NO bond at 343 nm was used to monitor the denitrosation. However, no significant denitrosation was observed when DTT or homocysteine was used as the reducing agent. This suggests that PDI denitrosation activity is specific to the presence of glutathione, which is the primary reducing agent in the cell with a concentration of >1 mM (Pastore *et al.*., 2003). The PDI-dependent denitrosation reaction as a function of [GSNO] was probed via two independent methods: directly via the loss of the S–NO bond absorbance at 343 nm or indirectly with DAN. The K_M for GSNO estimated by spectrophotometric method was found to be ~65 ± 5 μM (Figure 2.9), whereas DAN assay gave a value of 65 ± 5 μM (Figure 2.14). Before proceeding further, we set out to determine the final product of GSNO denitrosation by PDI. Hemoglobin assay (Figure 2.15) showed that it is NO· and not NO^- being formed during the GSNO denitrosation by PDI, which is in agreement with a previous study presented on GSNO denitrosation (Nikitovic and Holmgren, 1996). On the basis of results obtained, we propose the PDI denitrosation mechanism as shown in Scheme 2.3.

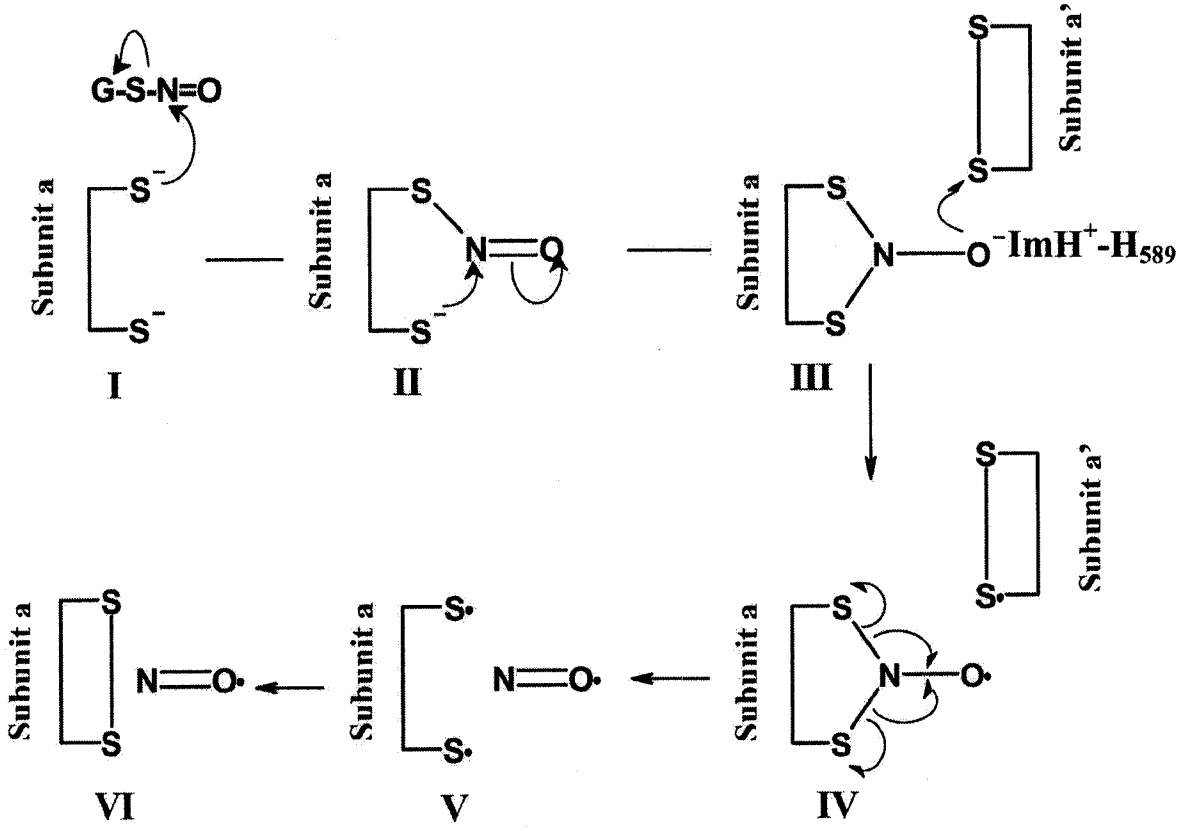

Scheme 2.3 PDI denitrosation mechanism

One of the vicinal thiols of PDI active site subunit ***a***, undergoes transnitrosation reaction (I) in the presence of RSNO, followed by the attack of the second cysteine at N of the S–N=O resulting in formation of a nitroxyl disulfide intermediate (III). The final product after one enzymatic turnover is an oxidized protein active site of subunit ***a*** and NO· (V and VI)

In this mechanism, one of the vicinal thiols (Scheme 4, I) in the CXXC sequence of PDI active site undergoes a transnitrosation reaction with the RSNO substrate (Scheme 4, II). The second active site cysteine then attacks the nitrogen of the S–N=O yielding a nitroxyl disulfide intermediate (Scheme 4, III). The formation of this intermediate could be facilitated via delocalization of electrons in N=O to yield N–O, which could be stabilized via a positively charged side chain in the vicinity of the active site, such as His^{160} in the ***a***-domain or His^{589} in the ***a'***-domain (GenBank™ accession number AK027647 [GenBank]). A one-electron oxidation results in the formation of nitroxyl disulfide radical (Scheme 4, IV), which could rearrange to yield an oxidized (–S–S–) PDI active site plus NO· (Scheme 4, V and VI). The formation of such a nitroxyl disulfide intermediate was proposed by Houk *et al.* (2003) in a recent computational study. In order for this mechanism to work, there is a requirement for an electron acceptor which could be the oxidized active site thiols of PDI itself in the antiparallel arrangement as proposed by Solovyov and Gilbert (2004). In support of this, it has been reported that PDI active site is the most oxidative (–180 mV) (Wilkinson and Gilbert, 2004) of all other members of thioredoxin family. In addition, it has been reported that oxidized active site thiols in DsbD (PDI-like protein) can serve as electron transporter (Collet *et al.*., 2002; Rietsch *et al.*., 1997). The flow of electrons within DsbD have been proposed to occur via succession of disulfide exchange reactions (Rietsch *et al.*., 1997).

Additional evidence for thiyl radical production was obtained with the Ac-Tempo probe. When equimolar GSNO was mixed with PDI, thiyl/dithiyl radicals were generated (Figure 2.16) supporting the proposed mechanism. In contrast, GSNO alone or BSA used

instead of PDI did not result in production of radicals, nor did PDI and GSNO in the presence of GSH, which would reduce the thiyl/dithiyl radicals. In further support of the proposed mechanism, the rate of thiyl/dithiyl radical formation paralleled NO formation. The estimated stoichiometry of the reaction indicates that 3 mol of thiyl/dithiyl radical is formed per 1 mol of NO. This stoichiometry is well accommodated by Scheme 4, suggesting that the two active sites S· plus the S–S· (i.e. 3 mol of thiyl/dithiyl) plus 1 mol of NO· (Scheme 4, IV and V) form in a concerted manner rather than sequentially.

It was observed that almost half-of the reduced PDI was reoxidized within 2.5 h (Figure 2.19A) after which it remained fairly stable. Furthermore, upon exposure of native PDI to DEA-NO, all of the free thiols of PDI could be nitrosated. Interestingly, when $HgCl_2$ or PDI was added to this fully *S*-nitrosated PDI-SNO, ~50% of the S–NO was rapidly released as NO (Figure 2.19B).

We further confirmed that active site thiols of PDI were essential for the release of NO from DEA-NO-exposed PDI. In these experiments, the free thiols of PDI were blocked with NEM. When PDI-NEM was exposed to DEA-NO and production of NO was monitored in the presence of $HgCl_2$, NO release was not observed. However, NO was released when thiols in the form of GSH was introduced to this mixture (Figure 2.17, light line).

In conclusion, the results presented here have very important implications with respect to the role of PDI in the transport of NO equivalents from NO-producing cells to the serum and in the release of NO from RSNOs. Our results show that PDI denitrosates GSNO

when NO levels are low, as is the case on the cell surface. However, in the presence of large amounts of generated NO, as in the intracellular environment of endothelial cells, PDI becomes a NO carrier via an N_2O_3-mediated auto-*S*-nitrosation of its active site thiols. Because PDI is continuously excreted, this might be an important route for the transport of intracellular NO equivalents to the serum. Once excreted, PDI-SNO can be denitrosated by PDI yielding NO on the cell surfaces of endothelial cells and platelets. This could be a cyclic process because it has been speculated that excreted PDI may be recycled back into intracellular environment (Terada *et al.*., 1995).

Chapter 3

Development of Fluorescent Probes for Monitoring Disulfide Reductase Activity of PDI

3.1 Introduction

The catalytic activity of PDI is generally monitored by either the insulin turbidity assay or scrambled RNase assay. The insulin turbidity assay is based on monitoring increase in turbidity at 630 nm caused by the reduction of disulfide bond between the α- and β-chains of insulin (Lundstrom and Holmgren, 1990). Once the disulfide bond in broken, the two chains separate from each other and β-chain precipitate resulting in increase of turbidity. The Scrambled RNase assay is based on PDI-dependent isomerization of scrambled RNase to its catalytically active, native form that, in turn, acts on its substrate RNA (Hilson *et al.*, 1984) or cCMP (Lyles and Gilbert, 1991) resulting in the increase in absorbance monitored at 260 nm or 295 nm respectively. These assays are performed in the presence of reducing agents like DTT or GSH that are required to reduce enzyme active site after one turn over. Although the assays are widely used for estimating enzyme activity, there are several issues associated with them:

(i) There is always significant non-enzymatic blank rate due to the presence of reducing agent that makes the assays unsuitable for detecting activity in the samples with smaller enzyme concentrations

(ii) Long lag phases make it difficult to estimate true initial rates.

(iii) Non-stoichiometric increase in the enzymatic rates with insulin assay with stoichiometric increase in enzyme concentration.

(iv) Assays are insensitive to study single turnover of enzyme in the absence of reducing agent or at lower concentrations of reducing agents and

(v) Assays cannot be performed with precision in crude samples like platelet suspensions containing small amounts of enzyme.

3.1.1 Fluorescence self quenching

When two identical fluorescent molecules are in close proximity, their fluorescence is quenched due to homo resonance energy transfer (Jablonski, 1955) resulting from intermolecular interaction between two molecules. This phenomenon is termed fluorescence self-quenching (FSQ) and is generally characterized by decrease in quantum yield, anisotropy and fluorescence life time. If the distance between these two molecules is increased, their interaction with each other would decrease resulting in the increase in fluorescence. This phenomenon has been exploited in the past to study biochemical processes such as protease activity (Jones *et al.*, 1997), protein dimerization (Wendt *et al.*, 1995) protein folding (Zhuang *et al.*, 2000) and distance measurement (Kalinin *et al.*, 2003). As FSQ requires labeling of protein by same fluorescent molecule, the labeling technique is much simpler than fluorescence resonance energy transfer (FRET), where attachment of two different molecules is required to monitor quenching. However quenching observed in FRET is generally very high as compared to FSQ and therefore it is more commonly used and preferred technique than the latter.

3.1.2 Use of Fluorescence-quenched substrates for monitoring PDI activity

Fluorescence-quenched peptides have been used in past for quantitative analysis of PDI disulfide reduction activity using disulfide linked synthetic peptides containing a fluorescent probe and a quencher (Christiansen *et al.*., 2004; Westphal *et al.*., 1998) (Figure 3.1). However, synthesis for these peptides requires expensive chemicals and

peptide synthesizer that restricts its wider acceptance as a commonly used assay for PDI activity. Moreover, the performance of assay has not been established in crude samples.

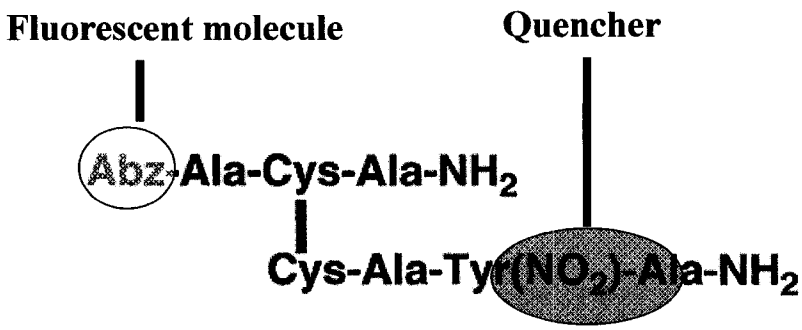

Figure 3.1 Fluorescent peptide as a PDI substrate.

We have previously described that *o*-aminobenzoyl-*S*-nitrosohomocysteine could be used as a probe for thiol detection (Root and Mutus, 2003). The excitation overlap between isatoicanhydride and S-NO (343 nm) quenches the fluorescence of former, which, in turn, could be removed by denitrosating the probe with the help of thiols.

The PDI pseudo-substrates presented here are prepared by single step synthesis using readily available oxidized glutathione. Furthermore the observed self-quenching of the fluorescent probes in the disulfide linked probe negates the need for incorporation of quencher. The assay was optimized to monitor disulfide reduction activity with purified human recombinant PDI and platelet surface PDI in standard fluorometer and was shown to be more kinetic-friendly and more sensitive compared to commonly used PDI assay.

3.2 Materials and Equipment

3.2.1 Materials

Acetone; Sigma-Aldrich Canada Ltd., Oakville, Ontario

Ammonium persulfate; Sigma-Aldrich Canada Ltd., Oakville, Ontario

Ammonium sulfate; Sigma-Aldrich Canada Ltd., Oakville, Ontario

Biorad Protein Assay (Bradford Reagent); Bio-Rad Laboratories USA, Hercules, California

4,4-difluoro-5,7-dimethyl-4-bora-3a,4a-diaza-*s*-indacene-3-propionic acid (BODIPY FL), Invitrogen Canada Inc., Burlington, Ontario

Copper sulfate; Sigma-Aldrich Canada Ltd., Oakville, Ontario

Eosin isothiocyanate; Sigma-Aldrich Canada Ltd., Oakville, Ontario

Ethylene diamide tetraacetic acid; Sigma-Aldrich Canada Ltd., Oakville, Ontario

Fluoroscein isothiocyanate; Sigma-Aldrich Canada Ltd., Oakville, Ontario

Monoclonal anti-PDI antibody RL90; Abcam USA, Cambridge, MA

Oxidized glutathione; Sigma-Aldrich Canada Ltd., Oakville, Ontario

Phenylarsine oxide; Sigma-Aldrich Canada Ltd., Oakville, Ontario

Potassium phosphate; Sigma-Aldrich Canada Ltd., Oakville, Ontario

Reduced glutathione; Sigma-Aldrich Canada Ltd., Oakville, Ontario

Rhodamine 1,2,3; Invitrogen Canada Inc., Burlington, Ontario

Sephadex G-25; Sigma-Aldrich Canada Ltd., Oakville, Ontario

Sodium Chloride; Sigma-Aldrich Canada Ltd., Oakville, Ontario

Sodium phosphate monobasic; Sigma-Aldrich Canada Ltd., Oakville, Ontario

3.2.2 Equipment

Agilent 8453 UV-VIS Spectrophotometer;
Agilent Technologies Canada Inc, Mississauga, Ontario

BioRad Fraction Collector Model 2110;
Bio-Rad Laboratories (Canada) Ltd., Mississauga, Ontario

Hemocytometer;
Reichert Co, Buffalo, NY

Jouan CR3i Centrifuge;
Jouan Inc., Winchester, Virginia

Labconco FreeZone 4.5 Liter Benchtop Freeze Dry Systems;
Laconoco Corporation, Kansas City, Missouri

Mettler AJ100 Balance;
Mettler Toledo Canada, Mississauga, Ontrio

Microtiter 96-well Solid Plate;
Thermo Electron Corp. Canada, Burlington, Ontario

Northen Eclipse 6.0 Imaging Software;
Empix Imaging Inc., Mississauga, Ontario

NUAIRE Biological Safety Cabinet Class II Type A/B3;
Thermo Electron Corp. Canada, Burlington, Ontario

Orion Model 420A pH Meter;
Thermo Electron Corp. Canada, Burlington, Ontario

Stir Plate 360 Series;
VWR International, Mississauga, Ontario

Varian Eclipse Fluorescence Spectrophotometer;
Varian Canada, Mississauga, Ontario

Zeiss Axiovert 200inverted Fluorescence Microscope;
Empix Imaging Inc., Mississauga, Ontario

3.3 Methods

3.3.1 PDI Assay Buffer

PDI assay buffer contained 0.1 M potassium phosphate buffer, pH 7.0 and 2 mM EDTA. This buffer was used throughout the study unless otherwise specified.

3.3.2 Preparation of di (*o*-aminobenzoyl) glutathione disulfide (diabz-GSSG)

Oxidized glutathione is incubated with 10 fold molar excess of isatoic anhydride in phosphate buffer (100 mM sodium phosphate, EDTA 2 mM, pH 8.5) for four h at room temperature. 100 μM of this sample is then passed through Sephadex G-10 column (100 mm x 10 mm) and 500 μL aliquots are collected with the help of fraction collector. The samples were tested for maximum fluorescence on a Varian Cary Eclipse fluorescence spectrometer with excitation at 312 nm and emission at 415 nm after addition of 10 mM DTT. All the fractions that show 95-100% increase in the fluorescence are pooled and stored at -80 °C.

3.3.3 Preparation of Abz-GSH

Abz-GSH was prepared by treating 10 mM diabz-GSSG with 100 mM DTT for 1 h and then separating the mixture with Sephadex G-10 column. First few aliquots showing high absorbance at 312 nm were pooled together and quantified using ϵ = 4600 $M^{-1}cm^{-1}$ (Churchich, 1993). Auto oxidation of Ant-GSH (10 μM) was studied in the presence of Cu^{2+} (10 μM) .

3.3.4 Quantification of [abz-GSH] formation

Increase in fluorescence was monitored as a function of [abz-GSH] (ϵ = 4600 $M^{-1}cm^{-1}$) (Churchich, 1993) and the standard plot was generated with excitation at 312 nm and emission at 415 nm. This standard plot was used wherever quantification of reduction of [Diabz-GSSG] to [Abz-GSH] was required.

3.3.5 Mass Spectrometry

Oxidized glutathione and the purified diabz-GSSG were analyzed by MALDI-TOF mass spectrometry by Dr. Vacratsis, University of Windsor, Canada. All spectra were acquired on a Voyager DE-Pro (Applied Biosystems) equipped with a nitrogen laser operating at 337 nm. The matrix used was cyanocinnamic acid dissolved in 50% acetonitrile containing 1% formic acid. MALDI- post source decay (PSD) was performed to obtain structural information on the parent ions.

3.3.6 PDI Purification

Recombinant human PDI was expressed using E. *coli* strain BL21 (DE3) and expression vector pET-28a as described elsewhere (Seslija, 2005). This plasmid encodes a fusion protein containing the entire human PDI sequence with an N-terminal His_6 tag (Pihlajaniemi *et al.* 1987). Recombinant PDI was purified from the soluble fraction of the cell lysate using Ni-CAM™ HC Resin (Sigma), which is a high-capacity nickel-affinity matrix. Bound PDI was eluted using 250 mM imidazole in 50 mM Tris/HCl (pH 8.0) and collected in 2.0 mL fractions. The fractions containing PDI were pooled and dialyzed

against 0.1 M potassium phosphate buffer (pH 7.0). Protein quantification was performed using the Bradford assay (Bradford, 1976).

3.3.7 PDI-dependent disulfide reduction kinetics

PDI disulfide reduction activity was monitored in PDI assay buffer by adding PDI (2.5 nM to 1 μM) to diabz-GSSG (15 μM) in the presence of 30 μM DTT. The increase in fluorescence was monitored at 415 nm with excitation at 312 nm. The activity was inhibited using phenylarsine oxide (16) (10 μM).

3.3.8 Cu^{2+}-catalyzed oxidation of abz-GSH

Cu^{2+} (10 μM) was added to the cuvette containing abz-GSH (~10 μM) in 100 mM Phosphate buffer and the fluorescence change was monitored with excitation at 312 nm and emission at 415 nm. After 5 min, 50 μM DTT was added followed by the addition of 0.5 μM PDI to the sample and fluorescence change was monitored for another 20 min.

3.3.9 Reduction or oxidation of PDI

25 μM PDI was reduced or oxidized by incubating it with 10 mM DTT or 10 mM GSSG respectively for 3 h at room temperature. The excess of DTT or GSSG was removed by using sephadex G-25 column. The thiol content of reduced or oxidized PDI was calculated using DTNB assay (Ellman, 1959).

3.3.10 Platelet isolation

Suspensions of washed human platelets were obtained by the method of Mustard *et al.*, (1989). Briefly, samples of peripheral venous blood were mixed 6:1 with ACD (acid citrate dextrose; 25 g/L trisodium citrate dihydrate, 15 g/L citric acid monohydrate and 20 g/L dextrose). Whole blood was centrifuged (15 min at 190 g at 37 °C) to yield platelet-rich plasma. Platelets were isolated by centrifugation (15 min at 2000 g at 37 °C) and washed three times in Tyrode-albumin solution (pH 7.4). The first wash contained heparin (2 units/mL) and apyrase (1 unit/mL); the second only apyrase (1 unit/mL); and the third wash contained Tyrode's solution without apyrase and heparin. Platelets were quantified using a hemocytometer.

3.3.11 Monitoring Platelet csPDI activity

Samples of washed human platelets were prepared in Tyrode's solution to final concentration of 10×10^8 mL^{-1}. 15 μM Diabz-GSSG was incubated with 10 μM DTT and Platelets (50 μL) and the activity was monitored continuously as a function of time. In addition, Variable volumes of Platelet (0, 25 μL, 50 μL) were incubated with diabz-GSSG (15 μM), in 1.2 mL PDI assay buffer for 15 min and centrifuged at 5000 rpm for 5 min. The supernatant was added to cuvette and fluorescence was monitored with excitation at 312 nm and emission at 415 nm. In addition, 50 μL of platelet was incubated with anti-PDI antibodies (10 μg/mL) in parallel to inhibit the activity of PDI (Lahav *et al.*, 2002).

3.4 Results

3.4.1 Synthesis of Diabz-GSSG

Isatoic anhydride (IA) is a fluorescent molecule with an anhydride functionality that reacts with terminal amino groups of proteins and peptides (Churchich, 1993). Here, IA was reacted with glutathione disulfide (GSSG, oxidized glutathione) to yield di-(*o*-amino benzoyl) glutathione disulfide (Abz-GSSG) (Figure 3.2)

To confirm successful formation of diabz-GSSG, MS/MS sequencing was performed (Figure 3.2). The molecular ion at m/z = 851.06 representing the diabz-GSSG was detected and subjected to MALDI-post source decay (PSD) sequencing (Figure 3.3, upper). The resulting fragmentation pattern was compared to the fragmentation pattern of a GSSG standard (Figure 3.3, lower) where several diagnostic GSSG fragmentation ions were observed. Additional fragment ions representing the Abz moiety were detected to unambiguously verify successful diabz-GSSG synthesis. In particular, the abundant fragment ion mass at m/z = 603 (Figure 3.3, upper) corresponds to the loss of glutamate-Abz. This indicates that the Abz moiety is located on the glutamate portion of GSSG as intended.

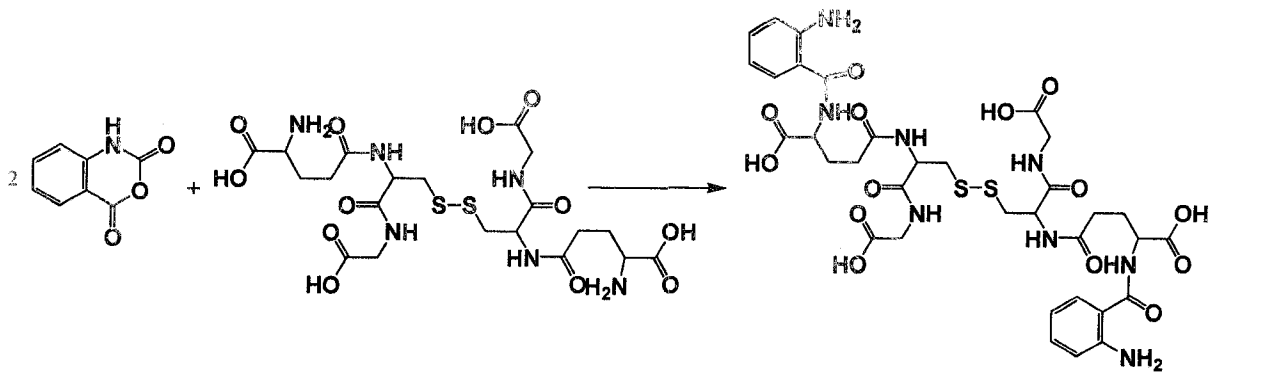

Isatoic anhydride **Oxidized glutathione** **di-(o-aminobenzoyl) glutathione disulfide**

Figure 3.2 Reaction of GSSG with Isatoic anhydride

Two molecules of isatoic anhydride react with two free amino groups of oxidized glutathione at pH 8.5 to give one molecule of diabz-GSSG.

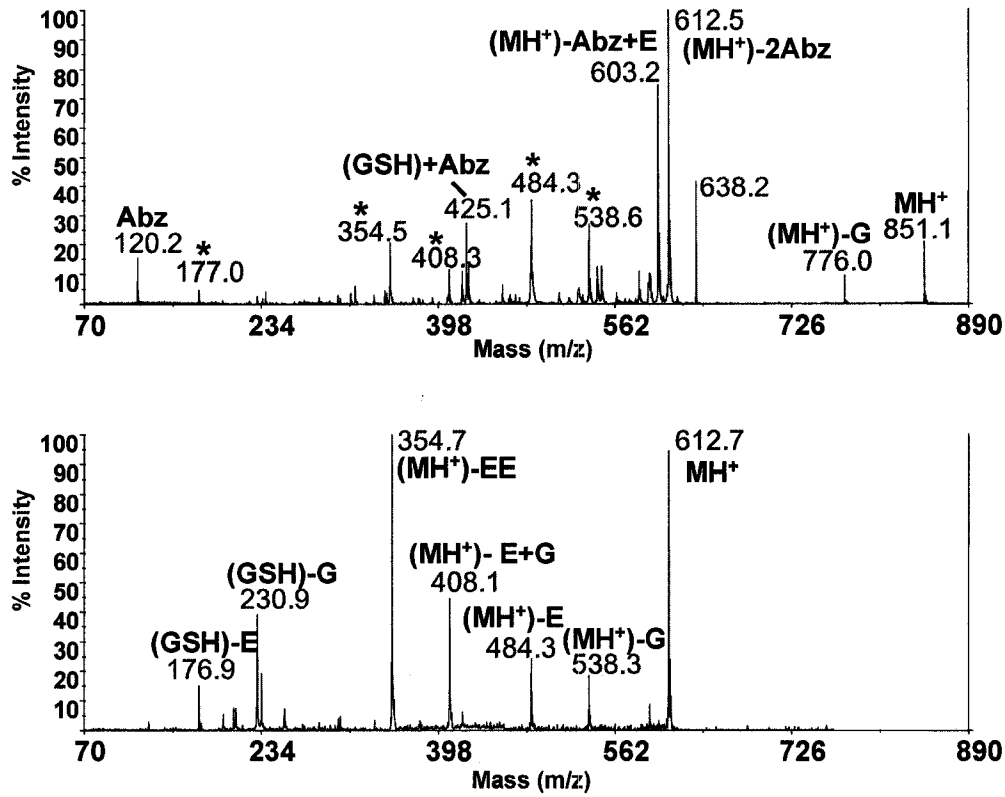

Figure 3.3 MALDI-PSD analysis of diabz-GSSG

Shown is the MS/MS fragmentation pattern of the diabz-GSSG parent ion (MH^+) at m/z 851 (Upper spectrum) and the GSSG standard parent ion (MH^+) at m/z 612.7 (Lower spectrum). Fragment ion masses corresponding to structural features of diabz-GSSG and GSSG are labeled. MH^+ - Abz, E, G, indicates the loss of amino benzoyl, glutamate, or glycine respectively. Common fragment ions observed between the standard and diabz-GSSG are indicated by asterisks (Upper spectrum).

3.4.2 Fluorescence of diabz-GSSG is sensitive to the reduction of the disulfide bond

Diabz-GSSG was fluorescent (ex. λ_{max} =312 nm, emission λ_{max}= 415 nm), however, upon addition of thiol reducing agent (250-fold molar excess) the fluorescence increased by ~100% (Figure 3.4). The fluorescent fraction, assumed to be abz-GSH, was separated from the excess DTT by chromatography on Sephadex G-10. The fluorescence of this compound was not altered by the addition of 300-molar excess of DTT, indicating that the observed enhancement diabz-GSSG fluorescence upon DTT addition is not due to interactions between DTT and the fluorophore. The most likely explanation of the fluorescence enhancement phenomenon is that in diabz-GSSG, the random movement of the *o*-aminobenzoyl residues brings them in close proximity of one another thus resulting in fluorescence self-quenching. Upon disulfide reduction the distance constraints are removed and the fluorescence increases. In order to test this hypothesis, molecular dynamic simulations (Alchemy 2000, Tripos, St.Louis MO) were carried out on diabz-GSSG. The simulations indicated that the aminobenzoyl residues can potentially come as close as 73 nm in a periodic fashion thus supporting the fluorescence self-quenching hypothesis (Figure 3.5).

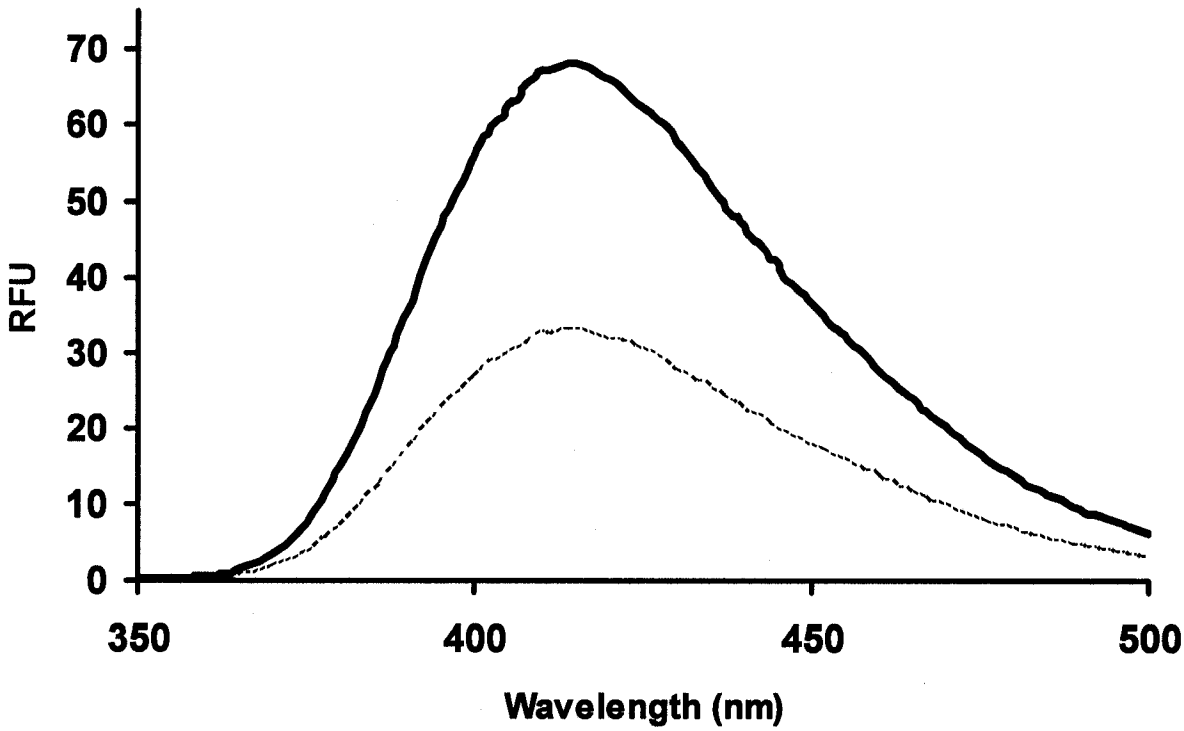

Figure 3.4 Fluorescence spectra of diabz-GSSG and abz-GSH

Diabz-GSSG (15 μM) spectrum in PDI assay buffer was taken with excitation at 312 nm and emission at 415 nm (dotted line). The same sample was then incubated with 10 mM of DTT for 15 min to completely convert diabz-GSSG to abz-GSH and the spectrum was taken under the same condition (dark line).

A.

B.

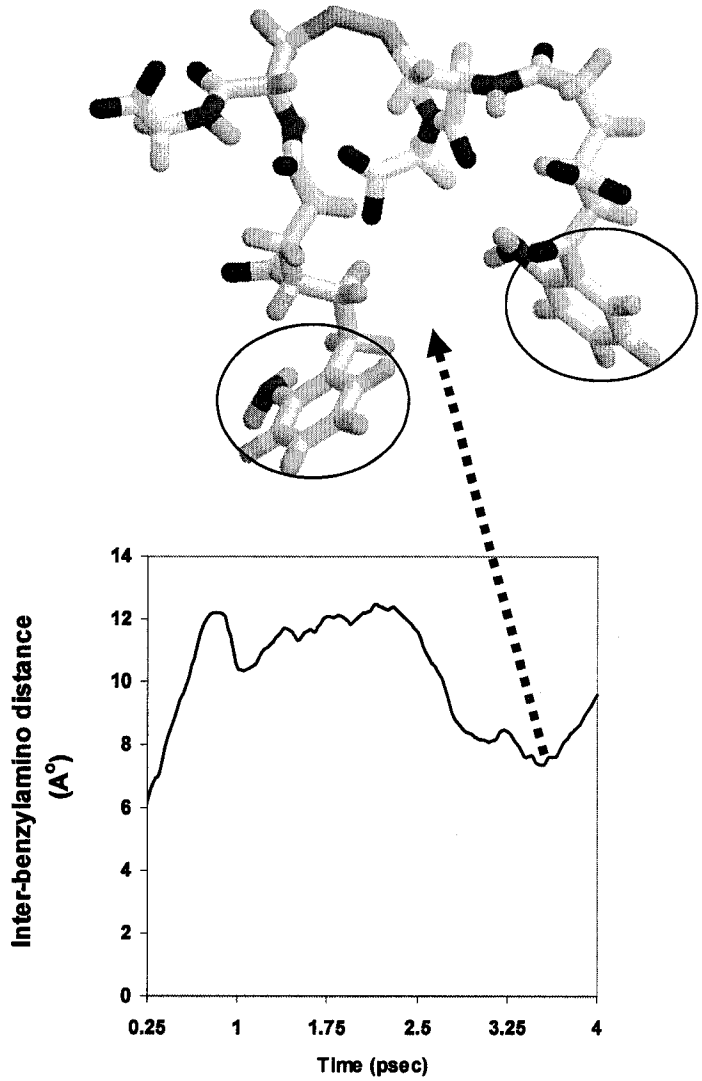

Figure 3.5 Molecular dynamics of diabz-GSSG

A. A plot of inter-benzoylamino distance as a function of time was performed by simulation of diabz-GSSG with Alchemy 2000 (Tripos, St. Louis MO). The initial temperature was 298 K, the simulation was run for 4 ps. **B.** The predicted diabz-GSSG conformation at a minimum inter-benzoylamino distance.

Further evidence for the fluorescence self-quenching being related to disulfide bond formation was obtained from Cu^{2+}-catalyzed oxidation of abz-GSH. When Cu^{2+} was added to the cuvette containing abz-GSH (~15 μM) and DTT (50 μM), a rapid decrease in the fluorescence was observed suggesting that once the fluorophores are linked via a disulfide bridge the fluorescence is quenched (Figure 3.6 continuous line).

When PDI (~0.5 μM) was added to this solution, the fluorescence increased to the same level observed for abz-GSH (Figure 3.6, dotted line). The results obtained with PDI were very significant in that ~10 mM DTT is required to achieve the same thiol reduction rates observed with 0.5 μM PDI (i.e the reduction conditions in Figure 3.4). This suggested that diabz-GSSG could be employed to assay the disulfide reduction activity of PDI as well as other enzymes.

3.4.3 Diabz-GSSG a pseudo-substrate for PDI

Diabz-GSSG (15 μM) is resistant to reduction by DTT (50 μM) (Figure 3.7, diamonds). Upon introduction of PDI (0.5 μM) to this solution, the fluorescence increased in a time dependent manner thus reporting disulfide bond cleavage (Figure 3.7, triangles). The PDI activity was completely inhibited in the presence of phenylarsine oxide, a known vicinal thiol blocker (Bennett *et al.*, 2000) (Figure 3.7, squares). For inhibition experiment, PDI (10 μM) was first incubated with PAO (100 μM) for 30 min and then added to reraction mixture such that final concentration of PAO is 5 μM.

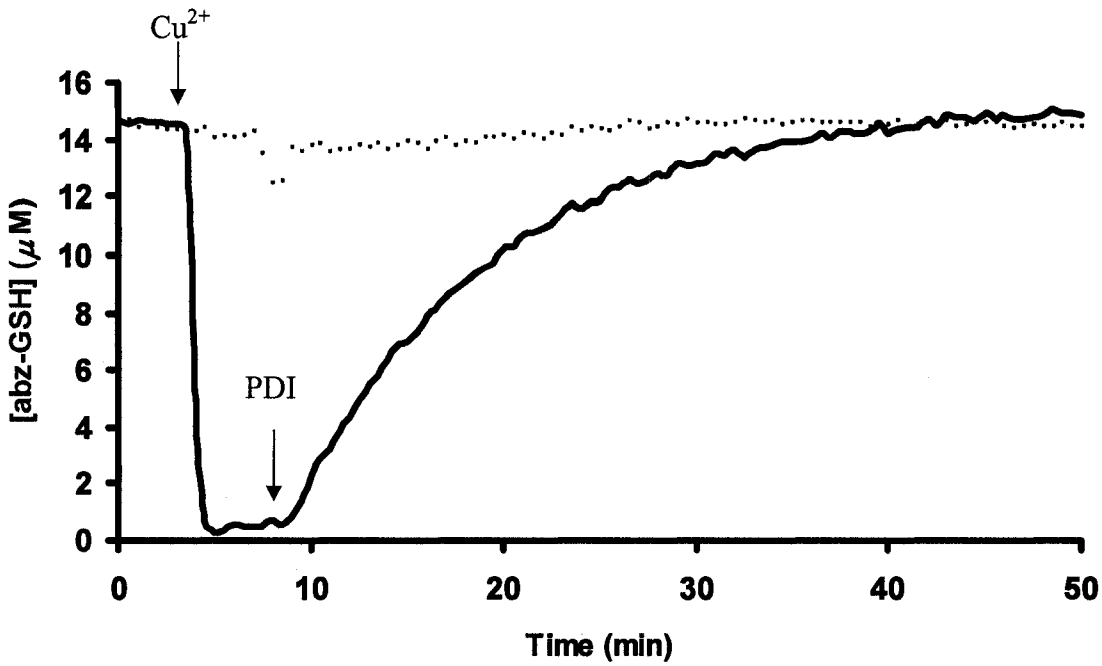

Figure 3.6 Cu^{2+}-catalyzed oxidation of abz-GSH

Cu^{2+} (10 μM) was added to the cuvette containing abz-GSH (~15 μM) in phosphate buffer (100 mM, pH 7) and the fluorescence decrease was monitored at room temperature with excitation at 312 nm and emission at 415 nm (continuous line). When PDI (~0.5 μM) was added to this solution after 5 minutes, the fluorescence increased to the same level observed for abz-GSH (continuous line). No change in the fluorescence was observed in sample containing no Cu^{2+} (dotted line). The total fluorescence produced was converted into [abz-GSH] via a standard curve.

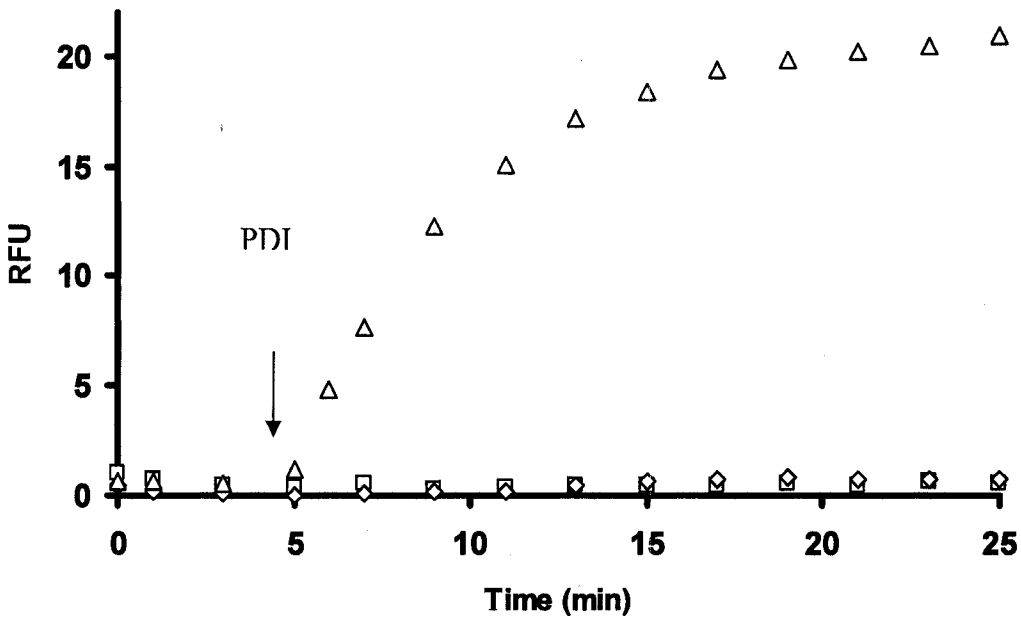

Figure 3.7 Detection of enzymatic activity and its inhibition by PAO

Diabz-GSSG (15 μM) was incubated with DTT (50 μM) in PDI assay buffer, pH 7 at room temperature in the presence of 0.5 μM PDI (triangles), 0.5 μM PDI blocked by PAO (squares) or DTT alone (diamonds).

If the fluorescence increase is enzymatic, the initial rates should vary directly with [PDI]. This was shown to be the case (Figure 3.8) and the assay is sensitive to estimate as low as 2.5 nM PDI activity under present experimental condition. The initial rates of Abz-GSH formation were monitored as a function of [Diabz-GSSG] with a view of estimating the affinity of PDI for Diabz-GSSG. The initial rate vs [Diabz-GSSG] data were well accommodated by the Michaelis–Menten equation with an estimated K_M of 15 ± 1 μM (Figure 3.9).

It is well established that free thiols like dithiothreitol (DTT) or GSH (Holmgren, 1979; Chen *et al.*, 1995) are required to maintain the thiol-disulfide exchange activity of PDI. Here PDI (1 μM, 4 μM in active sites; considering PDI as a homodimer) was incubated with diabz-GSSG (10 μM) and an excess DTT (50 μM). This yielded ~ 20 μM abz-GSH (Figure 3.10, squares) whereas diabz-GSSG (10 μM) incubated with DTT (50 μM) alone yielded no fluorescence increase (Figure 3.10, diamonds). In order to test the ability of diabz-GSSG to detect a single turnover, PDI (1 μM) was again incubated with diabz-GSSG (10 μM) but only in the presence of enough DTT to support one turnover (i.e. 4 μM) (Figure 3.10, triangles). Under these conditions, fluorescence increase equal to ~ 6 μM of abz-GSH was generated. This could be repeated with 2 subsequent additions of DTT (4 μM) to the sample. The total fluorescence increase upon addition of 3 aliquots of DTT corresponded to ~16 μM abz-GSH likely the result of incomplete reduction of enzyme active sites under near stoichiometric DTT: enzyme ratios.

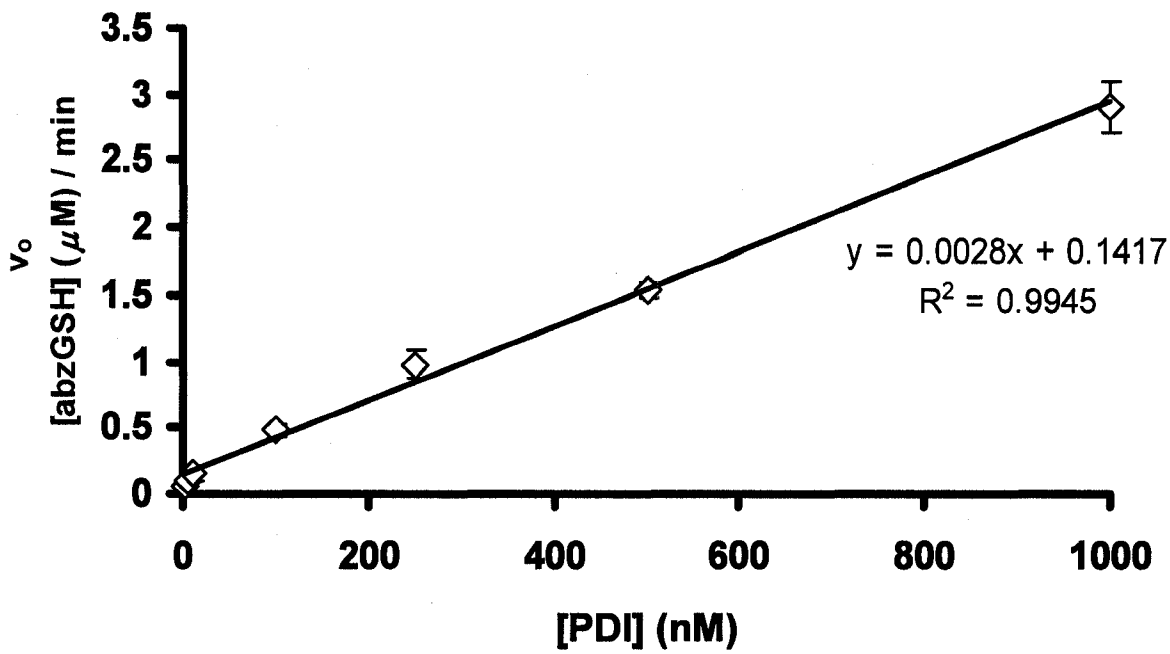

Figure 3.8 Linearity of enzymatic activity

Diabz-GSSG (15 μM) was incubated with DTT (50 μM) in PDI assay buffer, pH 7 at room temperature in the presence of varying concentration of PDI (2.5 nM to 1 μM) and rates of abz-GSH formation were monitored as a function of time. The total fluorescence produced was converted into [Abz-GSH] formed per minute via a standard curve.

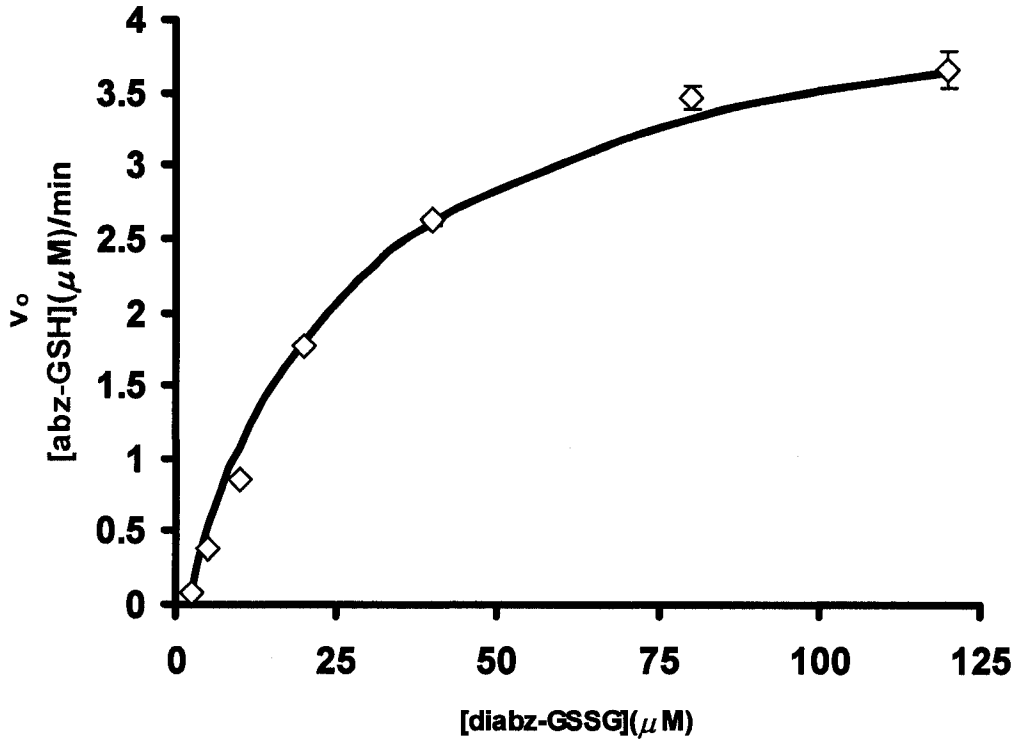

Figure 3.9 Estimation of K_M

PDI (0.5 μM) was incubated with variable concentration of diabz-GSSG (1 μM -150 μM) in PDI assay buffer at room temperature and initial rates of abz-GSH formation were monitored as a function of [Diabz-GSSG]. The total fluorescence produced was converted into [Abz-GSH] via a standard curve.

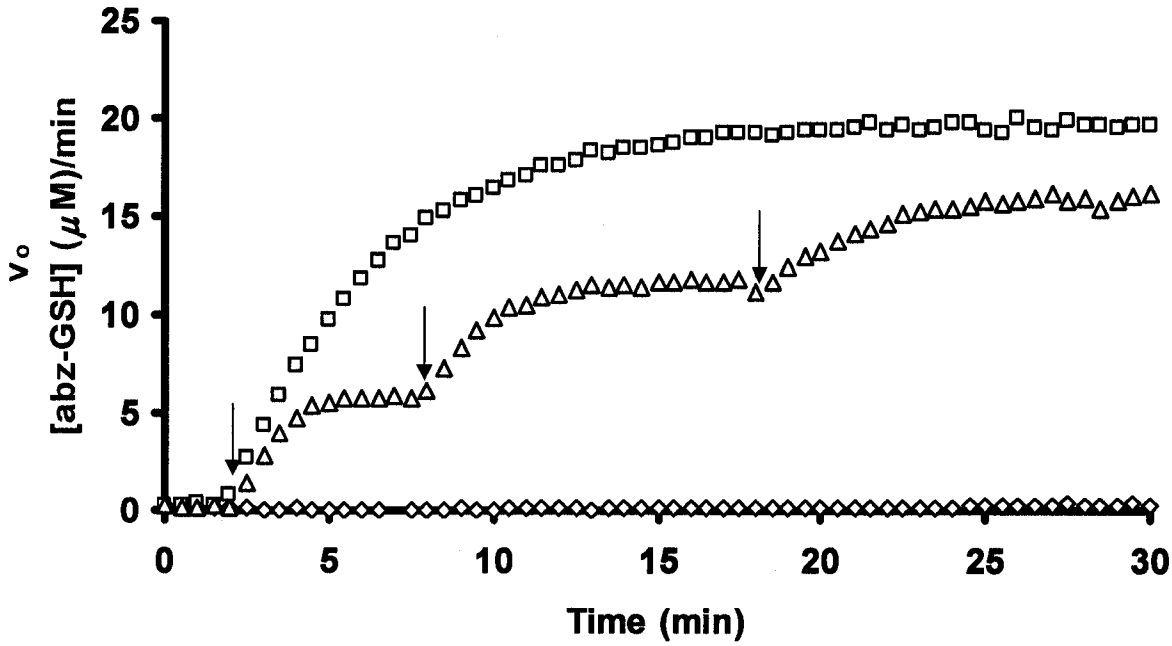

Figure 3.10 Single turnover of enzyme

PDI (1 μM) was incubated with diabz-GSSG (10 μM) and the disulfide reduction activity was monitored after the addition of 50 μM DTT (squares). In a separate sample, PDI (1 μM) was incubated with diabz-GSSG (10 μM) and 3 separate aliquots of 4 μM DTT were added as indicated by arrows (triangles). Fluorescence change of diabz-GSSG (10 μM) was also monitored in the presence of 50 μM of DTT alone (diamonds).

To further illustrate the sensitivity of the assay, 1 μM of completely reduced PDI, oxidized PDI or oxidized PDI with 4 μM DTT was incubated with diabz-GSSG (10 μM) and the rate was kinetically monitored for 30 min (Figure 3.11). While no increase in fluorescence was seen with oxidized PDI, equivalent fluorescence increase was observed with reduced PDI or oxidized PDI with equimolar DTT (Figure 3.11).

3.4.4 Monitoring platelet csPDI activity

Platelets have shown to have PDI on their surface and its activity has been studied in past using scrambled RNase assay (Essex *et al.*, 1995). However this discontinuous assay shows significant non-enzymatic rates. Here, we have developed diabz-GSSG assay for monitoring platelet csPDI activity. 15 μM Diabz-GSSG was incubated with 10 μM DTT and Platelets (50 μL) and the activity was monitored as a function of time. While no significant increase in fluorescence was observed without platelets (Figure 3.12A, squares), a time dependent increase was observed in sample containing platelets (Figure 3.12A, diamonds). This result clearly demonstrates that csPDI activity can be continuously monitored in a single step using this probe. The sensitivity of the assay can further be improved by centrifuging the samples before reading the fluorescence. To this end, platelets (0 μL-50 μL) were incubated with 15 μM Diabz-GSSG in the presence of 10 μM DTT for 15 min at room temperature and then centrifuged at 5000 rpm. The supernatant was tested for fluorescence at 415 nm with excitation at 312 nm. While no increase in fluorescence was observed in diabz-GSSG samples without platelets, stoichiometric increase in fluorescence was observed with corresponding increase in

platelet concentration suggesting reduction of diabz-GSSG by platelet csPDI (Figure 3.12B). The activity was completely inhibited by PDI antibodies.

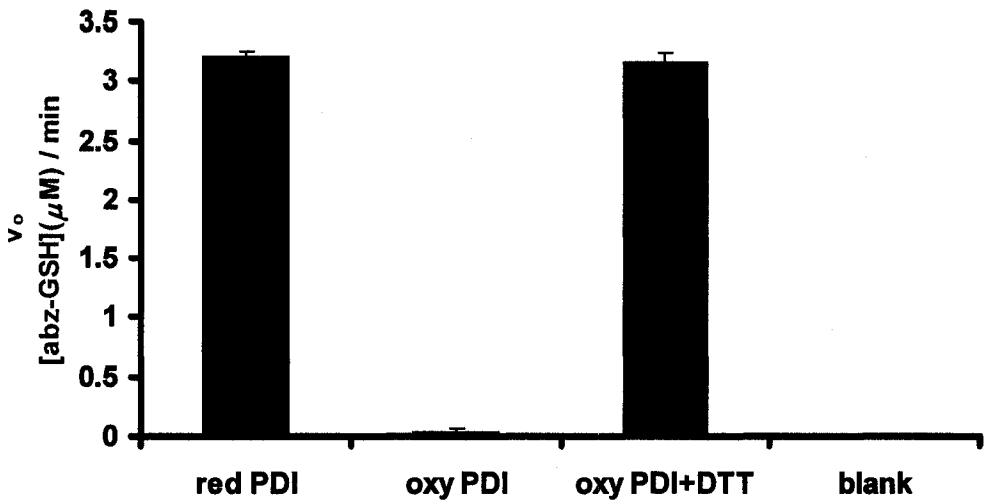

Figure 3.11 Reduction of probe by reduced or oxidized PDI

1 μM of completely reduced PDI, oxidized PDI (1 μM) or oxidized PDI (1 μM) with DTT (4 μM) was incubated with diabz-GSSG (10 μM) and the abz-GSH formation was monitored for 5 min.

A.

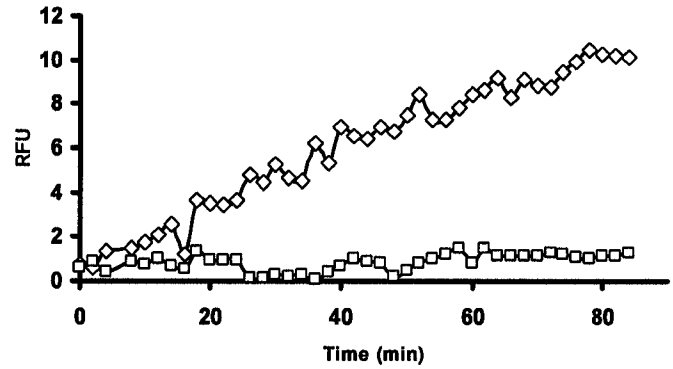

B.

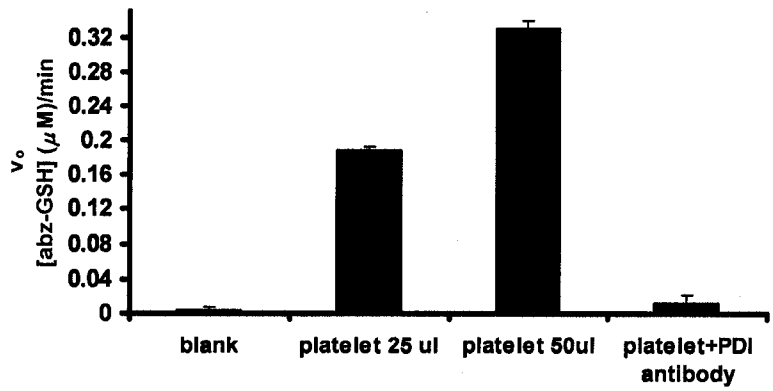

Figure 3.12 Monitoring platelet csPDI activity

A. 15 μM diabz-GSSG was incubated with 10 μM DTT and the activity was monitored in the absence (squares) or presence (diamonds) of 50 μL Platelets **B.** Platelets (0 μL, 25 μL & 50 μL) were incubated with 15 μM diabz-GSSG in the presence of 10 μM DTT for 15 min at room temperature and then centrifuged at 5000 rpm. The supernatant was tested for fluorescence at 415 nm with excitation at 312 nm. csPDI activity of platelets (50 μL) was completely inhibited in the presence of anti-PDI antibodies (10 μg/mL).

3.4.5 FSQ in GSSG with other fluorescent molecules

Although we have shown here that diabz-GSSG is sensitive probe for monitoring disulfide reductase activity, the level of quenching observed is only 50%. In an attempt to increase upon the sensitivity of probe, we modified GSSG by substituting isatoic anhydride with other fluorescent molecules and then observing the level of quenching. As shown in Figure 3.13, fluorescent molecules that showed significant quenching other than isatoic anhydride were fluorescein, rhodamine, texas red and bodipy and gave ~ 5-fold, ~ 4.5 fold, ~ 4-fold, ~25-fold and ~ 70-fold increase upon disulfide reduction respectively. Therefore, the sensitivity of the assay described before can be improved by simply replacing isatoic anhydride with these molecules as all of them show higher level of quenching. Based on percentage of quenching, dieosin glutathione disulfide (Di-E-GSSG) is, by far, the best probe for monitoring PDI activity as it is relatively non-fluorescent and gives very significant increase upon reduction of disulfide bond by either PDI or excess of reducing agent such as DTT (100 mM). Application of (Di-E-GSSG) as a probe for montoring PDI activity is described in detail in Chapter 4.

Although diabz-GSSG is least sensitive fluorescent molecule as compared to other derivatives of GSSG shown in Figure 3.13, it is the most stable derivative and, unlike other derivatives, can be stored at room temperature for 7 days without any appreciable loss in the fluorescence increase.

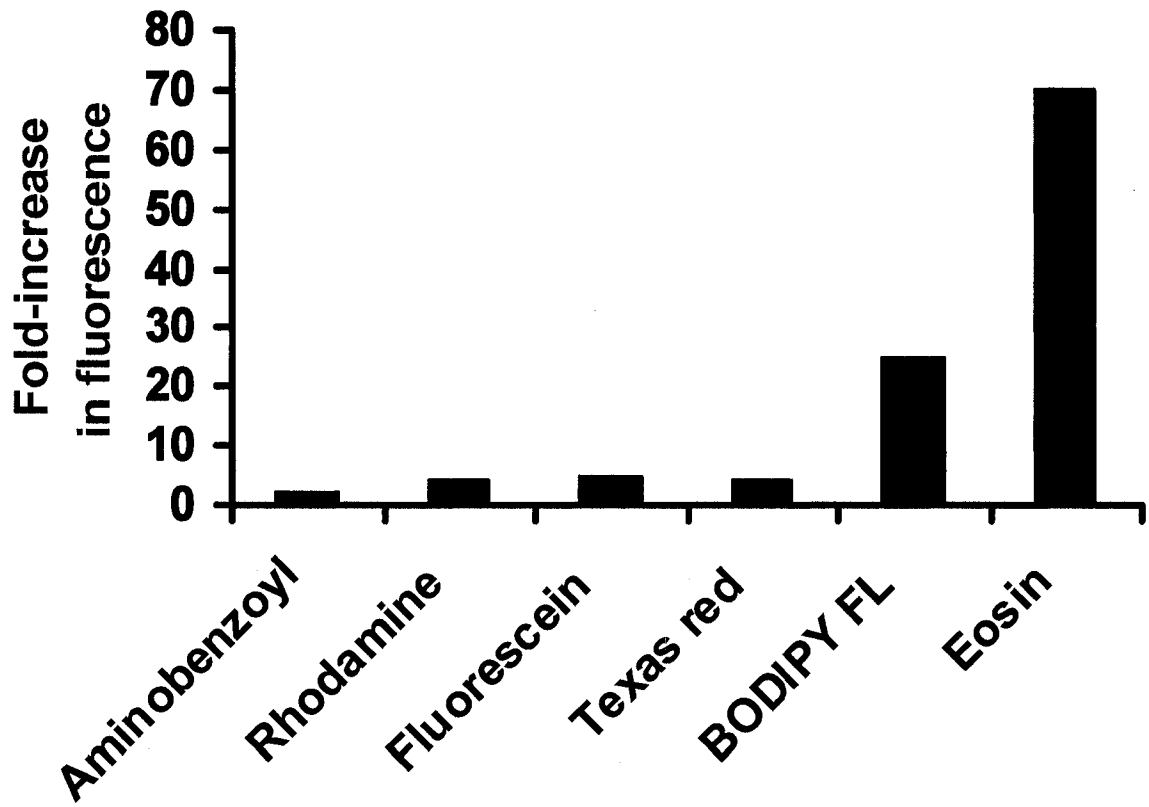

Figure 3.13 Relative fluorescence self quenching observed in GSSG using different fluorescent molecules.

3.5 Discussion

Fluorescence self-quenching (FSQ) has been used previously in various biochemical techniques (Wendt *et al.*, 1995; Zhuang *et al.*, 2000) including monitoring enzymatic activity (Wu *et al.*, 1995; Jones *et al.*, 1997). Here, we have used this phenomenon to develop a probe, diabz-GSSG, which has two amino benzoyl moieties attached to two free amino groups of oxidized glutathione. The structure of diabz-GSSG was confirmed by mass spectrometry. The fragmentation pattern of the diabz-GSSG along with the fragmentation pattern of the authentic GSSG standard revealed diagnostic GSSG fragment ions. Most importantly, fragment ions were detected that corresponded to the benzoyl moieties attached to the glutamate portion of GSSG, unambiguously verifying the successful synthesis of diabz-GSSG.

In order for FSQ to occur, the two amino benzoyl rings of diabz-GSSG must on average come closer than 100 nm. In order to test this, molecular dynamic simulations were performed. The simulations indicated that the *o*-aminobenzoyl residues could potentially come as close as 73 nm in a periodic fashion (Figure 3.5) suggesting the possibility of FSQ. This hypothesis was confirmed when ~2-fold increase in fluorescence was observed upon complete reduction of disulfide bond by DTT (10 mM) that removed the distance constraint resulting in the increase of fluorescence (Figure 3.6). The probe was then tested for enzymatic reduction by PDI in the presence of minimal concentration of DTT (50 μM). While no increase in fluorescence was observed with DTT alone (Figure 3.7, diamonds), the rapid increase in fluorescence was observed in time dependent manner in

the presence of PDI (0.5 μM) suggesting enzymatic reduction of disulfide bond (Figure 3.7, triangles). The final product of disulfide reduction of one molecule of diabz-GSSG would be two molecules of abz-GSH. If diabz-GSSG were to show the phenomenon of FSQ, there should be ~50% decrease in fluorescence upon re-oxidation of abz-GSH to diabz-GSSG. To this end, the auto-oxidation of abz-GSH was studied in the presence of cupric chloride, a commonly employed thiol oxidizing agent. The fluorescence decreased rapidly upon addition of cupric chloride to the sample containing abz-GSH confirming the FSQ due to the oxidation of abz-GSH to diabz-GSSG (Figure 3.6). This quenching was completely reversed by the addition of PDI plus DTT which reduced diabz-GSSG back to abz-GSH. Similar results were obtained when *o*-amino benzoyl cysteine (abz-Cys) was oxidized in the presence of Cu^{2+} to yield diabz-Cys. These results clearly illustrate the usefulness of abz-GSH / diabz-GSSG as a thiol redox probes.

One of the most important advantages of the diabz-GSSG fluorescent assay presented here is its higher sensitivity compared to two most commonly used assays. Scrambled RNase assay and insulin turbidity assay have long initial lag phases owing to which the actual initial rates for enzymatic activity cannot be determined. The diabz-GSSG assay presented here, shows instantaneous increase in fluorescence upon addition of PDI thus enabling the estimation of true initial rates. Diabz-GSSG was further used to study the single turnover of enzyme in the presence of minimal amount of DTT (Figure 3.10) or in the absence reducing agents (Figure 3.11) and results obtained clearly demonstrate the sensitivity as well as its potential usefulness as a kinetic probe to explore the active site environments of PDI and other members of the thioredoxin family of proteins.

Although Fluorescence-quenched peptides have been used in past for quantitative analysis of PDI disulfide reduction activity (Christiansen *et al.*, 2004; Westphal *et al.*, 1998) with sensitivity comparable to diabz-GSSG assay presented here, the method of preparation of these disulfide linked peptides is not straight forward. The probe presented here is synthesized in one simple step by incubating readily available chemicals, isatoic anhydride and oxidized glutathione. The end product of the reaction is always diabz-GSSG with no by-products that makes the purification process very simple.

Cell surface PDI activity has been studied earlier using scrambled RNase assay (Essex *et al.*, 1995). Here, we have optimized this assay to study platelet csPDI activity (Figure 3.12). This method of continuously monitoring platelet csPDI activity in one step is much simpler and more sensitive than previously described assay. The scRNase assay requires incubation of platelet with scRNase in the presence of reducing agent that would convert fraction of scRNase to native active form. The sample is then centrifuged and the supernatant that contains native RNase is transferred to solution containing its substrate RNA or CTP to further monitor the native RNase activity at 260 nm or 295nm respectively. Apart from this additional step required for scRNase assay, there is always significant blank rate associated with the process due to non-enzymatic conversion of scrambled RNase into native active form in the presence of DTT alone which makes the process less sensitive compared to diabz-GSSG assay. Platelet csPDI has shown to be actively involved in disulfide isomerization (Essex *et al.*, 1999; Lahav *et al.* 2002) as well as denitrosation (Root *et al.*, 2004) which affect the process of platelet aggregation. Studies involving platelet csPDI activity is not straightforward due to lack of sensitive

probes. Owing to the sensitivity of diabz-GSSG assay, the probe can be very useful for these studies. Moreover, it could be effectively used for studies involving the effect of redox buffers or reactive oxygen species (ROS) on platelet csPDI activity and its consequences on platelet functions.

Based on similar method of preparation as described for diabz-GSSG, we have synthesized series of glutathione disulfide derivatives by coupling it to variable fluorescent probes. It was observed that eosin derivative (Di-E-GSSG) showed maximum level of quenching (Figure 3.13) and therefore, potentially, is the most sensitive probe for monitoring PDI reductase activity.

In summary, here we have presented a series of new simple fluorescent disulfide probe for continuous detection of PDI disulfide reduction activity. The probe synthesis is simple, straight forward and inexpensive. The assay is rapid, sensitive and can be applied to cellular samples. The assay could be easily optimized for fluorescence plate reader and used for high throughput screening of PDI inhibitors from chemical libraries. The assay can be used for monitoring single turnover of enzyme and to estimate true initial rates of disulfide reduction in crude sample preparations.

Chapter 4

Characterization of Redox State of PDI under Variable Redox Environments Using a Sensitive Fluorescent Assay

4.1 Introduction

The activity of PDI, as described earlier, depends upon the redox state of its two active sites (Chapter 1, page 7). The enzyme will work as an oxidase when its active site is in the disulfide form whereas it will work as a reductase or isomerase when it is in the dithiol form. Therefore, it has been suggested that PDI dependent rearrangement of disulfide bonds in the ER lumen is thermodynamically controlled by its redox environment. Cellular redox environment is widely believed to be regulated by the ratio of reduced and oxidized form of glutathione (GSH / GSSG) which is significantly different in the cytosol, secretory pathways and extracellular environment.

4.1.1 Oxidation of PDI by GSSG

Formation of disulfide bond in the cytosol is not thermodynamically favored because of very high concentration of GSH (1 mM to 10 mM) and high [GSH] to [GSSG] ratio (30:1 to 100:1) which makes cytosolic environment highly reducing (Hwang *et al.*, 1992). However, in the ER lumen, the concentration of GSSG is relatively higher and [GSH] to [GSSG] ratio is 1:1 to 3:1 (Hwang *et al.*, 1992). This ratio has been shown to be ideal for *in vitro* oxidative folding of proteins (Bass *et al.*, 2004; Hwang *et al.*, 1992). Therefore, it is believed that GSSG is essential for oxidation of PDI active site, which, in turn, facilitates oxidative folding.

The oxidation of PDI dithiols by GSSG can be represented by Eq. 1

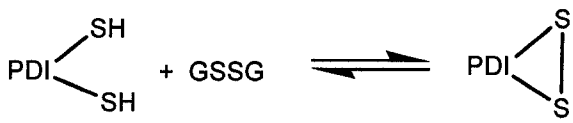

Eq. 1

Here, oxidized glutathione reacts with reduced active site of PDI to form oxidized PDI and 2 molecules of GSH.

The equilibrium constant for this reaction can be represented by Eq. 2

$$K_{OX} = \frac{[PDISS_2]\,[GSH]^2}{[PDISH_2]\,[GSSG]} \qquad \text{Eq. 2}$$

where K_{ox} is equilibrium constant for glutathione buffer system.

As evident from Eq 2, the K_{ox} would correspond to the concentration of $[GSH]^2$ / [GSSG] when red-PDI / ox-PDI = 1

The reduction potential for PDI active site can be obtained by substituting this value of K_{ox} in Nernst equation (Eq. 3)

$$E = E^{o} - \frac{RT}{nF} \ln K_{ox} \qquad \text{Eq. 3}$$

Where **E** is reduction potential for active site, $\mathbf{E^{o}}$ is standard reduction potential for glutathione buffer system, **R** is gas constant and **F** is Faraday constant. Therefore by knowing the value for K_{ox}, **E** can be calculated.

4.1.2 Methods for calculating reduction potential of PDI

(i) By using scRNAse assay and iodoacetic acid (IAA) (Hawkins *et al.*, 1991)**:** In this method, the active site of PDI was first blocked by alkylation using IAA and the effect of blocking on the isomerase activity was then measured using scRNase assay. The reaction of IAA with thiols can be represented as shown in Figure 4.1.

The extent of alkylation of PDI active sites by IAA will depend upon its redox state in glutathione buffer system.

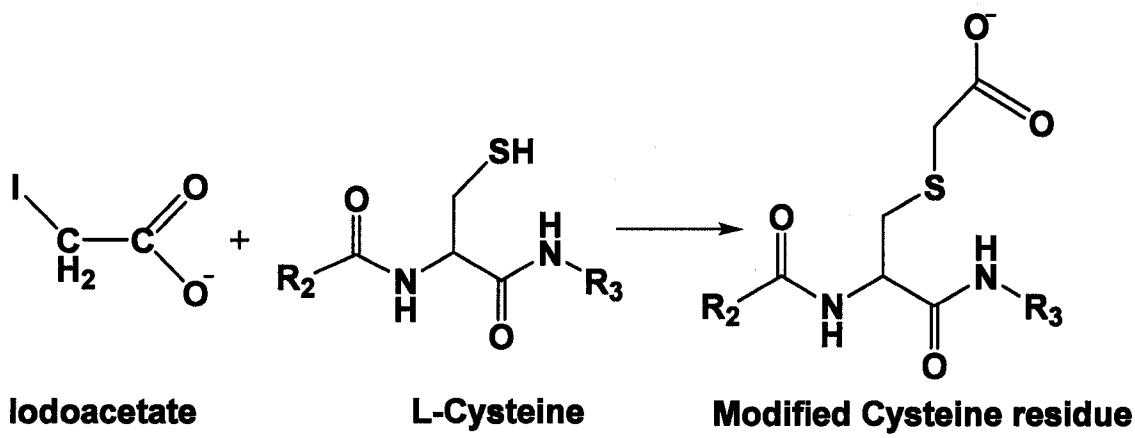

Figure 4.1 Reaction of IAA with cysteine

The effect of blocking PDI active sites on its activity was calculated by comparing it with activity of IAA-untreated PDI. The alkylation of PDI thiols permanently blocks them and as a result, they would not participate in isomerization of scRNase. Therefore, the fraction of isomerase activity would be the measure of redox state of PDI.

This method gave the equilibrium constant of 45 μM which corresponded to redox potential of -110 mV. This value is very small compared to values obtained from other methods. It was later suggested that the trapping of active site thiols by IAA is not precise in the presence of high concentrations of GSH because the rate at which active site thiols reacts with IAA is comparable to reduction of active site disulfide with GSH (Darby and Creighton, 1995). Due to this, IAA traps more active site thiols then are actually present by 'pulling' the equilibrium resulting in very low value of K_{ox}.

(ii) By using radioactive IAA (Lundstorm and Holmgren, 1993): In this method the radioactive IAA was used to alkylate PDI active site thiols equilibrated in glutathione buffer system in the similar fashion as in method (i) except that the reaction was performed in denaturating condition (6 M guanidium hydrochloride). The equilibrium constant obtained by this method was 3 mM corresponding to redox potential of -170 mM. The higher value obtained here as compared to method (i) is believed to be associated with denaturating condition because the disulfide bonds of unfolded proteins are more stable than native proteins. Therefore, the disulfide bonds would be more resistant to cleavage by GSH and the 'pulling effect' of IAA at equilibrium, as discussed in method (i), would be minimal resulting in more accurate blocking and higher value of K_{ox} (Darby and Creighton, 1995).

(iii) By monitoring IAA blocked PDI in HPLC (Darby and Creighton, 1995)**:** This method was used to study the redox properties of ***a*** and ***a'*** domains of PDI separately. The active sites of ***a*** and ***a'*** domains were acid trapped with IAA after equilibration in variable [GSH] / [GSSG] in denaturating as well as non-denaturating conditions followed

by their HPLC analysis. It was shown that all the products of this trapping reaction can be resolved by HPLC and the relative amounts of dithiols or disulfide can be estimated based on the extent of blocking of active site by IAA. This method gave the average K_{ox} value of 0.9 mM and 1.87 mM for ***a*** and ***a'*** domain respectively.

(iv) By gel shift assay (Schwaller *et al.*, 2003**):** In this method, the redox state of PDI was captured by using Mal-PEG, a conjugate of polymeric polyethylene glycol and maleimide. PDI is incubated with Mal-PEG after equilibration in variable ratio of [GSH] / [GSSG]. The Mal-PEG would react with cysteines of reduced PDI and cause a shift in the position of PDI band in SDS-PAGE depending upon extent of labeling. For example, the shift of one or two SH groups would indicate that one of the two active sites is oxidized, whereas a shift of three or four SH groups would indicate a completely reduce PDI. The fraction of reduced active sites was estimated by integrating the band intensities and gave the value of 0.7 mM for K_{ox}.

In summary, all the methods that have been used in past to calculate equilibrium constant gave significantly different values in glutathione buffer system ranging from 45 μM to 3 mM suggesting the dependence of value obtained in the method of estimation. The artifacts associated with the particular method, in part, may be responsible for the differences in estimated equilibrium constant.

Here, we have synthesized a fluorogenic pseudosubstrate for PDI and used it to develop an assay for studying its redox properties. The assay is sensitive enough to detect the thiols of reduced enzyme in the absence of any reducing agent. Therefore, the redox state of PDI can be reported as a function of change in the activity of reduced enzyme. We

have utilized this assay to study redox state of active site dithiols of PDI under variable [GSH] / [GSSG] buffer systems and extended our study to see the affect of these variable redox ratios on platelet surface PDI activity.

4.2 Materials and Equipment

4.2.1 Materials

Acetone; Sigma-Aldrich Canada Ltd., Oakville, Ontario

Ammonium persulfate; Sigma-Aldrich Canada Ltd., Oakville, Ontario

Ammonium sulfate; Sigma-Aldrich Canada Ltd., Oakville, Ontario

Biorad Protein Assay (Bradford Reagent); Bio-Rad Laboratories USA, Hercules, California

Eosin isothiocyanate; Sigma-Aldrich Canada Ltd., Oakville, Ontario

Ethylene diamide tetraacetic acid; Sigma-Aldrich Canada Ltd., Oakville, Ontario

Monoclonal anti-PDI antibody RL90; Abcam USA, Cambridge, MA

Oxidized glutathione; Sigma-Aldrich Canada Ltd., Oakville, Ontario

Phenylarsine oxide; Sigma-Aldrich Canada Ltd., Oakville, Ontario

Potassium phosphate; Sigma-Aldrich Canada Ltd., Oakville, Ontario

Reduced glutathione; Sigma-Aldrich Canada Ltd., Oakville, Ontario

Rhodamine 1,2,3; Invitrogen Canada Inc., Burlington, Ontario

Sephadex G-25; Sigma-Aldrich Canada Ltd., Oakville, Ontario

Sodium Chloride; Sigma-Aldrich Canada Ltd., Oakville, Ontario

Sodium phosphate monobasic; Sigma-Aldrich Canada Ltd., Oakville, Ontario

4.2.2 Equipment

Agilent 8453 UV-VIS Spectrophotometer;
Agilent Technologies Canada Inc, Mississauga, Ontario

BioRad Fraction Collector Model 2110;
Bio-Rad Laboratories (Canada) Ltd., Mississauga, Ontario

Hemocytometer;
Reichert Co, Buffalo, NY

Jouan CR3i Centrifuge;
Jouan Inc., Winchester, Virginia

Labconco FreeZone 4.5 Liter Benchtop Freeze Dry Systems;
Laconoco Corporation, Kansas City, Missouri

Mettler AJ100 Balance;
Mettler Toledo Canada, Mississauga, Ontrio

Microtiter 96-well Solid Plate;
Thermo Electron Corp. Canada, Burlington, Ontario

Northen Eclipse 6.0 Imaging Software;
Empix Imaging Inc., Mississauga, Ontario

NUAIRE Biological Safety Cabinet Class II Type A/B3;
Thermo Electron Corp. Canada, Burlington, Ontario

Orion Model 420A pH Meter;
Thermo Electron Corp. Canada, Burlington, Ontario

Stir Plate 360 Series;
VWR International, Mississauga, Ontario

Varian Eclipse Fluorescence Spectrophotometer;
Varian Canada, Mississauga, Ontario

Zeiss Axiovert 200 inverted Fluorescence Microscope;
Empix Imaging Inc., Mississauga, Ontario

4.3 Methods

4.3.1 PDI assay buffer

PDI assay buffer contained 0.1 M potassium phosphate buffer (pH 7.0) and 2 mM EDTA. This buffer was used throughout the study unless otherwise specified.

4.3.2 Preparation of dieosin glutathione disulfide (Di-E-GSSG)

GSSG was incubated with 10-fold molar excess of eosin in phosphate buffer (100 mM sodium phosphate and 2 mM EDTA, pH 8.5) at room temperature (25 °C). 100 μL aliquots were taken at different time intervals and passed down G-25 column (100 mm × 10 mm) using PDI assay buffer and 500 μL aliquots were collected with the help of a fraction collector. Free eosin binds to the top of the G-25 column and did not elute in phosphate buffer.

The elution time for GSSG alone, as estimated by monitoring absorbance increase at 220 nm in separate experiment, was 6 min. After 30 min of incubation time, an intense pink band that eluted at ~5 min was tested for fluorescence increase before and after addition of DTT (10 mM). The fluorescence increase of the fluorescent fractions was ~2-fold at 30 min and increased as a function of reaction time, reaching a plateau after 6 h (~70-fold) suggesting completion of reaction and the attachment of two eosin moieties to two free amino termini of GSSG. All the fractions that showed ~70-fold increase in the fluorescence were pooled and stored at -80 °C. The purity of the product was ascertained by thin layer chromatography (TLC) in a methanol-acetone solvent system (30:70).

4.3.3 Preparation of eosin-GSH

Eosin-GSH (EGSH) was prepared by treating 100 μM of purified Di-E-GSSG with 10 mM DTT for 30 min and then separating the mixture with a Sephadex G-25 column. The eluted sample did not show any increase in the fluorescence after addition of DTT (10 mM), confirming that all the Di-E-GSSG has been converted to EGSH. The aliquots were pooled together and quantified using molar absorption coefficient e = 88000 $M^{-1} \cdot cm^{-1}$ (Lettinga, 2004).

4.3.4 Quantification of EGSH formation

Increase in fluorescence was monitored as a function of [EGSH] (e = 88000 $M^{-1} \cdot cm^{-1}$) (Lettinga, 2004) and the standard plot was generated with excitation at 525 nm and emission at 545 nm. This standard plot was used wherever quantification of the reduction of [Di-E-GSSG] to [E-GSH] was required.

4.3.5 PDI purification

Recombinant human PDI was expressed using the Escherichia *coli* strain BL21 (DE3) and expression vector pET-28a as described elsewhere (Seslija, 2005). This plasmid encodes a fusion protein containing the entire human PDI sequence with an N-terminal His_6 tag (Pihlajaniemi *et al.*, 1987). Recombinant PDI was purified from the soluble fraction of the cell lysate using Ni-CAM™ HC resin (Sigma), which is a high-capacity nickel-affinity matrix. Bound PDI was eluted using 250 mM imidazole in 50 mM Tris/HCl (pH 8.0) and collected in 2.0 mL fractions. The fractions containing PDI were

pooled and dialysed against 0.1 M potassium phosphate buffer (pH 7.0). Protein quantification was performed by the Bradford assay (Bradford, 1976).

4.3.6 Kinetics of PDI-dependent disulphide reduction

PDI disulphide reduction activity was monitored in PDI assay buffer by adding PDI (5 nM to 20 nM) to Di-E-GSSG (150 nM) in the presence of 5 μM DTT. The increase in fluorescence was monitored at 545 nm with excitation at 525 nm.

Alternatively, the kinetics of reduction were also monitored by visible spectrophotometry at 525 nm or 550 nm as a function of time in the presence of 5 μM DTT and 100 nM PDI.

Reduction of substrate by red-PDI was studied under different redox environment by first incubating PDI in variable [GSH] / [GSSG] (1:1 to 20:1, [GSH] 200 μM to 4 mM and [GSSG] 200 μM) for 15 min and then transferring 10 μL (15 nM PDI) to PDI assay buffer containing 150 nM Di-E-GSSG. The final [GSH] and [GSSG] in the reaction mixture was from 1-20 μM and 1.6 μM respectively.

4.3.7 Reduction or oxidation of PDI

PDI (50 μM) was reduced or oxidized by incubating it with 10 mM DTT or 10 mM GSSG respectively for 3 h at room temperature. The excess of DTT or GSSG was removed by using a Sephadex G-25 column where the elution time for PDI was 2 min which was well separated from either GSSG or DTT with the elution time of greater than

6 min. The thiol content of reduced or oxidized PDI was calculated using the DTNB [5,5′-dithiobis-(2-nitrobenzoic acid); Ellman's reagent] assay (Ellman, 1959).

4.3.8 Platelet isolation and monitoring psPDI activity

Samples of peripheral venous blood were mixed 6:1 with acid citrate dextrose (25 g/L trisodium citrate dihydrate, 15 g/L citric acid monohydrate and 20 g/L dextrose). Whole blood was centrifuged (190 g for 15 min at 37 °C) to yield platelet-rich plasma. Platelets were isolated by centrifugation (700 g for 15 min at 37 °C) and washed two times in HEPES buffer containing 2 mM EDTA (pH 7.4). Platelets were quantified using a haemocytometer.

Final concentration of washed human platelets was adjusted to 10×10^9 mL^{-1} prepared in HEPES buffer containing 2 mM EDTA. Di-E-GSSG (150 nM) was incubated with 5 μM DTT and variable concentration of platelets (1×10^7 to 8×10^7 mL^{-1}) and the activity was monitored continuously as a function of time. For redox study, platelets were incubated with variable [GSH] / [GSSG] (10:1 to 1:1, [GSH] 500 μM and [GSSG] 50 to 500 μM) for 15 min and then 10 μL of platelet was added to the reaction mixture (150 nM Di-E-GSSG in HEPES-EDTA buffer) such that final concentration of platelets was $4x10^8$ mL^{-1} and final [GSH] or [GSSG] did not exceed more than 5 μM.

4.4 Results

4.4.1 Di-E-GSSG a new pseudosubstrate for PDI

PDI pseudosubstrate Di-E-GSSG is similar in function to a reagent recently introduced from our lab (Raturi *et al.*, 2005). Oxidized glutathione was incubated with 5 molar excess of eosin isothiocyanate at pH 8.5 for 8 h so that the two free amino groups of GSSG are conjugated covalently to two eosin moieties forming Di-E-GSSG. The probe was separated from unreacted eosin isothiocyanate using chromatography on Sephadex G-25. The close proximity of the eosin moieties resulted in the self-quenching of their fluorescence and made the molecule relatively non-fluorescent (Figure 4.2, dashed line) (ex. λ_{max} = 525 nm, emission λ_{max} = 545 nm). However, upon addition of thiol reducing agent such as DTT (10 mM), the fluorescence increased by ~70-fold (Figure 4.2, dark line) due to the reduction of disulfide bond that released the distance constraints between two eosin molecules. We then studied the reduction of probe (150 nM) in the presence of minimal concentration of DTT (5 μM) with or without PDI (5 nM to 20 nM). While no increase in fluorescence was observed with DTT alone (Figure 4.3, diamonds), an instantaneous increase of signal was observed as a function of time in the sample containing PDI demonstrating its disulfide reductase activity (Figure 4.3 circles, squares and triangles). Therefore the attractive feature of Di-E-GSSG is that its disulfide bond is more resistant to reduction by DTT than the active site disulfides of PDI. This means that with nanomolar amounts of PDI, its reductase activity can be continuously monitored in the presence of as much as 5 μM DTT (Figure 4.4, diamonds) without any appreciable

blank rates. The reductase activity of PDI increased as a function of [Di-E-GSSG] with the apparent Km of 650 nM ± 40 nM (Figure 4.4). The k_{cat} and catalytic efficiency (k_{cat}/K_M) were estimated to be 3.5 ± 0.25 sec^{-1} be 8.9 X 10^4 ± 180 M^{-1} sec^{-1} respectively.

4.4.2 Absorption spectra of Di-E-GSSG

Another interesting feature of Di-E-GSSG is its spectral behaviour in visible range when it is reduced either by PDI or excess of reducing agent (Figure 4.5A and 4.5B). Upon complete reduction of probe (1.6 μM) by PDI (100 nM) in the presence of DTT (5 μM), the absorbance at 520 nm increases by 85% while there is decrease in 550 nm absorption by 60% with the isobestic point at 540 nm (Figure 4.5A). An isobestic point is defined as the wavelength at which the absorption or extinction coefficient of two or more species in identical. Therefore, these ratiometric changes in the visible spectra can also be used to estimate the catalytic activity of enzymes of PDI family (Figure 4.5B). As shown in figure 4.5B, with 100 nM of PDI, the reaction is over in 60 seconds which demonstrates the better sensitivity as well as rapidity of this assay over other UV-Vis spectrophotometric assays such as insulin turbidity and scRNAse assays where the time taken to visualize PDI activity under similar experimental condition is more than 30 minutes (Lundstrom and Holmgren, 1990).

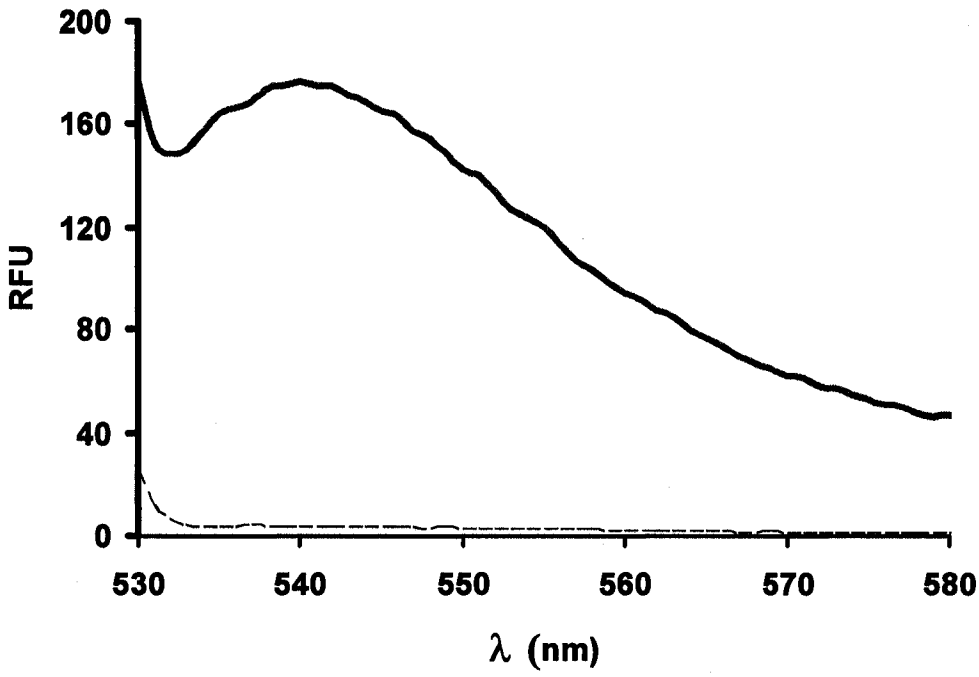

Figure 4.2 Maximum fluorescence increases in Di-E-GSSG after reduction

150 nM of Di-E-GSSG spectrum in PDI assay buffer was taken with excitation at 525 nm and emission at 545 nm (dashed line). The same sample was then incubated with 10 mM DTT for 15 min to completely convert Di-E-GSSG into EGSH and rescanned (solid line).

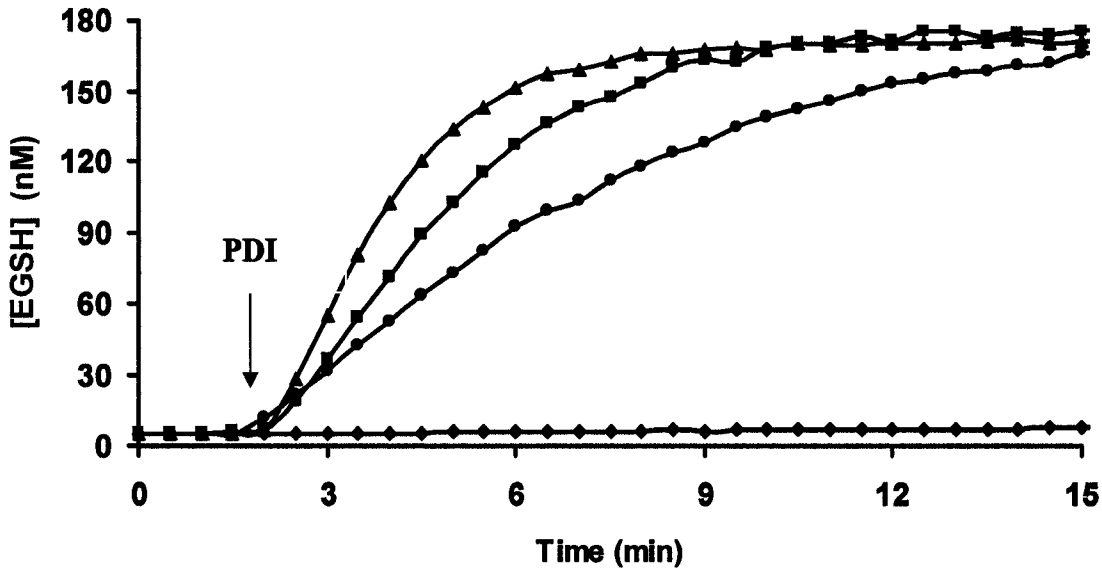

Figure 4.3 PDI disulfide reductase activity

Di-E-GSSG (150 nM) was incubated with DTT (5 μM) in PDI assay buffer (pH 7) at room temperature in the absence of any PDI (diamonds) or in the presence of 5 nM (circles), 10 nM (squares) and 20 nM (triangles) PDI.

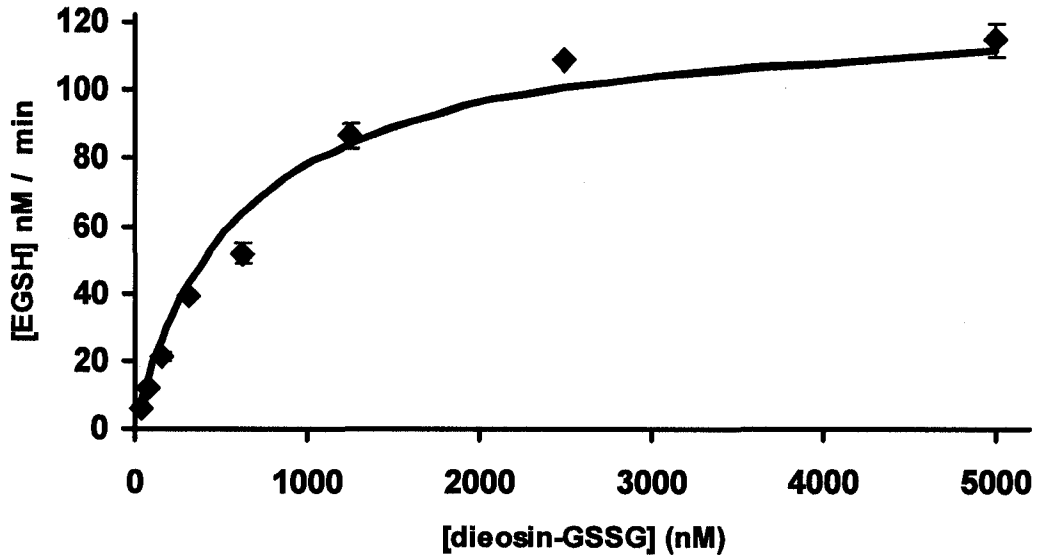

Figure 4.4 Estimation of K_M

Estimation of K_M: 40 nM of PDI was incubated with variable concentration of Di-E-GSSG (50 nM - 5 μM) in PDI assay buffer at room temperature and initial rates of E-GSH formation were monitored as a function of [Di-E-GSSG]. Theoretical best fit of the data to the Michaelis Menten equation (solid line): K_M = 650 units and Vmax =125 units.

A.

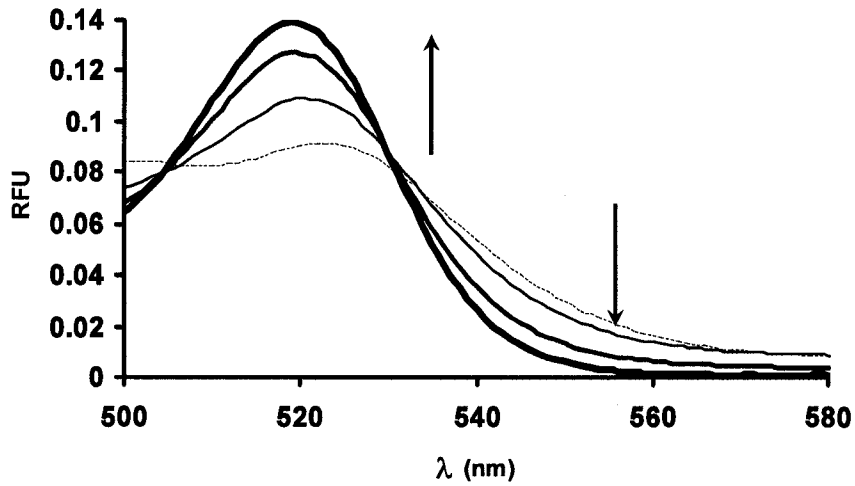

B.

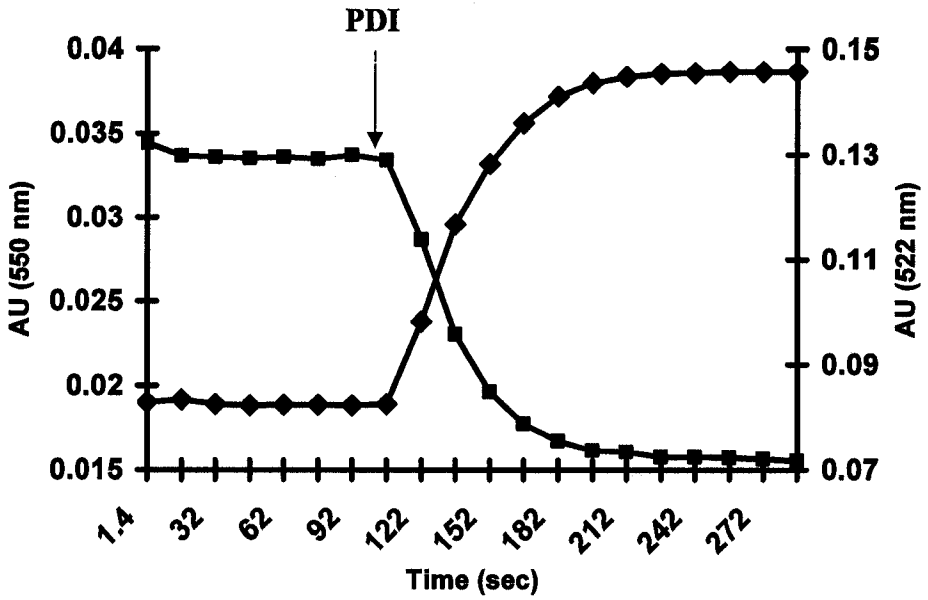

Figure 4.5 Ratiometric changes in visible spectra

A. Change in absorption spectra of Di-E-GSSG (1.6 μM) was monitored between 500 nm and 580 nm after reduction by PDI (100 nM).at 30 sec intervals. **B.** Change in absorption at 520 nm and 550 nm was monitored as a function of time.

4.4.3 Reduction of Di-E-GSSG by red-PDI

To further check the sensitivity of assay, red-PDI (4 nM to 32 nM) was added to probe in the absence of any reducing agent and the disulfide reduction (with no turnover), was monitored as a function of time. As shown in Figure 4.6 and Figure 4.7, the increase in substrate reduction was proportional to [PDI] even at lower nM range. Moreover, 4 nM of PDI released ~15.5 nM EGSH (Figure 4.6, triangles), confirming the sensitivity of assay at the lower [PDI] as 1 mole of red-PDI (2 active sites) should ideally give 4 mol of EGSH.

In order to compare the substrate specificity of PDI with Di-E-GSSG and PDI with GSSG, Di-E-GSSG reduction by red-PDI was monitored in the presence of variable [GSSG] (Figure 4.8). Di-E-GSSG (150 nM) was incubated with varying [GSSG] (0 – 4 mM) followed by addition of PDI (15 nM) and the substrate reduction was studied with excitation at 525 nm and emission at 545 nm. The inhibition constant for substrate inhibition with GSSG was found to be 200 ± 30 μM suggesting that PDI has much higher affinity for Di-E-GSSG as compared to GSSG and there would be no significant decrease in red-PDI activity with no turnover even in the presence of up to ~20 μM GSSG in reaction mixture.

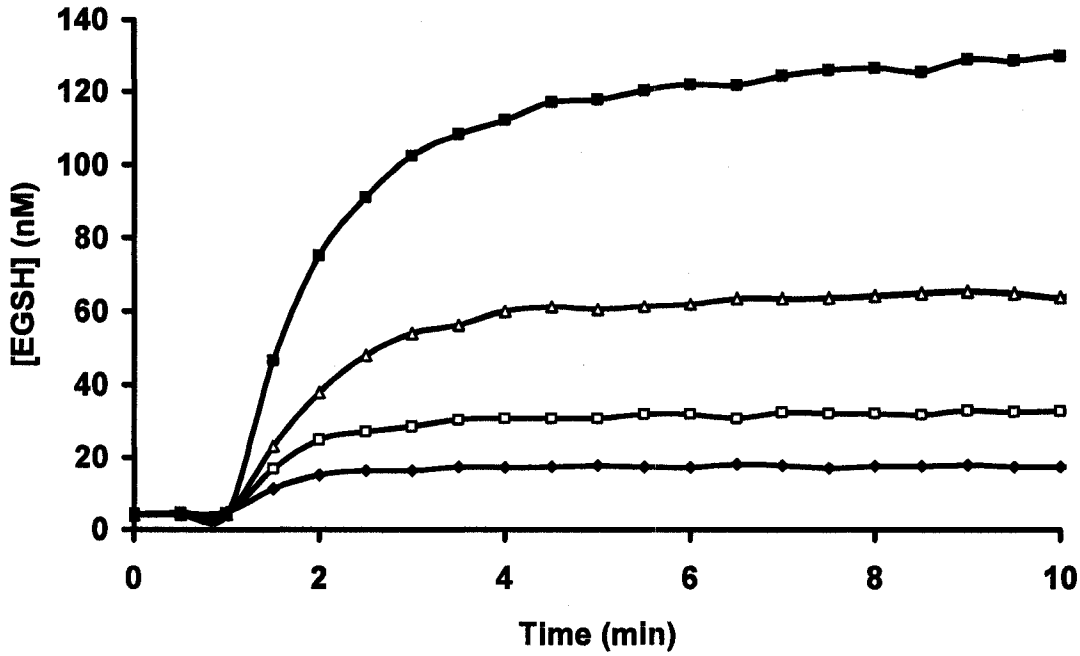

Figure 4.6 Di-E-GSSG reduction by red-PDI

Red-PDI was added to the reaction mixture containing Di-E-GSSG (150 nM) and and the disulphide reduction of substrate was monitored at 4 nM (diamonds), 8nM (hollow squares), 16 nM (hollow triangles) and 32 nM (filled squares) of red-PDI.

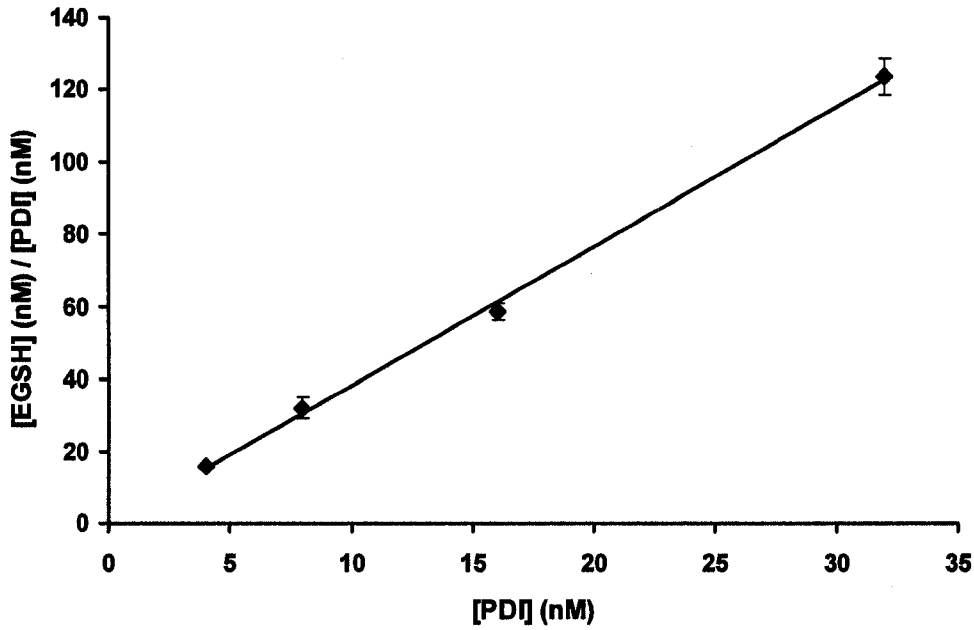

Figure 4.7 Reduction of Di-E-GSSG is linear with increasing [red-PDI]

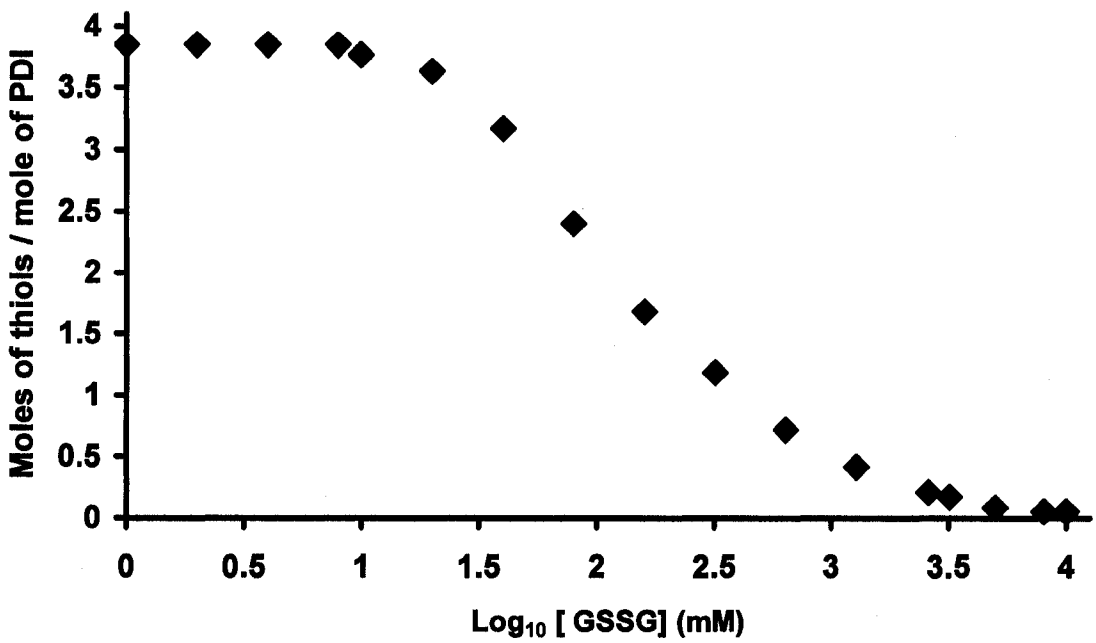

Figure 4.8 Inhibition of substrate reduction by PDI in the presence of variable [GSSG]

Di-E-GSSG (150 nM) was incubated with varying [GSSG] (0 nM to 4 mM) followed by addition of PDI (15 nM) and the substrate reduction was studied with excitation at 525 nm and emission at 545 nm.

4.4.4 Monitoring oxidation of PDI by Di-E-GSSG assay

PDI (50 μM) was reduced by incubating with 10 mM DTT for one hour followed by separation by G-25 column and its auto-oxidation was studied as a function of time at room temperature by DTNB assay. As shown in Figure 4.9 (squares), PDI (2 μM) is quite stable in reduced state in PDI assay buffer and shows only ~15% ± 7% oxidation in the interval of 5 h.

We then studied PDI-dithiol oxidation under the same conditions using our assay by hypothesizing that the loss in the reduced PDI activity could be attributed to conversion of fraction of red-PDI into oxidized PDI. In other words, reduction of probe by partially red-PDI compared to fully red-PDI would directly represent the fraction of red-PDI (fraction of oxidized PDI = 1 – residual activity). Red-PDI was added to 150 nM of Di-E-GSSG and the reduction of the probe was monitored as a function of time. The assay, similar to the DTNB assay, showed a loss of 16.5 ± 2% of thiols in 5 h (Figure 4.9 triangles) suggesting that Di-E-GSSG assay is rapid and simple technique to estimate redox state of PDI-dithiols and other proteins of the PDI super-family.

We then studied the oxidation of red-PDI by H_2O_2, a known potent thiol oxidant, and compared it with oxidation by GSSG, an important component of redox buffer in physiological environment. To this end, 2 μM of red-PDI was incubated with 100 μM of H_2O_2 (Figure 4.10 diamonds) or GSSG (Figure 4.10 squares) and the substrate reduction was monitored by adding 10 μL of PDI (final conc. 15 nM) to the assay buffer containing

150 nM of Di-E-GSSG at the interval of every 5 min for 1 h. As shown in Figure 4.10, the oxidation of PDI by GSSG was found to be 10-fold faster than H_2O_2 with the estimated half lives of 2 min and 20 min respectively.

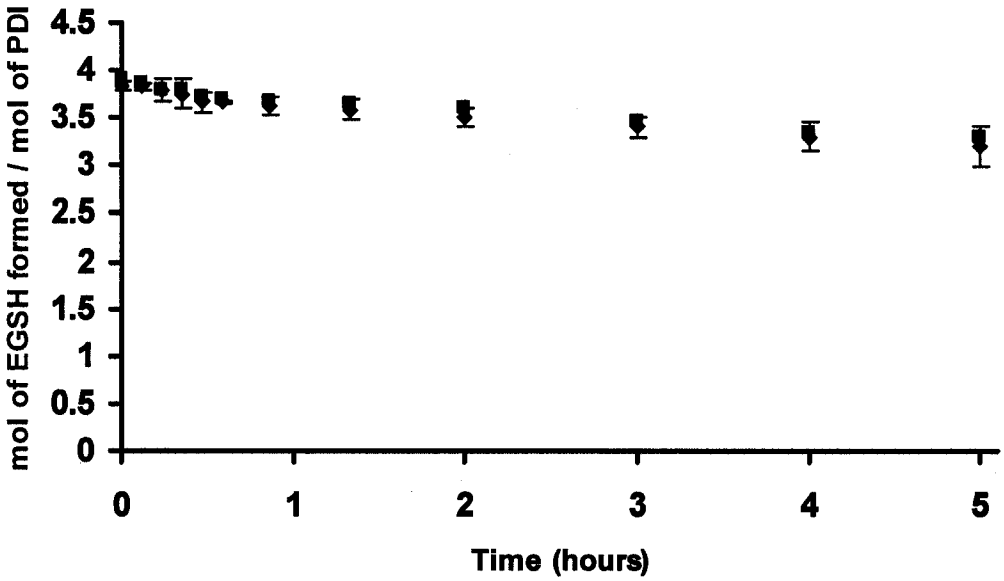

Figure 4.9 Monitoring auto-oxidation of PDI

red-PDI (2 μM) was incubated with DTNB (10 mM) in PDI assay buffer, pH 8 for 10 min at various time intervals and reading was taken at 412 nm (squares). PDI- substrate reduction (with no turnover) was measured in parallel by adding 10 nM of red-PDI to 150 nM Di-E-GSSG (diamonds) and fraction of red-PDI was calculated by converting final fluorescence units into mol of thiols using the standard curve for [EGSH].

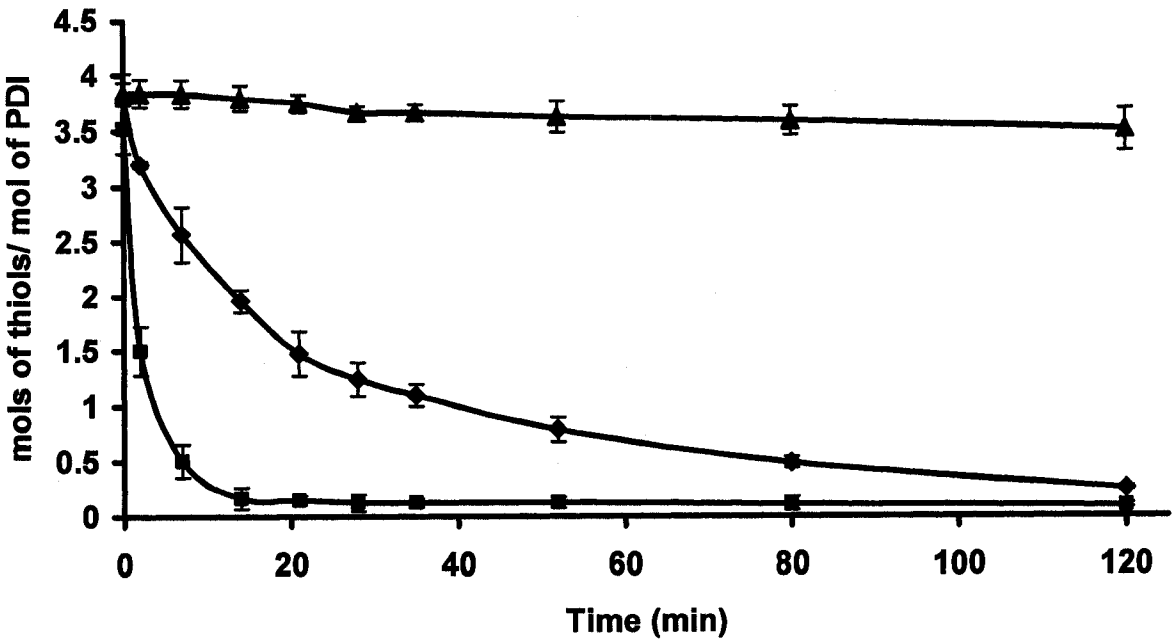

Figure 4.10 Oxidation of PDI by H_2O_2 or GSSG

PDI (2 μM) was incubated with 100 μM GSSG (squares) or H_2O_2 (diamonds) or just with buffer (triangles) for variable time intervals (0 to 60 min). An aliquot of PDI, (15 nM final concentration) was then removed after 15 min and added to 150 nM Di-E-GSSG. The fluorescence was monitored 545 nm (ex. 525 nm). The fluorescence units were converted to [EGH] by using the standard curve.

4.4.5 Substrate reduction by PDI in redox buffers with variable [GSH] / [GSSG]

Glutathione is the most abundant thiol in the cells and it has been shown that the ratio of thiol to disulfide ([GSH] / [GSSG]) affects the protein folding in the presence or absence of PDI. Previous reports have shown the dependence of PDI isomerase activity on the ratio of [GSH] to [GSSG] using scRNase assay (Lyles and Gilbert, 1991; Hawkins *et al.*, 1991; Lundstorm and Holmgren, 1993). Here we set out to study the fraction of red-PDI under different ratio of GSH to GSSG using our fluorescent substrate. The fraction of reduced PDI was estimated under variable [GSH] / [GSSG] ratio (1:1 to 20:1) by monitoring the decrease in the reduction of substrate by PDI. To this end, red-PDI (2 μM) was incubated with variable [GSH] / [GSSG] ([GSH] 200 μM to 4 mM and [GSSG] 200 μM) for 15 min at room temperature and then 10 μL (final [PDI] = 15 nM) was added to the reaction mixture containing 150 nM of Di-E-GSSG.

As shown in Figure 4.11, incubation of PDI with GSSG alone (200 μM) resulted in its complete oxidation whereas 10-fold excess of GSH over GSSG generated completely reduced PDI. Incubation of PDI for 30 min or 1 h in redox buffer gave same fraction of red-PDI and therefore 15 min of time interval was chosen for all the experiments in order to minimize the auto-oxidation of GSH during incubation. These experiments, when performed after removing unreacted GSSG or GSH from PDI by chromatography on Sephadex G-25 before adding to the reaction mixture, showed same activity as without separation confirming that presence of GSSG or GSH at these concentrations (GSH 1 μM to 20 μM and GSSG 1.6 μM) in reaction mixture do not alter no-turnover rates of PDI

and thus purification of excess GSSG or GSH is not required. Moreover, owing to very low affinity of PDI for GSSG (Figure 4.8) as compared to Di-E-GSSG, presence of low concentrations of GSSG is not expected to alter the rates of EGSH generation by red-PDI.

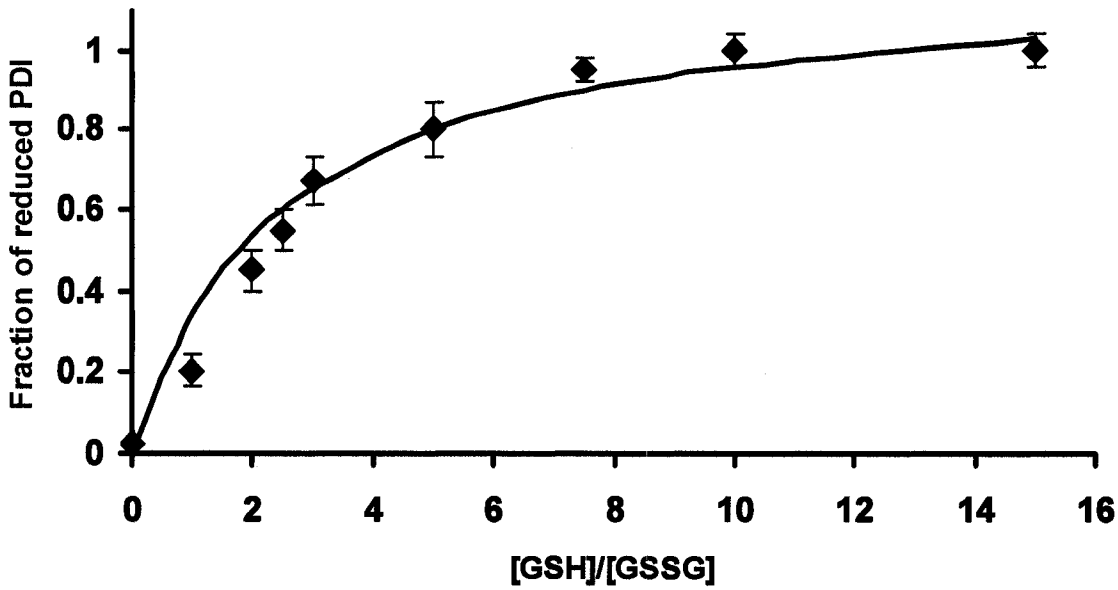

Figure 4.11 Estimation of fraction of red-PDI with variable GSH/GSSG ratio

2 μM of PDI was incubated with fixed concentration of GSSG (200 μM) and varying concentration of GSH (200 μM to 4 mM) at room temperature followed by addition of 10 μL of sample (Final [PDI] = 15 nM) to reaction mixture containing 150 nM Di-E-GSSG and . The fluorescence was monitored 545 nm (ex. 525 nm). The theoretical hyperbolic curve (solid line) is plotted using Michaelis Menten equation and by taking equilibrium constant value of 2.5.

In Figure 4.12, the redox state of PDI was plotted as a function of $[GSH]^2$ / [GSSG]. The plot was similar to Figure 4A showing the increase in reduced PDI fraction with the increase in $[GSH]^2$ / [GSSG] and gave the value for K_{ox} of 1.1 ± .075 mM. This value is similar to the value of ~1.3 mM reported by Darby and Creighton (1995) and comparable to the values of ~0.7 mM reported by Gilbert and coworkers (2003) and ~3 mM by Lundstrom and Holmgren (1993).

This experiment suggests that GSSG, that seems to be potent oxidant for PDI-dithiols, inhibits PDI disulfide reductase activity in concentration dependent manner. To further confirm this observation, we performed insulin turbidity assay, a well known PDI reductase assay (Lungstrom and Holmgren, 1990), at fixed [GSH] and varying [GSSG]. To this end, insulin (65 μM) was incubated with GSH (1 mM) and PDI (0.5 μM) and the enzymatic reduction was monitored as a function of time against increasing [GSSG] (Figure 4.13). As expected, the initial reductase activity decreased linearly with increasing [GSSG] thus confirming our previous observation that GSSG can inhibit reductase activity at near physiological concentrations.

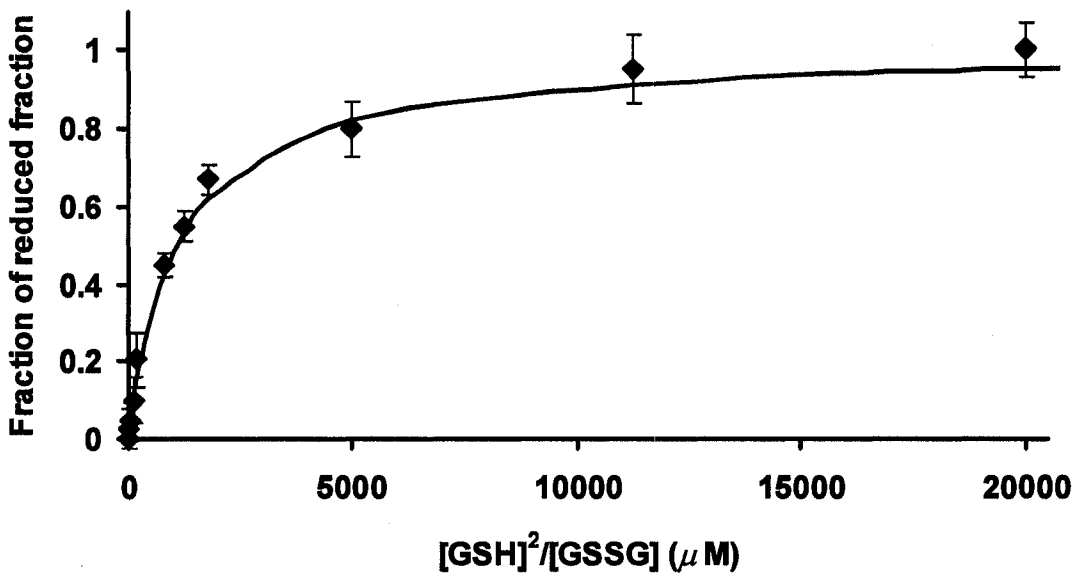

Figure 4.12 Caclulation of K_{ox}

Plot of red-PDI fraction against $[GSH]^2$ / [GSSG] was constructed with fixed concentration of GSSG (200 μM) and varying concentration of GSH (50 μM to 4 mM) under the similar conditions as described above. Theoretical best fit hyperbolic curve was created using Michaelis Menten equation and K_{ox} value of 1.1 mM (solid line).

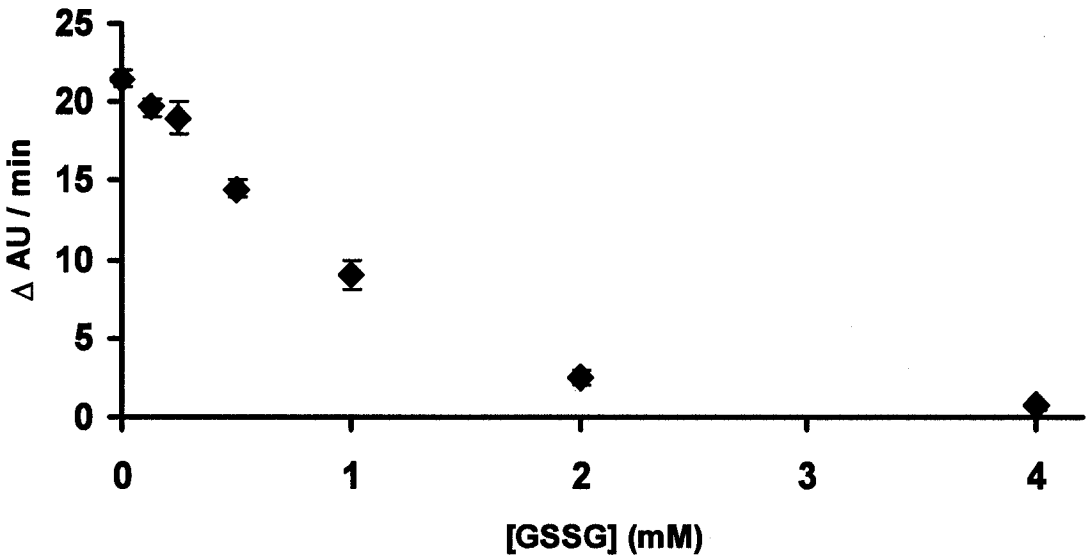

Figure 4.13 Inhibition of Insulin reduction by PDI

PDI (0.5 μM) was incubated with insulin (65 μM) in the presence of increasing concentration of [GSSG] (200 μM to 4 mM) at fixed concentration of [GSH] (1mM) and rate of reduction was measured as a function of turbidity at 620 nm.

4.4.6 Monitoring psPDI activity using fluorescent assay

PDI has been shown in past to account for ~40 % of total surface thiols (Jiang *et al.*, 1999) on platelets and is critical for platelet activation and secretion (Bennett *et al.*, 2000; Lahav *et al.*, 2002). Here, we optimized Di-E-GSSG assay for continuous monitoring of psPDI activity. Di-E-GSSG (150 nM) was incubated platelets (10^7 / mL to $8x10^7$ / mL) plus DTT (5 μM) and the fluorescence change was monitored as a function of time. While no significant increase in fluorescence was observed without platelets, a platelet-density dependent increase was observed in platelet-samples (Figure 4.14A and 4.14B) demonstrating that psPDI activity can be directly and continuously monitored using this assay. The platelet activity ($4x10^7$ / mL) was inhibited to 80% by using RL90 anti-PDI antibody confirming that majority of surface reductase activity is contributed by psPDI (Figure 4.14A, filled triangles and Figure 4.14B). To our knowledge, this is the most sensitive assay to monitor surface reductase activity that can be extended to other cell lines containing surface PDI.

It has been suggested earlier that attachment of PDI to the platelet surface is by electrostatic interactions (Terada *et al.*, 1995). We set out to explore the role of hydrophobic interaction with surface because of the fact that PDI has large hydrophobic patches through which it may bind to exofacial portions of transmembrane proteins.We tested this hypothesis by incubating platlelets ($8x10^7$ / mL) with varying concentration of isopropanol (IPA) (0.25% to 10%), for 5 min followed by the separation of supernatant from platelet by centrifugation at 2000 g for 15 min. The supernatant was then tested for PDI activity using Di-E-GSSG assay and subjected to western blot analysis (Figure 4.15).

The activity as well as PDI band intensity increased with the increase in IPA concentration suggesting that PDI, in part, may be attached to the platelet surface by hydrophobic interactions.

4.4.7 Effect of variable [GSH] / [GSSG] on psPDI-reductase activity

As we have observed that red-PDI activity was inhibited in the presence of [GSSG], we studied the effect of increasing [GSSG] (50 μM to 500 μM) at fixed [GSH] (500 μM) on psPDI reductase activity (Figure 4.14B). As expected, the reductase activity was also inhibited with the decrease in [GSH] / [GSSG] ratio and when the ratio approached 1:1 (Figure 4.16, filled diamonds), the activity overlapped with platelet sample containing no GSH or GSSG (Figure 4.16, hollow squares). This observation is important in view of the fact that csPDI primarily has a reductive role on the exofacial surface of cells (Couet *et al.*, 1996; Mandel *et al.*, 1993; Tager *et al.* 1997). It suggests that under oxidative stress or lower [GSH] / [GSSG] ratio in plasma, the reductive function of psPDI can be significantly inhibited.

A.

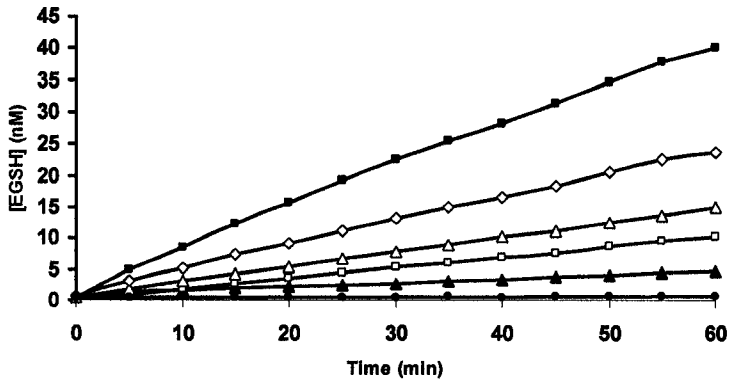

B.

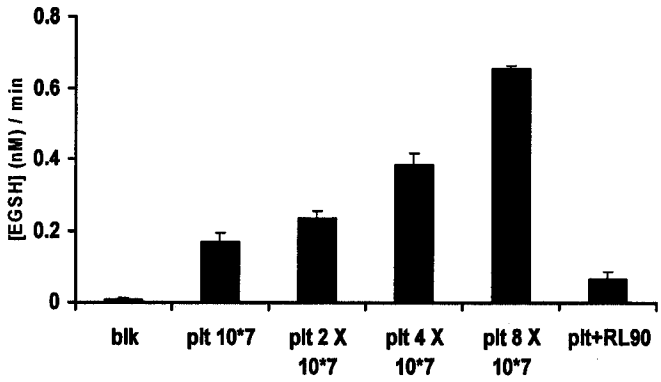

Figure 4.14 Monitoring psPDI activity

A. Di-E-GSSG (150 nM) was incubated with DTT (5 μM) and 10^7 / mL (squares), $2x10^7$ / mL (hollow triangles), $4x10^7$ / mL (hollow diamonds) and $8x10^7$ / mL (filled squares) of platelets and the activity was monitored as a function of time. Platelets activity ($4x10^7$ / mL) was also measured in parallel in the presence of RL90 anti-PDI antibody (filled triangles). Incubation of probe with DTT alone (5 μM) did not show any significant reaction (filled circles). **B.** The replot of the initial rates of [EGSH] generation (min^{-1}) by psPDI.

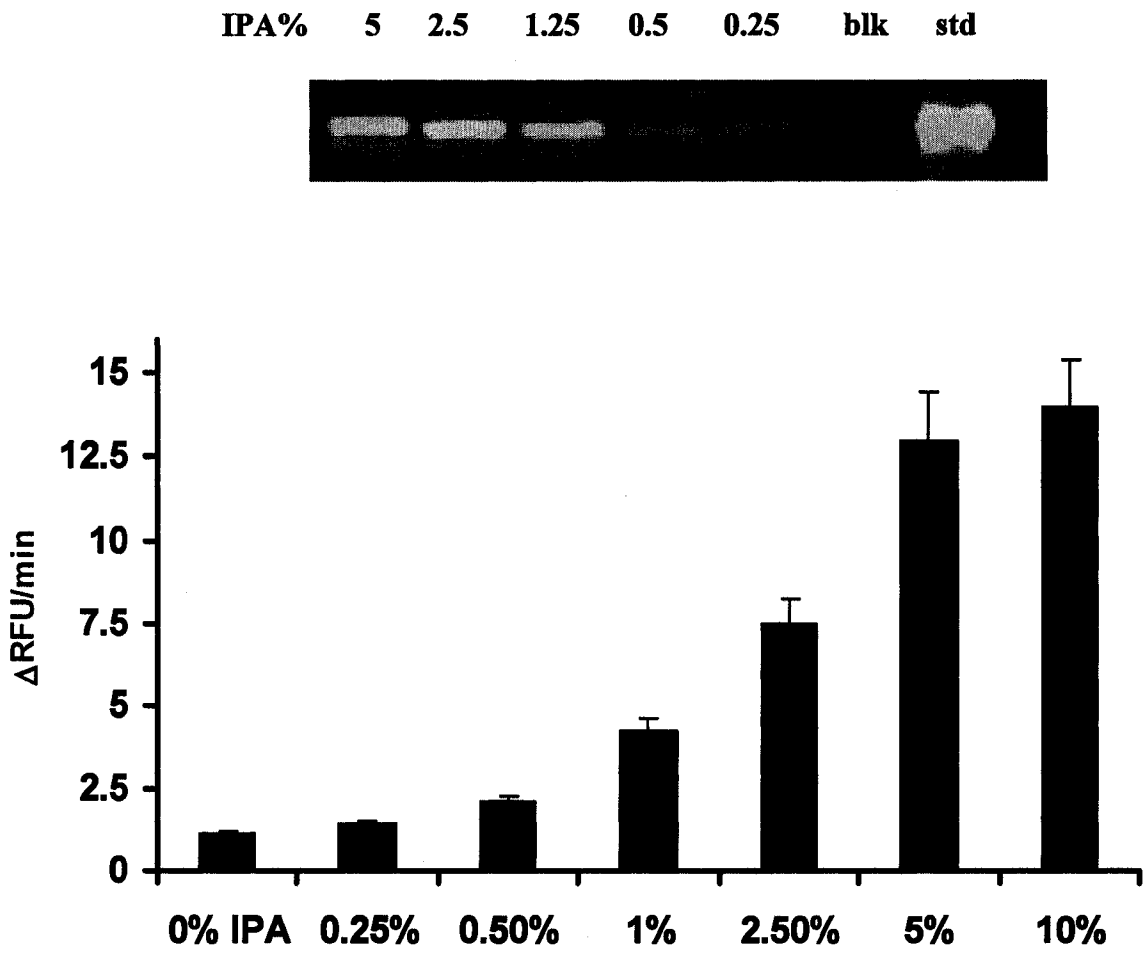

Figure 4.15 Washing of psPDI by IPA

Platlelets ($8x10^7$ / mL) were incubated with varying concentration of isopropanol (IPA) (0.25% to 5%) for 5 min followed by the separation of supernatant from the platelets by centrifugation at 2000g for 15 min. The supernatant was then tested to PDI activity using Di-E-GSSG assay as described earlier and subjected to western blot analysis.

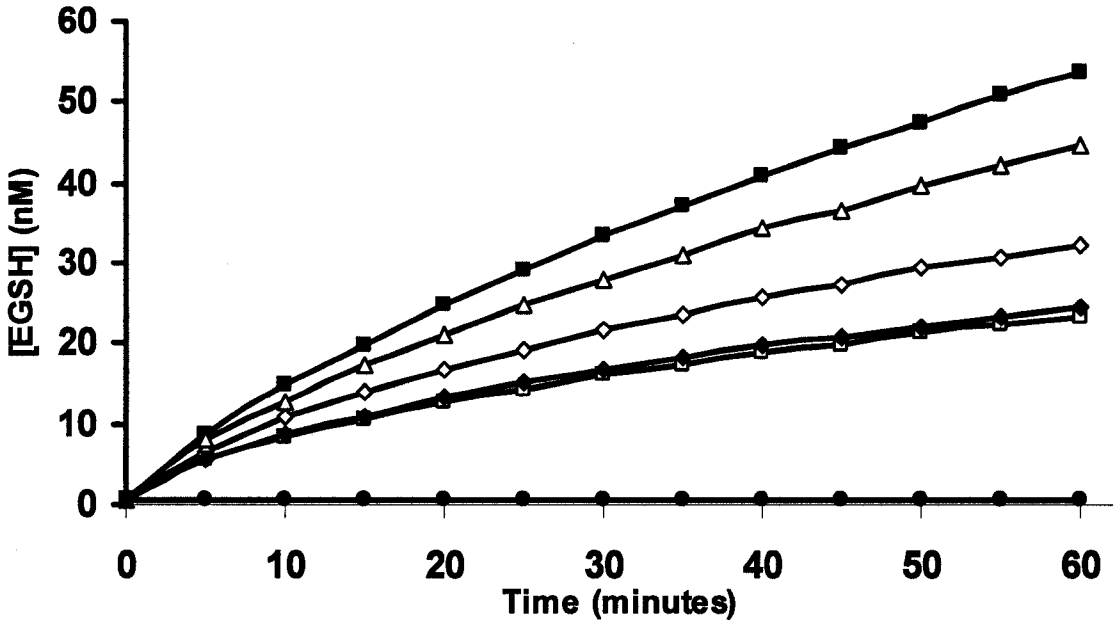

Figure 4.16 psPDI activity in variable [GSH] / [GSSG]

Platelets ($4x10^8$ / mL) were incubated with 500 μM GSH and 50 μM (filled squares), 100 μM (hollow triangles), 200 μM (hollow diamonds) and 500 μM (filled diamonds) GSSG for 15 min and then the activity was measured as described above. One sample of platelets was tested without any addition of [GSH] or [GSSG] (hollow squares). Incubation of substrate with GSH alone (20 μM) is represented by filled circles.

4.5 Discussion

Here, we have synthesized a fluorescent probe by covalently attaching two eosin molecules to the two free amino groups of glutathione disulfide so as to form Di-E-GSSG. The proximity of two eosin molecules leads to fluorescent self-quenching and makes the molecule relatively non-fluorescent. Upon addition of PDI (5 nM to 20 nM) at minimal concentration of DTT (5 μM), there was ~70-fold increase in fluorescence that saturates within 4 min, thus demonstrating the sensitivity as well as rapidness of the assay for reductase activity (Figure 4.2 and Figure 4.3).

This assay can be easily optimized to monitor the reductase activity of other enzymes of the PDI family. Even at these low concentrations, the assay was shown to reduce the substrate (~4 moles of EGSH per mole of PDI monomer) in the absence of any reductant. This encouraged us to exploit the assay for studying the redox state of PDI after incubating it in variable [GSH] / [GSSG] buffer. After equilibration of PDI redox state, it was incubated with the probe and substrate reduction with no turnover was monitored as a function of [GSH] / [GSSG] (1:1 to 20:1). The decrease in generation of reduced substrate was proportional to oxidation of reduced PDI and thus reported the fraction of red-PDI. Redox properties of PDI have also been studied in past using scRnase assay (Hawkins *et al.*, 1991; Lundstorm and Holmgren, 1993). In these methods PDI was incubated in variable [GSH] / [GSSG] ratio followed by blocking of reduced thiols with alkylating agent like iodoacetate. The alkylated PDI, after the removal of excess iodoacetate by dialysis or gel filteration, was then tested for its ability to convert scRNase into native active form and the loss in activity was attributed to loss of active site thiols of

PDI. This method of determining thiol content of PDI seems to differ from our method in two ways; 1) It involves an additional step of blocking of reduced thiols of PDI with iodoacetate and 2) Unlike our assay where the fraction of PDI-dithiols were directly calculated from the loss of red-PDI activity, in this method fraction of reduced PDI was calculated based on percentage of residual isomerase activity. However, the value obtained for K_{ox} with our method (Figure 4.12) is comparable to the values reported in literature using this method (Hawkins *et al.*, 1991) or other methods (Darby and Crieghton, 1995; Schwaller *et al.*, 2003) and corresponds to the redox potential of ~ -155 mV for PDI active site thiols.

The ratio of [GSH] / [GSSG] in cells varies from 30:1 to 100:1 making the environment highly reducing. Therefore under these conditions formation of disulfide bond is highly unlikely. Figure 4.11 shows that [GSH] / [GSSG] $\geq$ 8:1 gives complete one turnover and thus keeps PDI in completely reduced state suggesting the presence of only reduced form of PDI in cytosol (Turano *et al.*, 2002) or in any other environment where this, or higher ratio is maintained. However, Hwang *et al.* (1992) showed that the lumen of endoplasmic reticulum, a place for protein folding and disulfide bond formation, is 20 to 100 times more oxidizing than cytosol where the ratio of [GSH] / [GSSG] is 1:1 to 3:1. Our data (Figure 4.11) shows that at the ratio of ~ 2.5:1, half of PDI is in the reduced state suggesting that in the ER PDI is likely to be present in ~50% oxidized and ~50% reduced state. This observation is interesting in view of the fact that Schwaller *et al.* (2003) have proposed that catalysis of disulfide bond by PDI involves cycle of oxidation and reduction of substrate for proper folding. It is possible that redox ratio of 3:1 in ER favors

protein folding mediated by PDI by keeping it in half oxidized and half reduced state so that it can contribute effectively to the cycles of oxidation and reduction.

This assay was also optimized in the plate reader where it can detect continuous reductase activity even with 100 fmol of PDI (data not shown) and therefore, to our knowledge, is the most sensitive assay for monitoring disulfide reductase activity. In view of its high sensitivity, the assay is suitable for studying PDI activity on the exofacial surface of the various cells where it is expected to be in picomolar range. Figure 4.14 shows the assay can be used for continuous monitoring of psPDI activity. The presence of PDI on the surface of various cell lines is generally confirmed by immunological techniques. However, study of continuous exofacial reductase activity is severely hindered because of the lack of sensitive assay. We believe this assay, owing to its simplicity and sensitivity, can be easily extended to study cell surface reductase activity in various cell lines like hepatocytes, endothelial cells, fibroblasts, T-cells or monocytes where the presence of surface PDI has already been established.

When we challenged surface reductase activity of platelet with increasing [GSSG] (100 μM to 500 μM) at fixed [GSH] (500 μM), there was dose dependent decrease in activity suggesting the oxidation of PDI-dithiols by GSSG (Figure 4.15). Although the mechanism for the reduction of csPDI is not yet known, plasma [GSH] / [GSSG] ratio may contribute to the redox state of PDI. It has earlier been reported that short term exposure of cells to GSSG leads to overall decrease in surface thiols suggesting its regulatory role in maintaining the thiol content of exofacial proteins. Previous studies

have shown that the entry of HIV virus requires the exofacial reductive activity of PDI (Matthias and Hogg, 2003) or thioredoxin (Sahaf *et al.*, 2005) and therefore it can be hypothesized that reducing extracellular environment would promote reductive function of these enzymes that would facilitate viral entry in cells and the progression of disease. In line with this hypothesis, Sahaf *et al.* (2005) have shown that while the intracellular GSH level is low in HIV patients, the surface thiol content is higher suggesting that the exofacial surface in these patients are more reducing.

In summary, the work described here presents a new tool to monitor disulfide reductase activity of PDI with a sensitivity range that has not been reported in past. The assay was used to study the dithiol equilibrium state of PDI under variable ratio of GSH / GSSG and suggests that PDI in the ER is expected to be in closer to half reduced and half oxidized state whereas at the ratio $\geq$ 8:1, it is completely in reduced state. It also suggests that GSSG may play important role on the regulation of redox state of surface thiols where the primary function of PDI like proteins is believed to be reductive.

Chapter 5

Platelet Derived Microparticles have Surface Associated PDI: Implications for Platelet Aggregation and Type II Diabetes

5.1 Introduction

5.1.1 Platelets

Platelets are irregularly-shaped, colorless non-mitotic fragments present in the blood that are derived from the bone marrow cells called megakaryocytes. The formation of platelets from mitotic stem cells is regulated by thrombopoitin, a glycoprotein hormone, through a process known as thrombopoisis. Microscopically, platelets look like flattened discs or spiky ovals, with an average size of 1 to 3 μm.

(i) Structure: The overall structure of the platelet can be explained by the help of Figure 5.1. It contains an outer phospholipid bilayer, a microtubular cytoskeleton, secretory granules, mitochondria and lysosomes.

The outer coat of platelet's phospholipid bilayer is characterized by glycoproteins (GP). GP have essential roles in platelet activity and play a central role in platelet secretion and aggregation. The two most crucial surface receptors are GPIbIIa and GPIIb-IIIa for the binding of collagen and fibrinogen respectively. The surface of the platelet contains an open canicular network, through which its granular contents are secreted.

The internal surface has a dense tubular system that stores calcium ions and, together with cytoskeleton, regulates the shape of platelets once they are activated (Fuse, 1996). Internally, platelets contain dense bodies, alpha granules, lysosomes and mitochondria. The alpha granules are comprised of von Willebrand factor, platelet factor 4, platelet derived growth factor (PDGF), fibrinogen, fibronectin factor V and thrombospondin

while the dense granules contain ATP, ADP, calcium and serotonin. Once activated, these granules secrete their content through the open canicular network. The activation of platelet by various physiological agonists is mediated by their interaction with surface receptors that are summarized in Table 5.1.

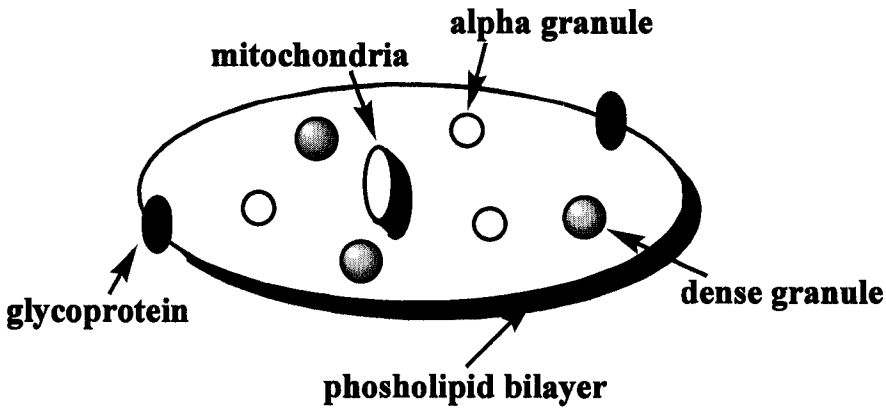

Figure 5.1 Overview of platelet structure and composition

Table 5.1 Summary of platelet activators and their platelet surface receptors

Agonist	Surface receptor
Collagen	GPIbIIa, GPVI
Fibrinogen	GP IIb-IIIa
Thrombin	PAR1, PAR1
ADP	P2Y1 and P2Y12
Adrenaline	alpha 2
Thromboxane A_2	TP
von-Willebrand factor	GPIb-IX-V
Human neutrophil elastase	$\alpha_{IIb}\beta_3$
Serotonin	5HT-2c

(ii) Function: The primary function of platelets are in hemostasis, a physiological process to minimize the blood loss at the time of vascular injury. Under basal condition platelets are non-adhesive and circulate in the resting stage without any interaction with the endothelium. Upon vascular injury, the subendothelial matrix is exposed to the platelets that initiate the surface interaction between collagen and surface receptors. Collagen interacts either directly with its receptor GPIbIIa or indirectly through von Willebrand factor to receptor GPIb/IX. The platelet-platelet interaction occurs by the

binding of fibrinogen to its receptor GPIIbIIIa resulting in the formation of primary hemostatic plug. Fibrinogen is further converted into insoluble network of fibrin by the catalytic activity of thrombin that eventually leads to the formation of an insoluble clot.

In general, the activation of the platelet by its agonists, such as thrombin and collagen, stimulates hydrolysis of membrane phospholipids that leads to the generation of more inositol 1,4,5-biphosphate (IP_3). The elevated levels of IP_3 results in the increase of intracellular calcium levels which cause polymerization of monomeric G actin into double helical microfilament called F actin as well as phophorylation of myosin (Leopold and Loscalzo, 1995). These modifications in the actin and myosin stimulate a change in shape of platelets. Platelet activation further results in the transport of phosphotidyl ethanolamine and phosphotidyl serine, negatively charged phospholipids, from the internal membrane to the outside. Due to this, the external surface of platelet becomes negatively charged and provides an ideal catalytic surface for the propagation of aggregation and secretion. It has been shown that the binding between collagen or fibrinogen to its integrin receptor, GPIbIIa or GPIIbIIIa, requires disulfide reshuffling that is mediated by PDI (Essex *et al.* 1999, Lahav *et al.*, 2002).

5.1.2 Microparticles

Microparticles are small vesicles that are derived from a variety of cell types upon activation or during apoptosis. These were first described by Wolf (1967) as 'platelet dust' that were present in normal human plasma as minute particles and showed procoagulant activity comparable to intact platelets (Hardisty and Hutton, 1966; Wolf, 1967). Later it was suggested that these microparticles are generated by the fracturing of

membrane buds from extended platelet peudopods (Crowford, 1971). Although the majority of microparticles circulating in the plasma are derived from platelets (PMP), they can also be derived from erythrocytes, monocytes, granulocytes, lymphocytes and endothelial cells.

5.1.2.1 Characterization and detection of microparticles

The size of microparticles, irrespective of their origin, is very small ranging in size from 0.1 to 1 μm. One interesting feature of MPs is that they have many exofacial antigens that are also exposed in their parent cells. Due to this, the cellular origin of microparticles can be ascertained by using antibodies against specific surface antigen. Table 5.2 summarizes the unique surface antigen present in microparticles derived from various cell types. Another important feature of microparticles is that their exofacial suface is negatively charged because phosphotidyl serine (PS),a negatively charged phospholipid that is present in inner membrane in non-stimulated cells, is exposed to the surface. Therefore, all the microparticles are positive to annexin V, a protein that binds to negatively charged phospholipids.

Table 5.2 Surface antigen in microparticles

Cell type	Antigens
Platelet	αIIbβ3 , CD42b, CD31, P-selectin, CD61
erythocytes	Glycophorin A
granulocyte	CD66
Lymphocyte	CD4, CD8
Endothelial cells	CD62E, CD31, CD34, CD51, CD146

Microparticles are generally detected using flowcytometry which is a powerful technique for monitoring, characterizing, counting and sorting microscopic particles. In this technique, the microparticles are characterized by size (forward scatter, FSC), density (side scatter, SSC) and positive signal obtained by labeling their surface antigens with fluorescently labeled antibodies (Table 5.2). The intensity of fluorescence obtained is the indirect measure of the amount of antigen exposed onto the surface of microparticles. Apart from flow-cutometry, electron microsopy and enzyme-liked immunosorbent assay (Nieuwland and Sturk, 2002) are other techniques that can also be utilized for their detection.

5.1.2.2 Generation of microparticles from platelets

Stimulation of platelets with endogenous agonists such as thrombin, collagen, thromboxane, serotonin, epinephrine or ADP results in their activation and secretion. Upon activation, platelets generate microparticles by membrane vesiculation. The mechanism resulting in generation of microparticles by activated platelets is still unclear and a matter of investigation. Preliminary evidence suggests that, upon activation, there is an increase in intracellular levels of calcium ions that result in the activation of enzyme calpain (Horstman and Ahn, 1999; Nieuwland and Sturk, 2002). This enzyme has been shown to degrade cytoskeletal proteins and inhibition of its activity inhibits agonist induced microparticle formation (Shcherbina and Remold, 1999). This observation is supported by the fact that addition of calcium ionophore directly enhances the generation of microparticles. Alternatively, microparticles are also generated upon prolonged storage of platelets (George *et al.*, 1986; Keuren *et al.*, 2006).

5.1.2.3 Role of PMPs in coagulation and diseases

It is now well established that, i*n vitro*, microparticles can both initiate and propagate coagulation (Ando *et al.*, 2002; Nomura, 1998; Warkentin *et al.*, 1994) The procoagulant activity of microparticles is generally attributed to the presence of negatively charged exofacial surface that binds to Gla-domains of coagulation factors (Va, IXa and VIIIa) in the presence of calcium ions and provides more binding site per unit surface area as

compared to activated platelets (Sabatier *et al.*, 2002). In addition, it has been shown that MP have surface exposed tissue factor (TF), a 45 kDa transmembrane protein that binds to factor VII and catalyzes the conversion of factor X (inactive) into factor Xa (active) which, in turn, converts prothrombin into thrombin and hence propagate aggregation. Recently it was shown that 10% of PMP expresses active tissue factor that, in part may be responsible for microparticle mediated aggregation.

The procoagulant activity of microparticles can be quantified using the thrombin generation assay where the conversion of chromogenic substrate by thrombin is monitored spectrometrically (Diamant *et al.*, 2002). In this system, microparticles supply the procoagulant surface and a possible initiator of coagulation, e.g. tissue factor, and plasma provides the necessary coagulation factors. In this assay, the generation of thrombin is completely dependent on the presence of microparticles, and in their absence no coagulation occurs.

The clinical relevance of PMP is currently under investigation in many diseases. Studies have shown significant differences between level of PMP circulating in healthy subjects and those found in patients suffering from various diseases such as cardiovascular diseases (VanWijk *et al.*, 2003), diabetes mellitus (Diamant *et al.* 2002; Nomura *et al.*, 1995), sepsis (Nieuwland *et al.*, 2000) and severe hypertension (Preston, 2003). PMPs have also been shown to be an important component of the human atherosclerotic plaque (Mallat *et al.*, 1999). Interestingly, the number of clinical disorders associated with elevated PMPs is increasing with new investigations.

Here we have shown by using fluorescent spectrophotometry, flowcytometry and immunological techiniques that platelet derived microparticles have surface-associated PDI (msPDI). Recently an increased level of microparticles were found in patients with type II diabetes (T2D) and was suggested to be related to enhanced platelet activation (Koga *et al.*, 2006; Nomura *et al.*, 1995). We have explored the role of microparticle surface PDI (msPDI) in platelet activation and aggregation and its possible implications in T2D.

5.2 Materials and Equipment

5.2.1 Materials

Ammonium persulfate; Sigma-Aldrich Canada Ltd., Oakville, Ontario

Ammonium sulfate; Sigma-Aldrich Canada Ltd., Oakville, Ontario

Biorad Protein Assay (Bradford Reagent); Bio-Rad Laboratories USA, Hercules, California

Bovine Insulin, Sigma-Aldrich Canada Ltd., Oakville, Ontario

Eosin isothiocyanate; Sigma-Aldrich Canada Ltd., Oakville, Ontario

Ethylene diamide tetraacetic acid; Sigma-Aldrich Canada Ltd., Oakville, Ontario

Monoclonal anti-PDI antibody RL90; Abcam USA, Cambridge, MA

Oxidized glutathione; Sigma-Aldrich Canada Ltd., Oakville, Ontario

Phenylarsine oxide; Sigma-Aldrich Canada Ltd., Oakville, Ontario

Potassium phosphate; Sigma-Aldrich Canada Ltd., Oakville, Ontario

Reduced glutathione; Sigma-Aldrich Canada Ltd., Oakville, Ontario

Sephadex G-25; Sigma-Aldrich Canada Ltd., Oakville, Ontario

Sodium Chloride; Sigma-Aldrich Canada Ltd., Oakville, Ontario

Sodium phosphate monobasic; Sigma-Aldrich Canada Ltd., Oakville, Ontario

5.2.2 Equipment

Agilent 8453 UV-VIS Spectrophotometer;
Agilent Technologies Canada Inc, Mississauga, Ontario

BioRad Fraction Collector Model 2110;
Bio-Rad Laboratories (Canada) Ltd., Mississauga, Ontario

Cytomics FC500 flow cytometer
Beckman Coulter, USA

Hemocytometer;
Reichert Co, Buffalo, NY

Jouan CR3i Centrifuge;
Jouan Inc., Winchester, Virginia

Labconco FreeZone 4.5 Liter Benchtop Freeze Dry Systems;
Laconoco Corporation, Kansas City, Missouri

Mettler AJ100 Balance;
Mettler Toledo Canada, Mississauga, Ontrio

Microtiter 96-well Solid Plate;
Thermo Electron Corp. Canada, Burlington, Ontario

Northen Eclipse 6.0 Imaging Software;
Empix Imaging Inc., Mississauga, Ontario

NUAIRE Biological Safety Cabinet Class II Type A/B3;
Thermo Electron Corp. Canada, Burlington, Ontario

Orion Model 420A pH Meter;
Thermo Electron Corp. Canada, Burlington, Ontario

Stir Plate 360 Series;
VWR International, Mississauga, Ontario

Varian Eclipse Fluorescence Spectrophotometer;
Varian Canada, Mississauga, Ontario

Zeiss Axiovert 200inverted Fluorescence Microscope;
Empix Imaging Inc., Mississauga, Ontario

5.3 Methods

5.3.1 Preparation of Dieosin-GSSG and Dieosin-Insulin

Dieosin-GSSG was prepared as described previously (Chapter 4, page 110). For preparing Dieosin-Insulin, Insulin (200 μM) was incubated with 5 fold excess of eosin isothiocyanate in phosphate buffer (100 μM sodium phosphate and 2 mM EDTA, pH 8.5) for 8 h at room temperature (25 °C). The sample (100 μL) was passed through a Sephadex G-25 column (100 mm x 10 mm) at 1 h intervals and 500 μL aliquots were collected with the help of a fraction collector. Aliquots were quantified for Insulin content by Bradford assay and for eosin by using e=88000 $M^{-1} \cdot cm^{-1}$ (Lettinga, 2004). Extent of eosin labeling was estimated by dividing [eosin] with [insulin]. It was observed that the predominant product after 4 hours of incubation was dieosin insulin. This sample was tested for maximum fluorescence on a Varian Cary Eclipse fluorescence spectrometer with excitation at 525 nm and emission at 545 nm after the addition of 10 mM DTT. All the fractions that showed 4-fold increase in the fluorescence were pooled and stored at -80 °C.

5.3.2 Diabetic Inclusion criteria: Healthy versus Diabetics

Healthy human subject (n=10), ages 35-70 years were chosen to participate in the study only if they showed no overt symptoms of disease and were taking no medication. Diabetic human subjects, ages 35-70 (n=10) were chosen to fulfill the criteria of the Expert Committee on the Diagnosis and classification of Diabetes Mellitus (Type 2).

Patients on diet treatment alone or diet treatment in combination with oral hypoglycemic agents were included in the study. However, subjects taking investigational agents, insulin or that were pregnant were excluded from the study. The experimental protocol was approved by University of Windsor Research Ethics Board.

5.3.3 Isolation of Microparticles

Platelet derived microparticles present in the plasma were isolated as described by George *et al.* (1982) with some modifications. Briefly, 1 unit of blood was centrifuged at 1000 g for 20 min at room temperature to separate platelet from plasma. The supernatant was separated and centrifuged at 5000 g twice for 15 min. The supernatant from the second centrifugation was then centrifuged at 35000 g for 45 min and the pellet obtained was stored in -80 °C after two washes in 100 μL of PBS and labeled as plasma-MP. For MP derived after platelet activation, the platelets obtained from first centrifugation was washed twice with HEPES-ACD buffer then 5 ml of $1x10^{10}$ platelets/mL was activated with 1U of thrombin for 15 min. The fractions were first centrifuged at 2000 g for 15 minutes and then the supernatant was centrifuged at 35000 g for 45 min at room temperature. The pellet was washed twice in PBS and then stored at -80 °C in PBS. Microparticle count was adjusted to $2.5x10^{7}$ /mL for disulfide reductase activity.

5.3.4 Monitoring platelet aggregation

Platelet aggregation (10^9 /mL) was studied with (hollow circles) or without (filled circles) thrombin. 5 μL (filled triangles) and 10 μL (filled squares) of MP ($2.5x10^7$ /mL) were added to the platelet suspension and the effect on aggregation was studied as a function of decrease in transmittance at 630 nm. 10 μL of MP was also added in parallel after 30 min incubation with anti PDI antibody (hollow squares).

5.3.5 Kinetics of PDI-dependent disulphide reduction

PDI disulphide reduction activity was monitored in PDI assay buffer of MPs (10 μL to 20 μL of $2.5x10^7$ /mL) to dieosin-GSSG (150 nM) in the presence of 2 μM DTT. The increase in fluorescence was monitored at 545 nm with excitation at 525 nm. The activity was inhibited using anti-PDI antibody (RL90) (10 μg/mL).

5.3.6 Analysis by Flow cytometry

Flow cytometry experiments were performed by Dr. Hudson, University of Windsor, Canada. Microparticles were analyzed in a Cytomics FC500 flow cytometer (Beckman Coulter, USA). Forward (FSC) and side scatter (SSC) were set at logarithmic gain and triggering were set at FSC. MP origin from platelet was established via binding to CD61 antibody (1:50 dilution). Surface characterization of MP was done using Annexin V and PDI antibody. For quantification of diabetic and non-diabetic plasma samples, 100 μL of plasma was directly analyzed for the presence of MP and the quantification was done as described earlier (Bode *et al.*, 1991).

5.4 Results

5.4.1 Monitoring MP-surface associated reductase activity using Dieosin glutathione disulfide (Di-E-GSSG)

As described earlier, in Di-E-GSSG, the fluorescent moieties are covalently attached to two N-terminal residues in GSSG that results in fluorescence self-quenching (FSQ) and makes the molecule relatively non-fluorescent. Upon addition of PDI, Di-E-GSSG disulfide bond was cleaved releasing proximity constraints and the fluorescence is enhanced by ~70-fold (Raturi and Mutus, 2006).

Owing to the sensitivity of the assay, we used it here for monitoring platelet derived microparticle-associated surface (msPDI) reductase activity. To this end, microparticles were added to the solution containing, Di-E-GSSG and DTT (2 μM). As shown in Figure 5.2, while no significant reduction of probe was observed with DTT alone, the sample containing microparticles showed continuous disulfide reductase activity. More importantly, this activity was blocked to ~85 % by RL90 PDI-antibody suggesting that the disulfide reductase activity is contributed by PDI present on the microparticles surface. The western blot of MPs showed the presence of a band at ~58 kDa (Figure 5.2, *inset*) that was immunoreactive to anti-PDI antibody thus establishing the presence of msPDI in microparticles.

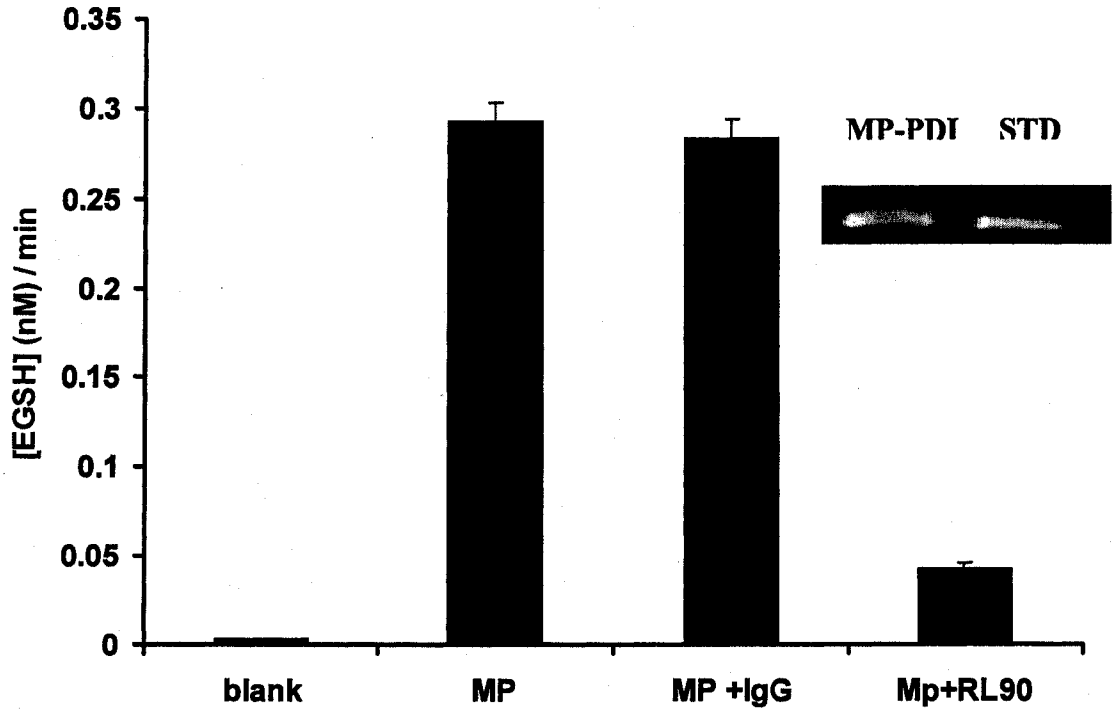

Figure 5.2 Activity and western blot analysis of msPDI

5 μL of MP ($2.5x10^7$ / mL) was added to PDI assay buffer containing 150 nM di-E-GSSG and 2 μM DTT and the activity was monitored as a function of time. In the figure 'blank' represents Di-E-GSSG incubated with DTT alone. The increase in fluorescence was converted to [EGSH] produced by using a standard of plot of [EGSH] vs fluorescence. Western blot of 20 μL MP shows an anti-PDI reactive band at 58 kDa.

5.4.2 Flow-cytometry analysis of MP

To further demonstrate the presence of surface associated PDI in MPs, plasma isolated MPs were subjected to flow-cytometry. The dot-plot showed the subpopulation of MPs that were identified by size (FSC/SSC) as well as by platelet positivity against FITC labeled annexin V [Figure 5.3, (i) and (ii)] and anti-PDI antibody [Figure 5.3, (iii) and (iv)]. The platelet origin of MPs was confirmed by using CD61 antibody. The Incubation of MPs with FITC-labeled anti-PDI antibody showed ~55 % positive binding (Figure 5.4) in the same subpopulation that showed positive binding to annexin V-FITC and CD61 confirming the presence of msPDI.

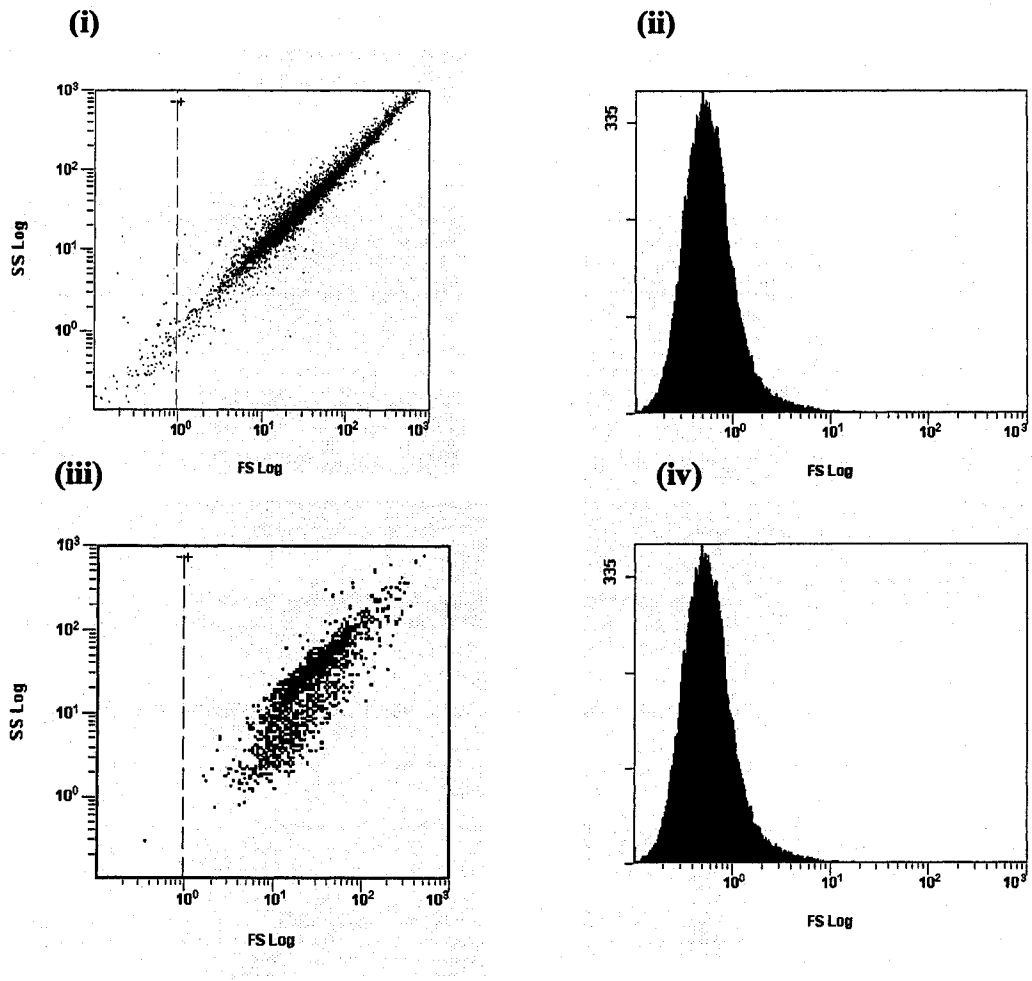

Figure 5.3 Flow cytometry of MP

MP were characterized first by FITC labeled Annexin V (i) and then by FITC labeled anti-PDI antibody (iii). Labeling with both markers gave uniform size distribution in the same region [(ii) and iv)].

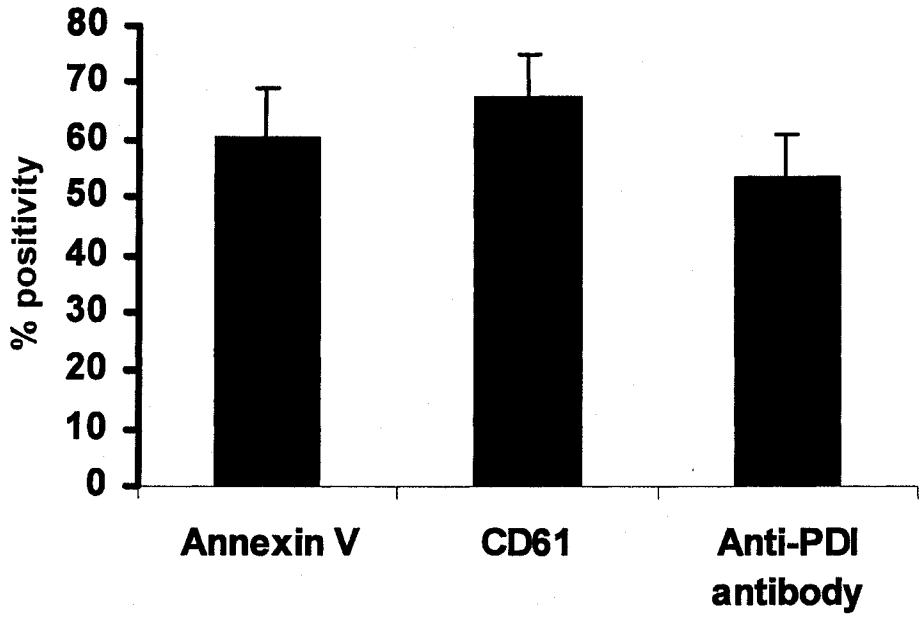

Figure 5.4 Immunoreactivity of MP with different antibodies

Anti-PDI antibody showed positive binding in same subpopulation which was positive for CD61 and Annexin V.

5.4.3 Role of msPDI in platelet aggregation

Earlier reports have suggested that microparticles enhance the activation of platelets (Berkmans 2001; Nomura, 2001). We set out to explore the role of msPDI on platelet aggregation. Addition of 20 μL of microparticles ($2.5x10^7$ /L) in platelet suspension increased the aggregation by 50% (Figure 5.5, triangles) supporting the previous reports of its proaggregatory affect. We hypothesized that this effect could be due to the msPDI that facilitates surface-surface interaction through disulfide isomerization. To test this we incubated MPs with RL90 anti-PDI antibody for 30 min followed by two washes to remove unbound antibody. Interestingly, the increase in activation was completely inhibited to control levels in the presence of anti-PDI antibody (Figure 5.5, hollow circle). These results strongly suggest the role of msPDI on the platelet aggregation.

5.4.4 MP levels in T2D and control subjects

The elevated levels of MP have been reported in numerous stress conditions including type 2 diabetes (Koga *et al.*, 2006; Nomura *et al.*, 1995). Here we compared the relative MP as well as MP-PDI content of plasma from normal (n=10) and T2D (n=10) subjects. As seen in Figure 5.6, the T2D plasma samples contained 50% more MPs per 100 μL of plasma. More significantly, the MP-PDI content (Figure 5.6) was ~ 80% larger in T2D than in controls.

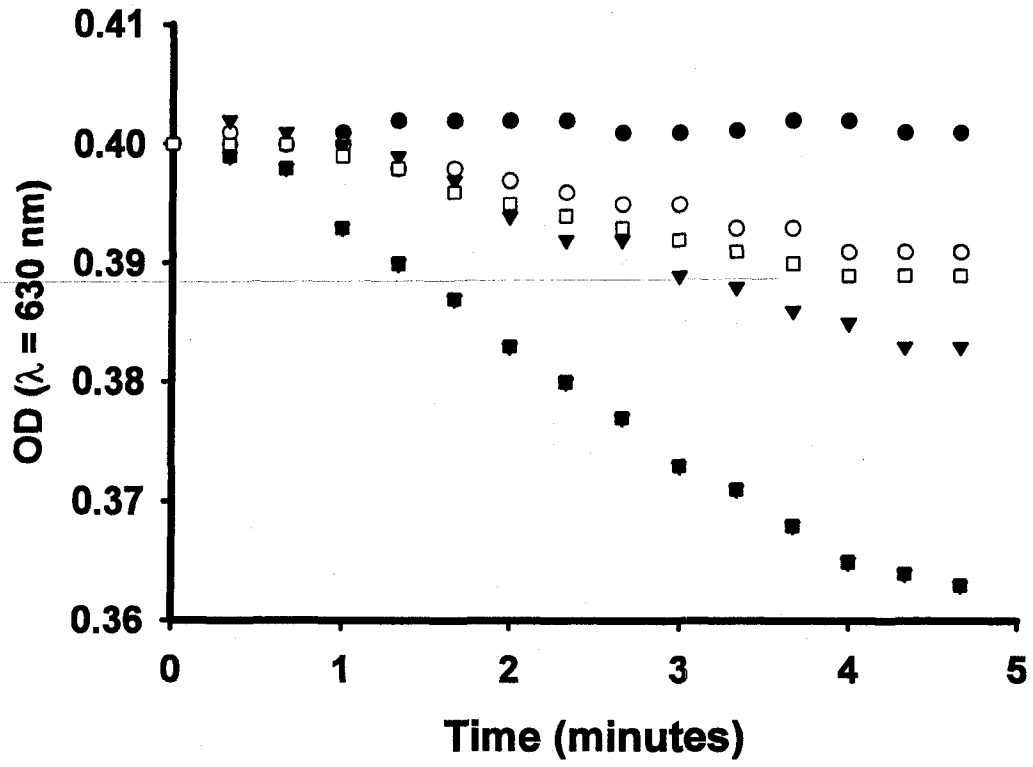

Figure 5.5 Aggregation of platelet in the presence of MP

Platelet aggregation (10^9 / mL) was studied with (hollow circles) or without (filled circles) thrombin. 5 μL (filled triangles) and 10 μL (filled squares) of MP ($2.5x10^7$ / mL) were added to the platelet suspension and the effect on aggregation was studied as a function of decrease in transmittance. 10 μL of MP was also added in parallel after 30 minutes incubation with anti PDI antibody (hollow squares).

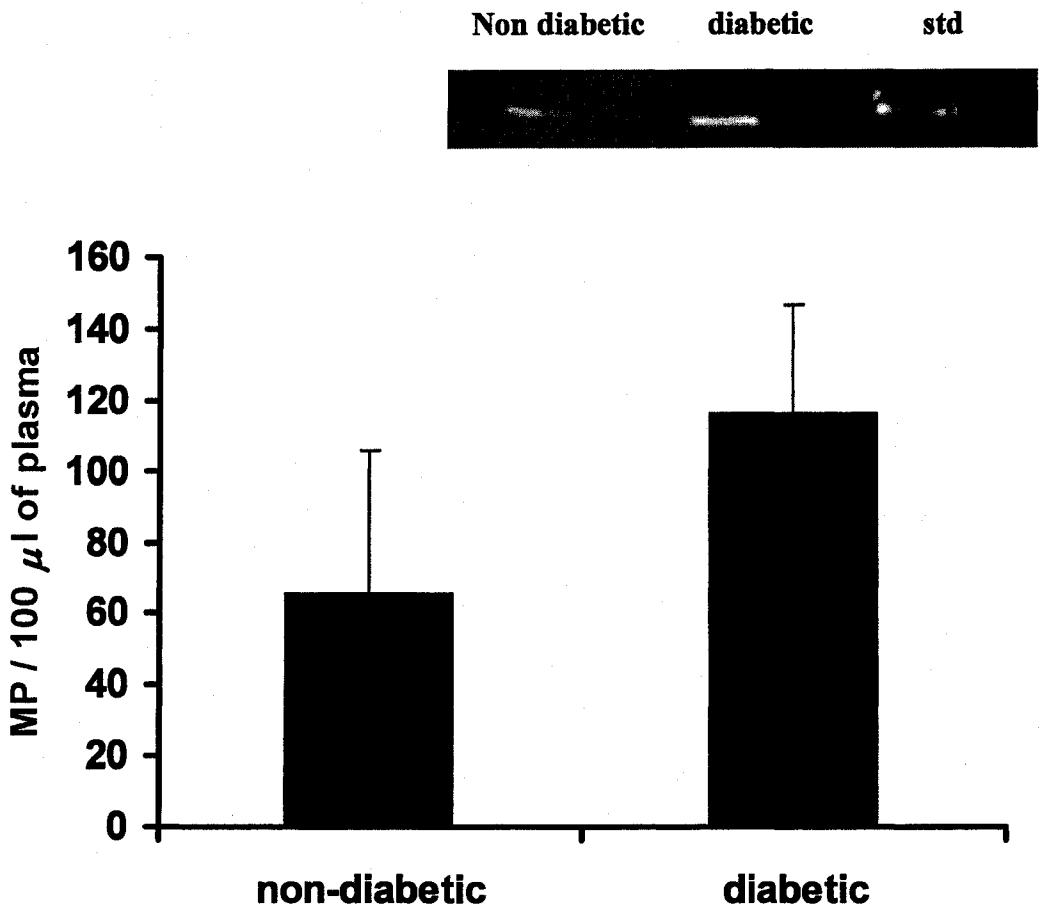

Figure 5.6 The quantification of MP from diabetic and non diabetic subjects was done using flow cytometry. For each run, the volume loaded was fixed to 100 μL. *Inset* shows the western blot analysis of MP for the presence of PDI that is obtained from 10 mL of diabetic or non-diabetic plasma.

5.4.5 Degradation of Insulin by msPDI

Insulin has two polypeptide chains, α and β, that are joined together by two disulfide bonds. It is well established that PDI can break these bonds that leads to the separation of two chains. Here, we utilized fluorescently labeled insulin at near physiological plasma concentrations to test whether msPDI can cleave disulfide bonds of insulin.

Di-E-Insulin, similar to Di-E-GSSG, has two molecules of eosin attached to N-terminus of α and β chains causing fluorescence self quenching. Upon reduction of disulfide bonds by PDI, there is ~4-fold increase in the fluorescence (Figure 5.7). Therefore, PDI mediated enzymatic reduction of insulin can be estimated by monitoring fluorescence increase caused by separation of two chains after reduction. The reduction of Insulin by PDI was found to be linear with increasing concentration of Di-E-Insulin (Figure 5.7B) even at lower nanomolar levels. Therefore assay is suitable to study csPDI mediated reduction of insulin at its near-physiological plasma concentrations. As can be seen in Figure 5.8, while no increase in the fluorescence was observed in sample containing Di-E-Insulin and DTT (Figure 5.8, diamonds), addition of MP (Figure 5.8, squares) caused time dependent increase in the fluorescence suggesting reduction of insulin by msPDI. More importantly, the reductase activity was completely inhibited in the presence of RL90 antibody confirming that the reduction of insulin was attributed to surface PDI (Figure 5.8, triangles). The fact that diabetic patients have higher number of circulating MPs in the plasma (Figure 5.6) clearly suggests higher levels of msPDI mediated reduction of Insulin.

A.

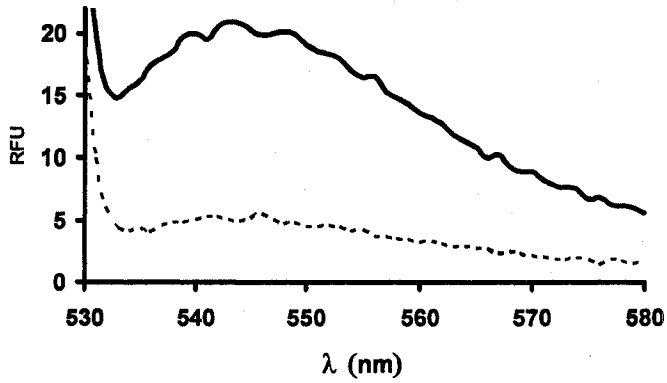

B.

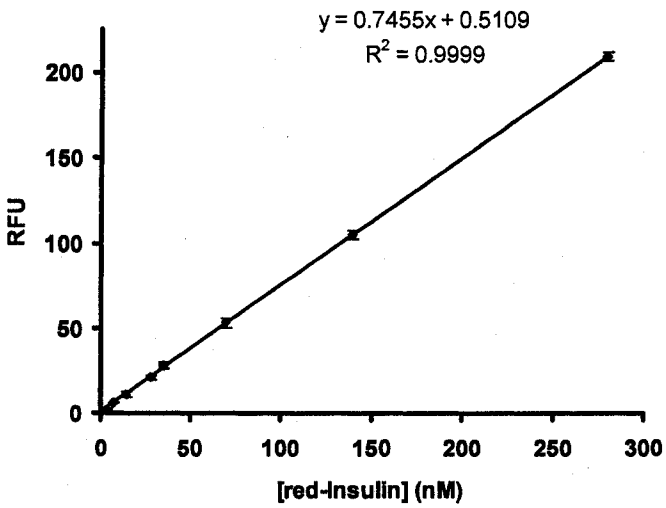

Figure 5.7 Reduction of Di-E-Insulin by either DTT or PDI

A. Maximum fluorescence before (dashed line) and after (dark line) the addition of PDI in the presence of 5 μM DTT **B.** Reduction of [Di-E-Insulin] by either DTT (10 mM) or PDI (10 nM) showed complete linearity with Increasing [Di-E-Insulin].

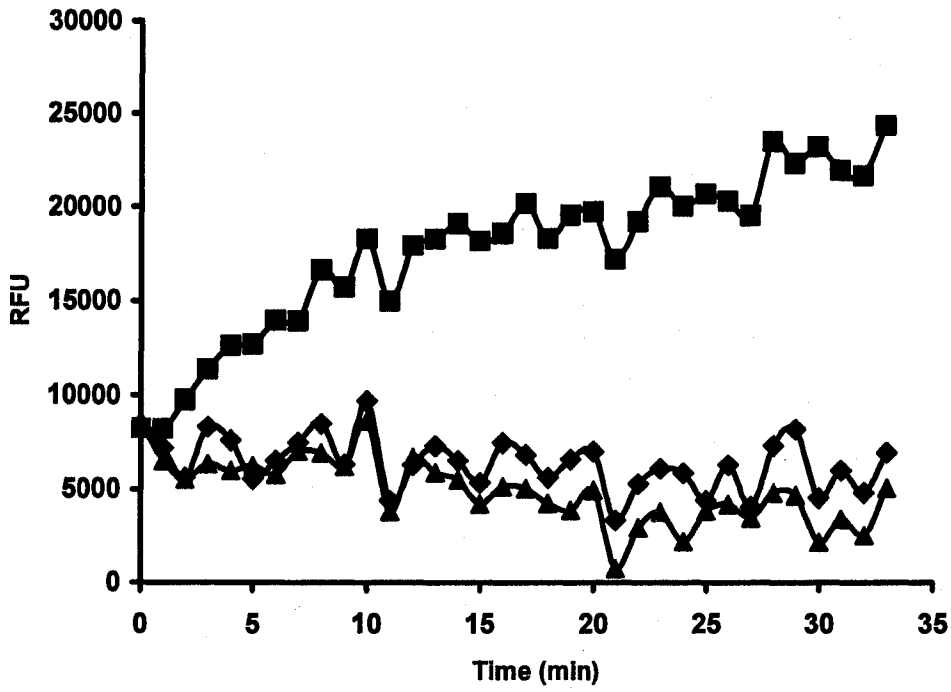

Figure 5.8 Reduction of Di-E-Insulin by msPDI

100 nM of Di-E-Insulin was incubated with 5 μM DTT in the absence (triangles) or presence (squares) of MP (10^7/mL) and the fluorescence increase was monitored as a function of time at 525 nm. The assay was also performed in the presence of MP and RL90 antibody (diamonds).

5.5 Discussion

In this study we have described, for the first time, the presence of PDI on the surface of microparticles. The activity of PDI was studied using fluorescently labeled glutathione disulfide (Di-E-GSSG) that clearly demonstrated the presence of surface PDI in catalytically active form (Figure 5.2). The presence of msPDI was further confirmed by western blot analysis (Figure 5.2, inset) as well as by flow-cytometry (Figure 5.3).

The procoagulant activity of microparticles is known for decades and has been compared to intact platelet aggregation (Wolf, 1967). The bleeding disorder associated with Scott syndrome and Castaman's disease has been attributed to low levels of plasma microparticles (Castaman *et al.*, 1997; Toti *et al.*, 1996). On the contrary, elevated levels of plasma microparticles are shown to be present where there is thromboembolic risk or vascular damage (Kahn *et al.*, 1973) as well as in cardiovascular disease (VanWijk *et al.*, 2003) and diabetes mellitus (Koga *et al.*, 2006; Nomura *et al.*, 1995).

In agreement with previous studies, we also observed that platelet aggregation increases significantly in the presence of MP (Figure 5.5). Moreover, levels of platelet derived microparticles as well as msPDI were higher in T2D by 50 % and 80 % respectively as compared to control (Figure 5.6 and *inset*). However, this proaggregatory effect of MP was reversed to control levels in the presence of RL90 antibody (Figure 5.5, hollow circles) that clearly demonstrates the role of PDI in MP mediated proaggregation. In view of the large contribution of msPDI to platelet aggregation demonstrated here,

elevated numbers of MP containing larger than normal PDI activity could potentially be a major contributing factor to platelet hyperactivity observed in T2D.

We have also shown here that msPDI can break insulin into its two polypeptide chains by reducing the disulfide bonds between them. The biological action of insulin is mediated via its binding to insulin receptor (IR), a transmembrane tyrosine kinase consisting of two exofacial α-subunits and two intracellular ß-subunits. Insulin binds to the extracellular α-subunit that results in the conformational changes in the protein leading to autophosphorylation of tyrosine residues of the β-subunit (Figure 5.9) (Tiang, 2005; Le Roith and Zick, 2001).

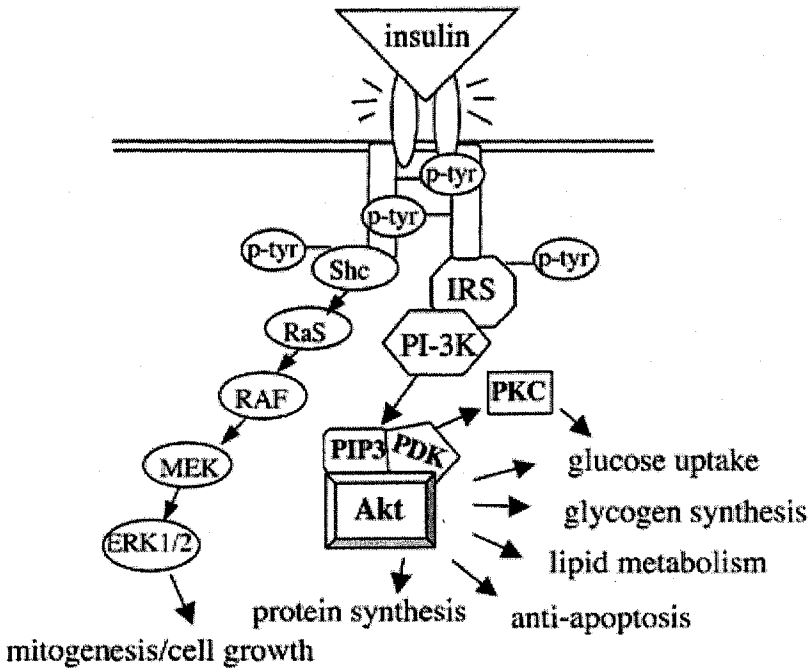

Figure 5.9 Insulin signaling after receptor binding (Tiang, 2005).

This autophosphorylation of IR results in activation of the receptor kinase and tyrosine phosphorylation of substrates for IR that serve as docking sites for downstream effectors (Figure 5.9). It is likely that PDI mediated insulin degradation will impair its binding to receptor that may contribute, in part, to the development of insulin resistance. This hypothesis is supported by an earlier finding where it was shown that defect in insulin binding to its receptor may lead to insulin resistance (Roach *et al.*, 1994).

The procoagulant activity of microparticles is generally attributed to the presence of negatively charged exofacial surface that binds to Gla-domains of coagulation factors (Va, IXa and VIIIa) in the presence of calcium ions and provides more binding site per unit surface area as compared to activated platelets (Diamant *et al.*, 2004). In addition, it has been shown that MP have surface exposed tissue factor (TF), a 45 kDa transmembrane protein that binds to factor VII and catalyzes the conversion of factor X (inactive) into factor Xa (active) which, in turn, converts prothrombin into thrombin and hence propagate aggregation. Recently Chen *et al.*, (2006) showed that the TF is generally in its cryptic form where its exofacial Cys186-Cys209 disulfide bond is in the reduced state and its activation requires formation of disulfide bond. This hypothesis was based on the observation that addition of reducing agent diminished TF activity while addition of oxidizing agent potentiated it. Our results, together with this observation, demonstrate the need of studying the co-localization of PDI and TF on MP membrane. It is possible that activation of TF is mediated by the catalytic activity of PDI that converts the cryptic form of TF into active disulfide form. Higher levels of TF exposing MP have

been reported in uncomplicated T2D (Diamant *et al.*, 2002). This could be linked to elevated aggregation in diabetic patients through PDI activity which is likely to be in oxidized state on account of elevated oxidative-stress in T2D. Therefore, PDI would more effectively convert reduced-cryptic form of TF into its disulfide-active form on account of its high reduction potential that makes it a better oxidant for protein thiols.

Chapter 6

Conclusions

Although PDI is primarily known to act on disulfide bonds or thiols, its *S*-denitrosation activity has also been reported in several studies. However, this activity has not been well characterized. Here we set out to kinetically analyze the GSNO denitrosation activity of human recombinant PDI. In Chapter 2 we studied the denitrosation activity of PDI by means of simple and sensitive assays. To date, the only probe used for monitoring the denitrosation activity of PDI is N-dansyl-S-nitrosohomocysteine (DansylHCysNO). We have presented another means for monitoring the denitrosation activity of PDI. DAN is a relatively nonfluorescent compound and reacts with NOx to form the highly fluorescent compound napthotriazole NAT. Our findings suggest that DAN is a highly sensitive tool for studying PDI denitrosation activity which is also unique in deciphering the fate of nitric oxide once it is released from RSNOs. Furthermore, *S*-nitrosoglutathione (GSNO) denitrosation activity of recombinant human PDI was kinetically optimized and characterized by monitoring the loss of the S-NO absorbance at 343 nm.

By using these sensitive assays, we have proposed a catalytic mechanism for PDI that involves a nitroxyl disulfide intermediate. Our results suggest that it is NO· and not NO^- being formed during the GSNO denitrosation by PDI, which is in agreement with a previous study presented on GSNO denitrosation. It has been established that PDI is continuously secreted from cells like endothelial cells that are net producers of Nitric oxide. Our study has demonstrated that PDI can be *S*-nitrosated to form PDI-SNO which, in turn, can be denitrosated by PDI suggesting that this enzyme could be intimately involved in the transport of nitric oxide across the membrane.

In Chapter 3 and Chapter 4, we set out to characterize PDI-disulfide reductase activity. Disulfide reductase activity of PDI is generally monitored by insulin turbidity assay or scrambled RNase assays, both of which are performed by UV-visible spectroscopy and thus lacks required sensitivity. We have established a sensitive fluorimetric assay for continuous determination of disulphide reduction activity of PDI. A new fluorogenic pseudosubstrate designed for PDI is Di-E-GSSG that is relatively non-fluorescent and gives ~70-fold increase in the fluorescence signal upon reduction of disulfide bond. The substrate was used to develop highly sensitive disulfide reductase assay that can detect as low as 100 femtomoles of PDI. The assay is sensitive enough to detect enzyme activity in the absence of any reducing agent and thus, to our knowledge, is the most sensitive assay for monitoring disulfide recustase activity of PDI.

We have utilized this assay to study the oxidation kinetics of PDI-dithiols under variable redox environment. Based on our findings we have reported that, PDI would be in ~ ½-reduced state where [GSH] / [GSSG] ratio is between 1:1 to 3:1, conditions similar to the lumen of endoplasmic reticulum or in the extracellular environment. On the other hand, ratio of ~ 8:1 or higher, such as in cytosol, would keep PDI in completely reduced state. Furthermore, we showed that GSSG plays important role on the regulation of redox state of surface thiols of platelets where the primary function of PDI like proteins is believed to be reductive.

In Chapter 5 we utilized our sensitive fluorescent assays as well as immunological techniques and flow cytometry to demonstrate that the platelet derived microparticles contain protein disulfide isomerase. These microparticles were previously reported to enhance platelet activation. Our results suggest a central role for surface associated PDI on the proaggregatory effect of microparticles on platelets. In addition, we detected increased levels of PDI-containing microparticles in patients with type II diabetes. This observation strongly suggests that platelet hypersensitivity observed in diabetes can partially be attributed to microparticle-surface-PDI activity.

In order to characterize PDI's role in cellular processes, it is imperative to know the physicochemical basis by which it identifies its substrates. Recently we have obtained evidence that substrates dihedral angles play important role in substrate recognition by PDI (unpublished results). Future studies could be aimed towards finding a correlation between the substrate-dihedral angles and PDI disufide reductase activity. In addition, we have recently observed that PDI is also secreted into the plasma in its catalytically active form at the levels where it can inactivate insulin by breaking the disulfide bonds between the two chains. It would be interesting to study the physiological implications of soluble plasma PDI in normal and diseased state (T2D) and identify the cellular parameters that result in enhanced secretion of PDI into blood stream.

References

Abell, B.A., and Brown, D.T., (1993), *J. Virol.*, **67**, 5496-5501.

Aledort, L.M., Troup, S.B., and Weed, R.I., (1968), *Blood*, **31,** 471-479.

Ando, M., Iwata, A., Ozeki, Y., Tsuchiya, K., Akiba, T., and Nihei, H., (2002), *Kidney Int.*, **62,** 1757-1760.

Arnelle, J.S., and Stamler, J.S., (1995), *Arch. Biochem. Biophys.*, **318,** 279–285.

Askew, S.C., Butler, A.R., Flitney, F.W., Kemp, G.D., and Megson, I.L., (1995), *Bioorg. Med. Chem.*, **3,** 1-9.

Bass, R., Ruddock, L.W., Klappa, P., and Freedman, R.B., (2004), *J. Biol. Chem.*, **279,** 5257-5262.

Bazylinski, D.A., and Hollocher, T.C., (1985), *J. Am. Chem. Soc.*, **107,** 79828–79860.

Beckman, J.S., Beckman, T.W., Chen, J., Marshal, P.M., and Freeman, B.A., (1990), *Proc. Natl. Acad. Sci., USA,* **87,** 1620-1624.

Bell, S.E., Shah, C.M., and Gordge, M.P., (2006), *Biochem. J.*, in press.

Bennett, T.A., Edwards, B.S., Sklar, L.A., and Rogelj, S., (2000), *J. Immunol.*, **164**, 4120-4129.

Berckmans, R.J., Neiuwland, R., Boing, A.N., Romijn, F.P., Hack, C.E., and Sturk, A., (2001), *Haemost.*, **85**, 639-646.

Bode, A.P., Orton, S.M., Frye, M.J. and Udis, B.J. (1991), *Blood*, **77**, 887-895.

Borisenko, G.G., Martin, I., Zhao, Q., Amoscato, A.A., and Kagan, V.E., (2004), *J. Am. Chem. Soc.*, **126,** 9221–9232.

Bradford, M.M., (1976), *Anal. Biochem.*, **72**, 248-254.

Butler, A.R., Flitney, F.W., and Williams, D.L.H., (1995), *Science,* **16,** 18-22.

Cai, H., Wang, C.C., and Tsou, C.L., (1994), *J. Biol Chem.*, **269**, 24550-24552.

Castaman, G., Yu-Feng, L., Battistin, E., and Rodeghiero, F., (1997), *Br. J. Haematol.*, **96**, 458-463.

Chen, K., Detwiler, T.C., and Essex, D.W., (1995), *Br. J Haematol.,* **90**, 425-451.

Chen, V.M., Ahamed, J., Versteeg, H.H., Berndt, M.C., Ruf, W., and Hogg, P.J., (2006) *Biochemistry,* **45**, 12020-12028.

Christiansen, C., St Hilaire, P.M., and Winther, J.R., (2004), *Anal. Biochem.,* **333,** 148–155.

Churchich, J.E., (1993), *Anal. Biochem.,* **213**, 229–233.

Collet, J.-F., Riemer, J., Bader, M.W., and Bardwell, J.C.A., (2002), *J. Biol. Chem.,* **277,** 26886–26892.

Conant, C.G., and Stephens, R.S., (2006), *Cell. Microbiol.*, in press.

Couet, J., de Bernard, S., Loosfelt, H., Saunier, B., Milgrom, E., and Misrahi, M., (1996), *Biochemistry,* **35**, 14800-14805.

Crawford, N., (1971), *Br. J. Haematol.* **21**, 53-69.

Dai, Y., and Wang, C.C., (1997), *J. Biol. Chem.,* **272,** 27572-27576.

Darby, N.J., and Creighton, T.E., (1995), *Biochemistry,* **34**, 16770-16780.

Darby, N.J., Kemmink, J., and Creighton, T.E., (1996), *Biochemistry,* **35**, 10517--10528

Diamant, M., Nieuwland, R., Pablo, R.F., Sturk, A., Smit, J.W., and Radder, J.K., (2002) *Circulation*, **106**, 2442-2447.

Diamant, M., Tushuizen, M.E., Struk, A., and Nieuwland, R., (2004), *Eur. J. Clin. Invest.*, **34**, 392-401.

East, A.L.L., McKellar, A.R.W., and Watson, J.K.G., (1998), *J. Chem. Phys.,* **109,** 4378-4383.

Ellgaard, L., and Ruddock L.W., (2005a), EMBO Rep.**6**, 28-32.

Ellgaard, L., and Beckwith, J., (2005b), *J. Mol. Biol.*, **179,** 125-142.

Ellman, G.L., (1959), *Arch. Biochem. Biophy.,* **82**, 70-77.

Essex, D.W., Chen, K., and Swiatkowska, M., (1995), *Blood,* **86**, 2168–2173.

Essex, D.W., Miller, A., Swiatkowska, M., and Feinman, R.D., (1999), *Biochemistry,* **38,** 10398-10405.

Essex, D.W., Li, M., Miller, A., and Feinman, R.D., (2001), *Biochemistry,* **40**, 6070-6075.

Fenouillet, E., Barbouche, R., Courageot, J., and Miquellis, R., (2001), *J. Infect. Dis.,* **183,** 744-810.

Ford, P.C., Wink, D.A., and Stanbury, D.M., (1993), *FEBS Lett.,* **326,** 1-3.

Furchgott, R.F., and Vanhoutte, P.M., (1989), *FASEB J.,* **9**, 2007-2018.

Fuse, I., (1996), *Crit. Rev. Oncol. Hematol.,* **22,** 1-25.

George, J.N., Thoi, L.L., McManus, L.M., and Reimann, T.A., (1982), *Blood,* **60**, 834-840.

George, J.N., Pickett, E.B., and Heinz, R., (1986), *Blood,* **68,** 307-309.

Girard, P., and Potier, P., (1993), *FEBS Lett.,* **320,** 7–8.

Goldberger, R., Epstein, C. J., and Anfinsen, C.B., (1963), *J. Biol Chem.,* **238,** 628-635.

Goretski, J., and Hollocher, T.C., (1988), *J. Biol. Chem.,* **263,** 2316-2323.

Goss, S.P., Singh, R.J., Hogg, N. and Kalyanaraman, B., (1999), *Free Radic Res.,* **31,** 597–606.

Grey, W.R., (1997), *Protein Structure,* (IRL Press at Oxford University Press, Oxford).

Hawkins, H.C., De Nardi, M., and Freedman, R.B., (1991), *Biochem. J.,* **275**, 341-348.

Hardisty, R.M., and Hutton, R.A., (1966), *Br. J. Haematol.,* **12,** 764-766.

Hart, T.W., (1985), *Tetrahedron Lett.,* **26,** 2013–2016.

Hillson, D.A., Lambert, N., and Freedman, R.B., (1984), *Methods in Enzymol.,* **107**, 281-294.

Holmgren, A., (1979), *J. Biol. Chem.,* **254,** 9627–9632.

Horstman, L., and Ahn, Y.S., (1999), *Crit. Rev. Omcol. Hematol.,* **30,** 111-142.

Hotchkiss, K.A., Matthias, L.J., and Hogg, P.J., (1998), *Biochim. Biophys. Acta,* **1388,** 478-488.

Houk, K.N., Hietbrink, B.N., Bartberger, M.D., McCarren, P.R., Choi, B.Y., Voyksner, R.D., Stamler, J.S., and Toone, E.J., (2003), *J. Am. Chem. Soc.*, **125,** 6972–6976.

Hwang, C., Sinskey, A.J., and Lodish, H.F., (1992), *Science*, **257**, 1496-1502.

Ignarro, L.J., Wood, K.S., and Wolin, M.S., (1984), *Adv. Cyclic Nucleotide Protein Phosphorylation Res.*, **17,** 267-274.

Ignarro, L.J., (1991), *Biochem. Pharm.*, **43,** 485-490.

Ignarro, L.J., Buga, G.M., Wood, K.S., Byrns, R.E., and Chaudhuri, G., (1987), *Proc. Natl. Acad. Sci., U. S. A.*, **84,** 9265-9259.

Ignarro, L.J., (2000), *Nitric Oxide Biology and Pathobiology* (Academic Press, New York).

Jablonski, J., (955), *Acta Phys. Pol. XIV,* 295-307.

Jensen, D., Belka, G., and Dubois, G., (1998), *Biochem. J.*, **331,** 659-668.

Jiang, X.-M., Fitzgerald, M., Grant, C.M., and Hogg, P.J., (1999), *J. Biol. Chem.*, **274**, 2416-2423.

Johnson, S., Michalak, M., Opas, M., and Eggleton, P., (2001), *Cell Biol.*, **11,** 122-129.

Jones, L.J, Upson, R.H., Haugland, R.P., Panchuk-Voloshina, N., Zhou, M., and Haugland, R.P., (1997), *Anal. Biochem.*, **251**, 144-152.

Jourd'heuil, D., Hallen, K., Feelisch, M., and Grisham, M.B., (2000), *Free Radic. Biol. Med.*, **28,** 409–417.

Jourd'heuil, D., Laroux, F.S., Miles, A.M., Wink, D.A., and Grisham, M.B., (1999), *Biochem. Biophys.*, **361,** 323-330.

Kahn, I., Zucker-Franklin, D., and Karpatkin, S., (1973), *Br. J. Haematol.*, **31**, 449-460.

Kalinin, S., Molotkovsky, J.G., Johansson, L.B.-A., (2003), *J. Phys. Chem. B.*, **107,** 3318-3324.

Kandel, E.R., and O'Dell, T.J., (1992), *Science,* **258,** 243-245.

Kemmink, J., Darby, N.J., Dijkstra, K., Nilges, M., and Creighton, T.E., (1996), *Biochemistry*, **35**, 7684-7691.

Kemmink, J., Darby, N.J., Dijkstra, K., Nilges, M., and Creighton, T.E., (1997), *Curr. Biol.*, **7**, 239-245.

Keuren, J.F.W., Magdeleyns, E.J.P., Govers-Riemslag, J.W.P., Lindhout, T., and Curvers, J., (2006), *Br. J. Haematol.*, **134,** 307-313.

Kivirikko, K.I., and Myllyharju, J., (1998), *Matrix Biol.*, **16,** 357-368.

Kleinhenz, D.J., Fan, X., Rubin, J., and Hart, C.M., (2003), *Free Radic. Biol. Med.*, **34,** 856–861.

Koga, H., Sugiyama, S., Kugiyama, K., Fukushima, H., Watanabe, K., Sakamoto, T., Yoshimura, M., Jinnouchi, H., and Ogawa, H., (2006), *Eur Heart J.*, **27**, 817-823.

Lahav, J., Gofer-Dadosh, N., Luboshitz, J., Hess, O., and Shaklai, M., (2000), *FEBS Letters,* **475**, 89-92.

Lahav, J., Jurk, K., Hess, O., Barnes, M.J., Farndale, R.W., Luboshitz, J., and Kehrel, B. E., (2002), *Blood,* **100**, 2472-2478.

Lamberg, A., Jauhiainen, M., Metso, J., Ehnholm, C., Shoulders, C., Scott, J., Pihlajaniemi, T., and Kivirikko, K.I., (1996), *J. Biochem.*, **315,** 533-536.

Leopold, J.A., and Loscalzo, J., (1995), *Coronory Artery Disease,* **6,** 923-929.

Le Roith, D., and Zick, Y., (2001), *Diabetes Care,* **24,** 588-597.

Lettinga, M.P., (2004), *J. Chem. Phys.*, **120**, 4517-4523

Lipton, A., Johnson, M., Macdonald, T., Lieberman, M., Gozal, D., and Gaston, B., (2001), *Nature,* **413,** 171-174.

Lincoln, T.M., and Cornwell, T.L., (1993), *FASEB J.,* **7,** 328-338.

Liu, X., Miller, M.J., Joshi, M.S., Thomas, D.D., and Lancaster, J.R., Jr. (1998), *Proc. Natl. Acad. Sci., U. S. A.,* **95,** 2175–2179.

Liu, L., Hausladen, A., Zeng, M., Que, L., Heitman, J., and Stamler, J.A., (2001), *Nature,* **410,** 490-494.

Lundstrom, J., and Holmgren, A., (1990), *J. Biol. Chem.*, **265**, 9114-9120.

Lundstrom, J., and Holmgren, A., (1993), *Biochem.*, **32,** 6649-6655.

Lyles, M.M., and Gilbert, H.F., (1991), *Biochemistry,* **30**, 619-625.

Macintyre, D.E., and Gorden, J.L., (1974), *Biochem. Soc. Trans.*, **2,** 873-875.

Mallat, Z., Hugel, B., Ohan, J., Leseche, G., Freyssiner, J.M., and Tedgui, A., (1999), *Circulation,* **99,** 348-353.

Mandel, R., Ryser, H.J., Ghani, F., Wu, M., and Peak, D., (1993), *Proc. Natl. Acad. Sci., USA,* **90,** 4112-4116.

Markovic, I., Stantchev, T.S., Fields, K.H., Tiffany, L.J., Tomic, M., Weiss, C.D., Broder, C.C., Strebel, K., and Clouse, K.A., (2004), *Blood,* **103,** 1586-1594.

Matthias, L.J., and Hogg, P.J., (2003), *Antiox. Redox Signal.*, **5**, 133-138.

McKellar, A.R.W., Watson, J.K.G., and Howard, B.J., (1995), *Mol. Phys.*, **86,** 273-286.

Moncada, S., Palmer, R.M., and Gryglewski R.J., (1986), *Proc. Natl. Acad. Sci., USA,* 83, 9164-9168.

Moncada, S., Palmer, R.M., and Higgs, E.A., (1991), *Pharmacol. Rev.*, **43,** 109-142.

Mustard, J.F., Kinlough-Rathborne, R.L., and Packham, M.A., (1989), *Methods Enzymol.*, **169**, 3–11.

Myers, P.R., Minor, R.L., Jr, Guerra, R. Jr, Bates, J.N., and Harrison, D.G., (1990), *Nature,* **345**, 161-163.

Naguleswaran, A., Alaeddine, F., Guionaud, C., Vonlaufen, N., Sonda, S., Jenoe, P., Mevissen, M., and Hemphill, A., (2005), *Int. J. Parasitol.*, **35**, 1459-1472.

Narindrasorasak, S., Yao, P., and Sarkar, B., (2003), *Biochem. Biophys. Res. Commun.*, **311,** 405–414.

Nedospasov, A., Rafikov, R., Beda, N., and Nudler, E., (2000), *Proc. Natl. Acad. Sci. U. S. A.*, **97,** 13543–13548.

Nieuwland, R., Berckmans, R.J., McGregor, S., Boing, A.N., Romijin, F.P., and Westendorp, R.G., (2000), *Blood,* **95,** 930-935.

Nieuwland, R., and Sturk, A., (2002), *Platelets,* (Academic Press, Elsevier Science, London).

Nikitovic, D., and Holmgren, A., (1996), *J. Biol. Chem.*, **271,** 19180–19185.

Noble, D.R., and Williams, D.C., (2001), *J. Chem. Soc. Perkin Trans.*, **1 2,** 13–17.

Nomura, S., (2001), *Int. J. Hematol.*, **74**, 397-404.

Nomura, S., Suzuki, M., Katsura, K., Xie, G.L., Miyazaki, Y., Miyake, T., Kido, H., Kagawa, H., and Fukuhara, S., (1995), *Atheroscleaserosis,* **116**, 235–240.

Noiva, R., and Lennarz, W.J., (1992), *J. Biol. Chem.*, **267,** 3553–3556.

Ohba, H., Harano, T., and Omura, T., (1981), *J. Biochem.*, **89,** 901-907.

Palmer, R.M., Ferrige, A.G., and Moncada, S., (1987), *Nature*, **327**, 524-526.

Pastore, A., Federici, G., Bertini, E., and Piemonte, F., (2003), *Clin. Chim. Acta,* **333,** 19-39.

Pfeiffer, S., Schrammel, A., Schmidt, K., and Mayer, B., (1998), *Anal. Biochem.*, **258,** 68–73.

Pihlajaniemi, T., Helaakoski, T., Tasanen, K., Myllyla, R., Huhtala, M.L., Koivu, J., and Kivirikko, K.I., (1987), *EMBO J.*, **6**, 643-649.

Pimeskoski, A., Klappa, P., Lobell, M., Williamson, R.A., Byme, L., Alanen, H.J., Sab, K.E., and Kivirikko, K.I., (2004), *J. Bio. Chem.*, **279**, 10374-10381.

Puig, A., and Gilbert, H.F., (1994), *J. Biol. Chem.*, **269,** 7764-7771.

Preston, R.A., Jy W., Jimenez, J.J., Mauro, L.M., Horstman, L.L., and Valle, M., (2003), *Hypertension,* **41,** 211-217.

Primm, T.P., Walker, K.W., and Gilbert, H.F., (1996), *J. Biol. Chem.*, **271,** 33664-33669.

Primm, T. P., and Gilbert, H.F., (2001), *J. Biol. Chem.*, **276,** 281–286.

Radomski, M.W., Palmer, R.M.J., and Moncada, S., (1987), *Br. J. Pharmacol.*, **92,** 181-187.

Rafikova, O., Rafikov, R., and Nudler, E., (2000), *Proc. Natl. Acad. Sci., U. S. A.*, **99,** 5913–5918.

Ramachandran, N., Root, P., Jiang, X.-M., Hogg, P.J., and Mutus, B., (2001), *Proc. Natl. Acad. Sci., USA,* **98**, 9539-9544.

Raturi, A., and Mutus, B., (2004), *Anal. Biochem.*, **326,** 281–283.

Raturi, A., Vacratsis, P.O., Seslija, D., Lee, L., and Mutus, B., (2005), *Biochem. J.*, **391**, 351-357.

Raturi, A., and Mutus, B., (2006), *Biochemical. J.,* in press.

Rietsch, A., Bessette, P., Georgiou, G., and Beckwith, J., (1997), *J. Bacteriol.,* **179,** 6602–6608.

Roach, P., Zick, Y., Formisano, P., Accili, D.,Taylor, S.I., and Gorden, P., (1994), *Diabetes,* **43,** 1096–1102.

Root, P., and Mutus, B., (2003), *Anal. Biochem.*, **320**, 299-302.

Root, P., Sliskovic, I., and Mutus, B., (2004), *Biochem. J.,* **382**, 575-580.

Ryser, H.J.P., Levy, E.M., Mandel, R., and DiSciullo, G.J., (1994), *Proc. Natl. Acad. Sci., USA,* **91**, 4559-4563.

Sabatier, F., Darmon, P., Hugel, B., Combes, V., Sanmarco, M., and Velut, J.G., (2002), *Diabetes,* **51,** 2840-2845.

Sahaf, B., Heydari, K., Herzenberg Leonard, A., and Herzenberg Leonore, A., (2005), *Arch. Biochem. Biophys.,* **434**, 26-32.

Schwaller, M., Wilkinson, B., and Gilbert, H.F., (2003), *J. Biol. Chem.,* **278**, 7154-7159.

Seslija, D., (2005) in *M.Sc. Thesis* (University of Windsor, Dept. of Chem. and Biochem., Windsor), pp. 31-32.

Sexton, D.J., Muruganandam, A., Mckenny, D.J., and Mutus, B., (1994), *Photochem. Photobiol.,* **59,** 463-467.

Shaw, A.W., and Vosper, A.J., (1977), *J. Chem. Soc. Faraday Tarns. I,* **8,** 1239-1244.

Shcherbina, A., and Remold-O.' Donnell, E., (1999), *Blood,* **93,** 4222-4231.

Sideraki, V., and Gilbert, H.F., (2000), *Biochemistry,* **39,** 1180–1188.

Solovyov A., and Gilbert, H.F., (2004), *Protein Sci.,* **13,** 1902–1907.

Song, J.L., and Wang, C.C., (1995), *Eur. J. Biochem.,* **231,** 312-316.

Stamler, J.S., Jaraki, O., Osborne, J., Simon, D.I., Keaney, J.F., Vita, J.A., Singel, D., Valeri, C.R., and Loscalzo, J., (1992a), *Proc. Natl. Acad. Sci., USA,* **89,** 7674-7677.

Stamler, J.S., Simon, D.I., Osborne, J., Mullin, M.E., Jaraki, O., Michel, T., Singel, D., and Loscalzo, J., (1992b), *Proc. Natl. Acad. Sci., USA,* **89,** 444-448.

Stanbury, D.M., (1989), *Adv. Inorg. Chem.,* **33,** 69-138.

Stone, J.R., and Marletta, M.A., (1994), *Biochemistry,* **33,** 5636–5640.

Tager, M., Kroning, H., Thiel, U., and Ansorge, S., (1997), *Exp. Hematol.,* **25**, 601-607.

Terada, K., Manchikalapudi, P., Noiva, R., Jauregui, H.O., Stockert, R.J., and Schilsky, M. L., (1995), *J. Biol. Chem.,* **270**, 20410-20416.

Tian, G., Xiang, S., Noiva, R., Lennarz, W.J., and Schindelin, H., (2006), *Cell,* **124,** 61-73.

Tiang, R., (2005), *Cir. Rev.*, **96,** 139-140.

Toti, F., Satta, N., Fressinaud, E., Meyer, D., and Freyssinet, J.M., (1996), *Blood,* **87**, 1409-1415.

Trujillo, M., Alvarez, M., Peluffo, G., Freeman, B., and Radi, R., (1998), *J. Biol. Chem.,* **273,** 7929-7934.

Turano C, Coppari S, Altieri F, and Ferraro A., (2002), *J. Cell. Physiol.* **193**, 154-163.

Vanin, A.F., Malenkova, I.V., and Serezhenkov, V.A., (1997), *Nitric Oxide,* **1,** 191-203.

VanWijk M.J., Vanbavel, E., Sturk, A., and Nieuland, R., (2003), *Cardiovas. Res.*, **59**, 277-287.

Vuori, K., Pihlajaniemi, T., Myllyla, R., and Kivirikko, K.I., (1992), *EMBO J.*, **11,** 5213-5217.

Warkentin, T.E., Hayward, C.P., Boshkov, L.K., Santos, A.V., Sheppard, J.A., and Bode, A.P., (1994), *Blood,* **84,** 3691-3699.

Wendt, H., Berger, C., Baici, A., Thomas, R.M., and Bosshard, H.R., (1995), *Biochemistry,* **34**, 4097-4107.

Westphal, V., Spetzler, J.C., Meldal, M., Christensen, U., and Winther, J.R., (1998), *J. Biol. Chem.,* **273**, 24992–24999.

Wetterau, J.R., Combs, K.A., Spinner, S.N., and Joiner, B.J., (1990), *J. Biol. Chem.,* **265,** 9800-9807.

Wilkinson, B., and Gilbert, H.F., (2004), *Biochim. Biophys. Acta,* **1699,** 35-44.

Williams, D.L., (1996), *Methods Enzymol.,* **268,** 299–308.

Wink, D.A., Kim, S., Coffin, D., Cook, J.C., Vodovotz, Y., Chistodoulou, D., Jourd'heuil, D., and Grisham, M.B., (1999), *Methods Enzymol.*, **301,** 201–211.

Wolf, P., (1967), *Br. J. Haematol.*, **13**, 269–288.

Wu, J.H., and Diamond, S.L., (1995), Anal. *Biochem.*, **224,** 83–91.

Yoshimori, T., Semba, T., Takemoto, H., Akagi, S., Yamamoto, A., and Tashiro, Y., (1990), *J. Biol. Chem.*, **265**, 15984-15990.

Zai, A., Rudd, M.A., Scribner, A.W., and Loscalzo, J., (1999), *J. Clin. Invest.*, **103**, 393-399.

Zhang, X., Cardosa, L., Broderick, M., Fein, H., and Davies, I.R., (2000), *Electroanalysis,* **12,** 425–428.

Zheng, J., and Gilbert, H.F., (2001), *J. Biol. Chem.*, **276,** 15747–15752.

Zhuang, X., Ha, T., Kim, H.D., Centner T, Labeit, S. and Chu, S., (2000), *Proc. Natl. Acad. Sci.*, U S A., **97**, 241-244.

Appendix

A. Buffers

i) Acid Citrate Dextrose (ACD)

25 g/L trisodium citrate dehydrate
15 g/L citric acid monohydrate
20 g/L dextrose

ii) *E.coli* Lysis buffer

100 mM Tris-HCL
200 mM NaCl
2 mM EDTA
100 µg/mL Lysozyme
50 µg/mL DNAse I
50 µg/mL RNAse
2 mM PMSF
1% Triton X 100
Adjust to pH 8

iii) Phosphate buffer saline (PBS)

8 g/L NaCl
1.44 g/L Na_2HPO_4
0.24 g/L KH_2PO_4
0.2 g/L KCl
Adjust to pH 7.4

iv) PDI assay Buffer

14.2 g/L K_2HPO_4
3.8 g/L KH_2PO_4
0.58 g/L EDTA
Adjust to pH 7.0

v) Terrific Broth (TB)

12 g/L Tryptone
24 g/L Yeast Extract
9.4 g/L K_2HPO_4
2 g/L KH_2PO_4
35 mg/L kanamycin
Adjust to pH 7.2

vi) Tyrode Buffer

8.0 g/L NaCl
0.2 g/L KCl
1.0 g/L $NaHCO_3$
0.05 g/L NaH_2PO_4
0.2 g/L $MgCl_2.6H_2O$
0.44 g/L $CaCl_2.6H_2O$
3.5 g/L bovine serum albumin
1.0 g/L dextrose
Adjust to pH 7.4

B. DTNB Assay for total thiol quantification

DTNB stock solution (10 mM) was prepared in 0.1 M TrisHCL pH 8.0. Free thiols were quantified by adding 100 μL of the DTNB stock solution to 800 μL of 0.1M phosphate buffer pH 8.0 and 100 μL of unknown thiol containing protein solution. Free thiols concentration were determined by measuring absorbance of the nitrothiolbenzoate anion (λ = 412 nm) using the extinction coefficient of 13600 L $mol^{-1}cm^{-1}$ (Ellman, 1959).

C. Protein estimation

Standard curve was generated by adding 100 μL of BioRad Protein Assay reagent with a series of known BSA concentrations (0 - 20 μg / mL). Unknown protein samples (100 μL) were mixed with 800 μL of PBS and 100 μL of BioRad's

reagent. The solutions were allowed to react for 15 min followed by absorbance measurements at 595 nm. The protein concentration in the unknown solution was obtained from the standard curve.

D. SDS-Polyacrylamide Gel Electophoresis

i) Preparation of the Resolving Gel

4.0 mL of H_2O
3.3 mL of 30% Acrylamide mix
2.5 mL of 1.5 M Tris (pH 8.8)
0.1 mL of 10% SDS
0.1 mL of 10% ammonium persulfate
0.002 mL of TEMED

The mixture was added to the gel casting cassettes. The cassettes were filled to ~2 nm from the top and layered with tert-butanol.

ii) Preparation of the Stacking Gel

tert-butanol was removed and the gel was rinsed with H_2O after the polymerization of separating gel (approx. ~30 min). The stacking gel was prepared by combining the following reagents:

3.4 mL of H_2O
0.83 mL of 30% Acrylamide mix
0.63 mL of 1.0 M Tris (pH 6.8)
0.05 mL of 10% SDS
0.05 mL of 10% ammonium persulfate
0.005 mL TEMED

iii) Sample Preparation

20 μL of protein sample was mixed with 20 μL of loading buffer and heated to 100 °C for 10 min. The molecular weight marker was loaded into the first lane, followed by 10 μL of each sample loaded their respective wells.

VITA AUCTORIS

Arun Raturi

Education

2002-2007	Ph.D. Biochemistry Department of Chemistry and Biochemistry University of Windsor, Windsor, ON
1998-2000	M.Tech. Biochemical Engineering School of Biochemical Engineering IT, BHU, Banaras, UP, India
1996-1998	M.Sc. Biotechnology Department of Biotechnology IIT Roorkee, Roorkee, UP, India
1992-1995	B.Sc. General Science Garhwal University Dehradun, Uttarakhand, India

Experience

2002- 2007	Research and Graduate Assistant
2000-2001	Research Associate, Wockhardt Research Centre Biotechnology Division, Aurangabad, India
2001-2002	Research Associate, Intas Pharmaceuticals Ltd. Biotechnology Division, Ahmedabad, India

Awards

1996-1998	Department of Biotechnology Scholarship, IIT Roorkee India
1998-2000	Department of Biotechnology Scholarship (GATE-Scholarship), IT BHU, Banaras, India
2003	The Award for Excellence in Research Presentation Chemical Biology Discussion Weekend, Universtiy of Windsor
2003-2004	University of Windsor International Visa Bursary award
2005-2006	University of Windsor Tuition Scholarship award

Publications

Raturi A, Miersch S, Vacratsis PO and Mutus B. Role of microparticle associated- and Plasma -PDI in degradation of circulating insulin: implications in development of insulin resistance (*manuscript under preparation*).

Raturi A, Hudson J, Miersch S and Mutus B. Platelets derived microparticles contain surface-associated protein disulfide isomerase: potential implications in diabetes (*manuscript submitted to FEBS letters*).

Raturi A, Mutus B. Characterization of redox state and reductase activity of protein disulfide isomerase under different redox environments using a sensitive fluorescent assay. *(submitted after revision, Free Radical Biology and Medicine)*

Miersch S, Sliskovic I, Raturi A and Mutus B. Rosuvastatin-dependent anti-oxidant and anti-platelet effects in a Syrian hamster model of type II diabetes. *In Press* (*Free Radical Biology and Medicine*).

Raturi A, Vacratsis PO, Seslija D, Lee L, Mutus B. A direct, continuous, sensitive assay for protein disulphide-isomerase based on fluorescence self-quenching. *Biochem J. 2005* Oct 15;391(Pt 2):351-7.

Sliskovic I *, Raturi A*, Mutus B. (*shared publication) Characterization of the S-denitrosation activity of protein disulfide isomerase. *J Biol. Chem.* 2005 Mar 11;280(10):8733-41.

Raturi A, Mutus B. Use of 2,3-diaminonapthalene for studying denitrosation activity of protein disulfide isomerase. *Anal. Biochem.* 2004 Mar 15;326(2):281-3.